DEVELOPMENT AND CHARACTERIZATION OF MULTIFUNCTIONAL NANOPARTICLES FOR DRUG DELIVERY TO CANCER CELLS

A Dissertation
Submitted to the Graduate Faculty
of the
North Dakota State University
of Agriculture and Applied Science

By

Rahul Rajaram Nahire

In Partial Fulfillment
for the Degree of
DOCTOR OF PHILOSOPHY

Major Department:
Pharmaceutical Sciences

May 2014

Fargo, North Dakota

North Dakota State University
Graduate School

Title

DEVELOPMENT AND CHARACTERIZATION OF MULTIFUNCTIONAL NANOPARTICLES FOR DRUG DELIVERY TO CANCER CELLS

By

RAHUL RAJARAM NAHIRE

The Supervisory Committee certifies that this ***disquisition*** complies with North Dakota State University's regulations and meets the accepted standards for the degree of

DOCTOR OF PHILOSOPHY

SUPERVISORY COMMITTEE:

SANKU MALLIK
Chair

JAGDISH SINGH

STEFAN VETTER

KATIE REINDL

Approved:

05/27/2014
Date

Dr. Jagdish Singh
Department Chair

ABSTRACT

Lipid and polymeric nanoparticles, although proven to be effective drug delivery systems compared to free drugs, have shown considerable limitations pertaining to their uptake and release at tumor sites. Spatial and temporal control over the delivery of anticancer drugs has always been challenge to drug delivery scientists. Here, we have developed and characterized multifunctional nanoparticles (liposomes and polymersomes) which are targeted specifically to cancer cells, and release their contents with tumor specific internal triggers. To enable these nanoparticles to be tracked in blood circulation, we have imparted them with echogenic characteristic. Echogenicity of nanoparticles is evaluated using ultrasound scattering and imaging experiments. Nanoparticles demonstrated effective release with internal triggers such as elevated levels of MMP-9 enzyme found in the extracellular matrix of tumor cells, decreased pH of lysosome, and differential concentration of reducing agents in cytosol of cancer cells. We have also successfully demonstrated the sensitivity of these particles towards ultrasound to further enhance the release with internal triggers. To ensure the selective uptake by folate receptor- overexpressing cancer cells, we decorated these nanoparticles with folic acid on their surface. Fluorescence microscopic images showed significantly higher uptake of folate-targeted nanoparticles by MCF-7 (breast cancer) and PANC-1 (pancreatic cancer) cells compared to particles without any targeting ligand on their surface. To demonstrate the effectiveness of these nanoparticles to carry the drugs inside and kill cancer cells, we encapsulated doxorubicin and/or gemcitabine employing the pH gradient method. Drug loaded nanoparticles showed significantly higher killing of the cancer cells compared to their non-targeted counterparts and free drugs. With further development, these nanoparticles certainly have potential to be used as a multifunctional nanocarriers for image guided, targeted delivery of anticancer drugs.

ACKNOWLEDGEMENT

I would like to thank my advisor, Dr. Sanku Mallik, for believing in me, and for giving me an opportunity to work in his laboratory under his supervision. During my stay in his laboratory, he was always encouraging me to learn new research techniques and methods. He never pushed me to work, instead he encouraged me to work harder by putting me on interesting projects and innovative ideas. I wish I become a teacher and researcher like him one day.

I would like to thank our department chair, Dr. Jagdish Singh, who encouraged me from the day I started my graduate studies in this department. I would like to thank Dr. Stefan Vetter and Dr. Katie Reindl, my dissertation committee members for their suggestions and comments on my preliminary proposal which really improved the quality of research. I would also like to thank S. Paul, Dr. Kausik Sarkar, Dr. D. K. Srivastava, Dr. K. Katti, Dr. K. Gange, Dr. W. Muhonen, Dr. J. Shabb, and for their help in some of the experiments.

I would like to thank Dr. Manas Haldar, for providing me with synthesized lipids and polymers. I would like to acknowledge his intellectual and practical contribution to my work. I would like to thank Erin Nyren Erickson- my former colleague, who trained me on all the research techniques and methods. I would also like to thank my labmate Prajakta, for helping with peptide synthesis and animal studies. Many rotation students have helped me during this period – Anaas, Rayat, and Rupa. I thank Jean and Janet, for always being very helpful with all the things in the department. I would like thank funding agencies (NIH and NSF), Department of Pharmaceutical Sciences, faculty, staff and everyone who helped me directly and indirectly during my PhD. My friends (Pancham, Nikhil, Anil, Deepak, Pravin, Harshal, Shrikant, Rahul, Ravi, Vikas Bhau), and family members (Mummi, Pappa, Tai, Daji, Satvik, in-law family, Akash, Sagar) for their love and support. I thank Dr. M. P. Wagh and Dr. Mrudula Bele who mentored and encouraged me for higher education during my graduation at NDMVPS's College of Pharmacy-Nasik. Finally, my wife Varsha – without whom, this wouldn't have been possible.

DEDICATION

To my Parents and in-law Parents

TABLE OF CONTENTS

LIST OF TABLES

LIST OF FIGURES

LIST OF SCHEMES

LIST OF ABBREVIATIONS

3D.....Three dimensional

ACS.....American Chemical Society

AFM.....Atomic Force Microscopy

ARLINs.....Acoustically Reflective Lipid Nanoparticles

ATCC.....American Type Culture Collection

Avg.....Average

BSA.....Bovine Serum Albumin

C.....Centigrade

Cm.....Centimeter

CD.....Circular Dichroism

CL.....Cross Linker

cm.....Centimeter

CO_2.....Carbon dioxide

CW.....Continuous Wave

CYS.....Cysteine

dB.....Decibel

DLS.....Dynamic Light Scattering

DNA.....Deoxyribonucleic Acid

DPPE-LR.....1,2-dipalmitoyl-*sn*-glycero-3-phosphoethanolamine-N-(lissamine rhodamine B sulfonyl) (ammonium salt)

DSC.....Differential Scanning Calorimetry

DSPC.....1,2-distearoyl-*sn*-glycero-3-phosphocholine

DSPE.....1,2-distearoyl-*sn*-glycero-3-phosphoethanolamine

DTT.....Dithiothreiotol

EDC.....Ethyl-3-(3-dimethylaminopropyl)-carbodiimide

ELIPs.....Echogenic Liposomes

EPR.....Enhanced Permeation and Retention

Em.....Emission

Ex.....Excitation

f.....Hydrophilic fraction

FDA.....Federal Drug Administration

g.....Grams

GSH.....Glutathione

h.....Hours

HBSS.....Hank's Blank Salt Solution

HER2.....Human Epidermal growth factor Receptor 2

HBTU.....O-Benzotriazole-N,N,N',N'-tetramethyl-uronium-hexafluoro-phosphate

HEPES.....4-(2-hydroxyethyl)-1-piperazineethanesulfonic acid

HOBT .....Hydroxybenzotriazole

HPLC.....High Performance Liquid Chromatography

kHz.....Kilo Hertz

kPa.....Kilo Pascal

Kv.....Kilo Volts

LFUS.....Low Frequency Ultrasound

LP4.....Lipopeptide 4

M.....Molar

MALDI-TOF.....Matrix-assisted laser desorption/ionization- Time of Flight

mg.....milligrams

MHz.....Mega Hertz

MI.....Mechanical Index

Ml.....Millilitres

mm.....Millimeters

mmol.....Millimolars

MMP.....Matrix metalloproteinase

MPa.....Mega Pascal

MPS.....Mononuclear Phagocyte System

m-PEG.....Methoxy Polyethyleneglycol

MW.....Molecular Weight

n.....Number

nm.....Nanometer

NMR.....Nuclear Magnetic Resonance

P4.....Polymersomes with PLA-3600

P5.....Polymersomes with PLA-5800

PBS.....Phosphate Buffered Saline

PC.....Phosphatidylcholine

PDI.....Polydispersity Index

PEG.....Polyethylene glycol

PLA.....Polylactic acid

PMDETA .....*N*,*N*,*N*′,*N*′,*N*′′-pentamethyldiethylenetriamine

PSD.....Particle Size Distribution

POPC..... 1-palmitoyl-2-oleoyl-*sn*-glycero-3-phosphocholine

POPE..... 1-palmitoyl-2-oleoyl-*sn*-glycero-3-phosphoethanolamine

POPE-G.....Gallate derivative with three propargyl groups coupled to POPE

RI.....Refractive Index

ROI..... Region of Interest

RPMI..... Roswell Park Memorial Institute medium

R_t.....Retention Time

RT..... Room Temperature

siRNA..... Small Interfering Ribose Nucleic Acid

TEM.....Transmission Electron Microscopy

Tg.....Glass Transition temperature

THF.....Tetrahydrofuran

µL.....Microliter

µmol.....Micro moles

US.....Ultrasound

USA.....United States of America

UV .....Ultravoilet

V .....Volts

W.....Watts

LIST OF APPENDIX TABLES

LIST OF APPENDIX FIGURES

GENERAL INTRODUCTION AND DISSERTATION ORGANIZATION

Nanomedicine: During the last few decades, nanotechnology has revolutionized the science of drug formulation and delivery. Recent years have witnessed unprecedented growth in the field of nanoscience and nanomedicine. The scientific community all over the world is very optimistic, hoping that nanomedicine will bring significant advances in the strategies of diagnosis and treatment of diseases. Although the term "nano" has varied connotations in different disciplines, there is consensus that nanotechnology means not just miniaturization of larger particles, but the preparation of nanomaterial whose properties change drastically from their bulkier versions because of their nanoscale size [1]. Although it's still a topic of debate, nanoparticles can be defined as ultra-dispersed, solid, supramolecular structures displaying submicron size, ideally smaller than 500 nm. It should also be noticed that many nanomedicine products don't fall into the category of nanoparticles as per definition of nanoscale materials (size range between 0.2 to 100 nm) by The Royal Society (2004) [2]. However, this does not necessarily have impact on their functional aspects in medical applications. Large-sized particles are needed for loading higher amounts of drug onto the particles. The reasons why nanoparticles find attractive applications in medicine is based on their unique features, such as large surface to mass ratio, their ability to adsorb/carry other compounds, and ability to change their physicochemical behavior just by change in the size. The composition of engineered nanoparticles can vary, and they can be of natural origin (e.g., phospholipids, lipids, chitosan, dextran, carbohydrates, lactic acid), or can be of "synthetic" origin (polymers, carbon, silica and metals) [2]. The most important goals behind the use of "nanomaterials" in drug delivery include:

- Target-specific delivery of drugs
- Improved efficacy, reduced toxicity
- Safety and biocompatibility

- Improved pharmacokinetics and bioavailability of drugs

The primary requisite of an ideal nanomaterial for drug delivery would be not only to have capacity to load high amounts of drug, but also the ability to release the drug at the intended site. Currently, different types of nanoparticles are being tested for their effectiveness as drug delivery vehicles (e.g., liposomes, polymersomes, micelles, dendrimers, nanosassemblies, microcapsules etc.). Among these, the most popular are the bilayered vesicles of lipids (liposomes) and amphiphilic polymers (polymersomes). These vesicles have higher loading capacity compared to other nanoparticles [3].

Liposomes as drug delivery vehicles: The first closed bilayered phospholipid vesicles were called liposomes by Alec Bangham and colleagues in 1965 [4]. Initially termed as "bangosomes" and then liposomes, were soon tested as drug delivery vehicles. Early pioneers such as Gregory Gregoriadis, established that liposomes can be an excellent drug delivery system [5-7]. Several publications showed the effect of liposomes on the *in vivo* distribution and overall pharmacokinetics of the drug entrapped [8, 9]. New methods were developed to improve and control the entrapment efficiency and size distribution [10, 11]. Sonication and extrusion of multilamellar liposomes through polycarbonate filters to produce smaller size liposomes was a major advancement in the field of liposomal drug delivery [12]. Subsequently, several reports demonstrated the *in vivo* efficacy of anticancer drug-encapsulated liposomes [13, 14]. Liposomal doxorubicin showed improved efficacy and reduced cardiotoxicity [15, 16], ultimately leading to the clinical studies with liposomal drugs [17].

Problems with liposomes: It soon became clear that conventional liposomes had several limitations with their *in vivo* use. Passive leakage of contents and rapid clearance of liposomes were hampering their efficacy as efficient drug carriers. Drug release was shown to be highly affected by the serum proteins. The opsonization of liposomes by serum proteins was proven to be the main mechanism behind rapid clearance of liposomes from the body. These problems

were partially solved by strengthening the bilayer (use of cholesterol and saturated lipids), pH gradient loading (remote loading/ammonium gradient), and PEGylation of liposomes (Stealth liposomes). Changing the composition of lipid bilayer, especially incorporation of cholesterol was shown to minimize the leakage by tightening the fluid bilayers. Switching from fluid bilayers (glass transition temperature below 37°C) to solid phase lipids (glass transition above 37°C) also decreased the passive leakage of contents from liposomes [18].

pH gradient method: One of the major advances in development of drug loading is the entrapment by pH gradient method. In this method, transmembrane pH gradient is created by encapsulating acidic buffer or proton-generating salts, such as ammonium sulfate, inside the aqueous interior of liposomes. The method is also known as remote loading, as the drug is loaded after formation of vesicles. Many currently used drugs possess amine groups and can be loaded using the pH gradient method. Some drugs (Doxorubicin) precipitate, and hence are retained efficiently in aqueous interior of liposomes whereas some drug (Ciprofloxacin) which do not precipitate readily are difficult to retain [19]. Drug precipitation can be enhanced by increasing the intraliposomal concentration of the compounds above their solubility. Drug that are not weak bases (Docetaxel) can be converted to weak base prodrugs [20].

Importance of PEGylation: To minimize the rapid clearance by MPS (Mononuclear Phagocyte System), initially smaller size liposomes showed some improvement. Addition of sphingomyelin for egg phosphatidylcholine resulted in longer circulating liposomes, likely due to the increase in surface hydrophilicity of liposomes. Earlier work of PEG attached to proteins to increase their circulation time, led to a simpler technique of making liposomes long circulating [21]. Several clinical studies showed that grafting of PEG to liposome surface resulted in substantial reduction in clearance [22, 23]. In 1995, the FDA approved the first nano-drug formulation of doxorubicin (Doxil®: passively targeted multilamellar PEGylated liposomes with remote loaded doxorubicin) for human use [24].

Need of targeting and triggering strategies: It soon became clear that there were still some unresolved problems with the use of these long circulating "stealth" liposomes. Although cardiac toxicity was minimized, because of lack of active targeting, the Doxil® liposomes would continue to leak contents slowly in circulation, and lead to side effects such as thrombocytopenia, neutropenia and hand-feet syndrome. Drug release rates have important implications for therapeutics activities of all types of drug delivery vehicles. The drug needs to be released from liposomes for bioavailability at the intended site of action. In the absence of any trigger, contents release was often slow, and hence, limited efficacy of treatment. Although Doxil® had an advantage of passive targeting due to the enhanced permeation and retention in cancer tumors, it had limitations [24]. As there was not active uptake of liposomes by the cells and no trigger to release the drug instantly, liposomes relied on passive release and convection to distribution in the tumor area. These might be some of the reasons why there are not many generic Doxil® versions in market.

Active targeting: One of the major problems with liposomal drug delivery is the intracellular delivery of drugs across the membranes of cells to the sites of action. Hydrophobic, uncharged drugs diffuse though the cell membrane, while some hydrophilic drugs use membrane transporters to enter the cytosol. Most of the drugs require delivery systems to transport them to the site of action inside the cytosol. The most popular approach today is to use receptor-mediated endocytosis of ligand-targeted liposomes, as long as the drug can sustain the acidic environment inside the endosomal-lysosomal compartment [25]. However, the uptake should be selective for diseased cells. Many cancer cells overexpress certain receptors on their surface (folate, transferrin, integrin, HER2, etc.) which can be utilized to increase the selectivity of drug carriers. There are many reports of higher uptake of ligand-targeted liposomes compared to non-targeted counterparts. Currently, there are several actively-targeted nanoparticles in clinical trials, showing better therapeutics profiles compared to passively-targeted nanoparticles [26, 27]. Active targeting can be classified into three types [28].

1. Angiogenesis associated targeting: by targeting growth of neovascular, the size and metastasis can be controlled [29] :
    - ❖ VEGF receptor [30]
    - ❖ Integrin receptor [31]
    - ❖ Vascular cell adhesion molecule [32]
    - ❖ MMPs [33]
2. Uncontrolled cell proliferation targeting:
    - ❖ Human epidermal factor (HER) [34]
    - ❖ Transferrin receptors [35]
    - ❖ Folate receptors [36]
3. Tumor cell targeting: [28]
    - ❖ Breast cancer
    - ❖ Colorectal cancer
    - ❖ Lung cancer
    - ❖ Prostate cancer

Folate targeting: Among all these targeting strategies, folate targeting is most widely used because folate ligand is inexpensive, nontoxic, easy to conjugate, non-immunogenic, has high binding affinity and is very stable on storage and in blood circulation [37]. Folate receptor is the most researched target for cancer therapeutics. Lung, ovarian, brain, head and neck, renal, and breast cancer tissues are known to overexpress folate receptors [38]. Because folate is essential for important cell functions (like purines and pyrimidine synthesis), the cargo attached to the ligand is retained within endocytic vesicle and released into the cytosol. Whereas, hormones, antibodies, and other ligands are internalized to clear the ligand from the receptor and to stop the activated signaling cascade, and thus, are shuttled into the lysosome for destruction [39]. Currently there are many folate targeted-formulations in clinical trials and some of those are ready to get the final FDA approval [40]. Vynfinit® (folate-targeted

vintafolide) is being evaluated in a global Phase 3 study named PROCEED for women with platinum-resistant ovarian cancer [41].

Triggering strategies: Stability of nanoparticles in blood circulation is very important to avoid side effects. At the same time, the carriers should release their contents instantly as they reach the targeted site. Doxil® formulation, although showed enhanced accumulation in tumors, had no trigger to release the drug [24]. Various triggering strategies have been studied, and many literature reports have demonstrated their efficiency both *in vitro* and *in vivo* [42]. Triggers can be classified into two categories: remote (external/exogenous) and local (internal/endogenous). Remote triggers can be heat [43], light [44], ultrasound [45] or magnetic field [46], whereas local triggers can be specific to disease sites such as elevated levels of enzymes (MMPs) [47], change in pH [48] or GSH levels [49]. There are reports of using combinations of multiple triggers to enhance the release from nanoparticles [50]. It should be noted that patient rarely die of their primary tumors as these tumors can be removed surgically or ablated with radiation [51]. In most cases, metastatic tumors cause morbidity, as these are not accessible via external triggers. Clearly, the local triggers can offer significant advantages in this situation. External triggers offer better temporal and spacial control over the release, whereas local triggers are important to target metastatic tumors. So it is important to focus on the smart use of a combination of these triggers to achieve maximum therapeutic outcomes.

The first study to demonstrate effectiveness of trigger release strategy was hyperthermia induced release of methotrexate from liposomes [52]. Use of lipids with phase transition a few degrees above the physiological temperature made heat as an effective trigger to release the contents. Many literature reports showed its effectiveness, and currently some formulations are in the clinical trials [53-57]. One of the major advances in the field is ThermoDox® (Celsion Corporation), which demonstrated significant improvements in drug release rates and uptake in heated tumors (around 41°C). This formulation is currently in phase III clinical trials [58].

Ligand-targeted nanoparticles, upon internalization into the target cells, can be designed to release the contents in response to high levels of GSH in the cytosol [59, 60], or the low pH environment inside lysosomes [61, 62].

Ultrasound in drug delivery technology: During the last decade, ultrasound has gained tremendous popularity in therapeutic and diagnostic applications. This is primarily due to its versatility, cost effectiveness, and highly encouraging applications in drug delivery techniques. With the introduction of gas bubbles and echogenic particles, research in the field of ultrasound-assisted drug delivery has really blossomed. Hyperthermia and cavitation are two important phenomena associated with use of ultrasound, and are primarily responsible for use of ultrasound in drug delivery [63]. Hyperthermia and acoustic cavitation lead to sonoporation, resulting in enhanced permeability of cell membranes. Different carriers are being developed for their responsiveness towards ultrasound. Echogenic liposomes [64], acoustically reflective liposomes [65], sonosensitive liposomes [66], "bubble" liposomes [67],and echogenic lipid nanoparticles [68] are essentially nanoparticles designed to carry air/gas either inside or on the surface. Many of these carriers are being proposed for simultaneous drug delivery and ultrasound imaging applications. Although microbubbles and echogenic particles carrying drugs have shown encouraging results for targeted drug delivery to cancer cells, they have certain limitations. Echogenic liposomes often show low and variable release of contents with application of diagnostic frequency ultrasound [69]. Although low frequency ultrasound have shown excellent results *in vivo*, their safety towards healthy tissues is always a concern. Microbubbles, because of their large size, cannot extravasate into the tumor tissues, and hence their clinical use in drug delivery is limited. For better control over the release from echogenic nanoparticles, we have designed them such that they are sensitive to an internal trigger and externally applied ultrasound.

In this dissertation, we have developed and characterized four drug delivery carriers/nanoparticles which are responsive to an internal trigger and ultrasound. This dissertation is paper-based, and each chapter has been published as an article in a peer reviewed journal. Scattering experiments were carried out by our collaborators Dr. Sarkar.

In Chapter 1, we have prepared liposomes which are responsive to elevated levels of MMP-9 enzymes at the tumor site, and are also responsive to ultrasound trigger. We have shown release kinetics with recombinant and cancer cells secreted MMP-9. These results are published in the American Chemical Society journal Molecular Pharmaceutics (Impact factor: 4.6).

In Chapter 2, we have prepared redox sensitive, polymer coated lipid nanoparticles which release their contents in the presence of millimolar concentrations of reducing agents and ultrasound. We have demonstrated their uptake and release in metastatic cancer cells. These results are published in the American Chemical Society journal Biomacromolecules (Impact factor: 5.4).

In Chapter 3, we have prepared liposomes which release their contents in acidic environment of lysosomes and tumor microenvironment. We have also studied their ultrasound responsiveness to further enhance the release. These results are currently under review in the journal Molecular Pharmaceutics (Impact factor: 4.6).

In Chapter 4, we have prepared polymersomes which are ultrasound reflective, and are redox sensitive. We have studied their effectiveness to carry and deliver a combination of two anticancer drugs using monolayer and spheroid cell cultures. These results are published in the Elsevier journal Biomaterials (Impact factor: 8.5).

CHAPTER I. ULTRASOUND ENHANCED MATRIX METALLOPROTEINASE-9 TRIGGERED RELEASE OF CONTENTS FROM ECHOGENIC LIPOSOMES

Abstract

The extracellular enzyme matrix metalloproteinase-9 (MMP-9) is overexpressed in atherosclerotic plaques and in metastatic cancers. The enzyme is responsible for rupture of the plaques and for the invasion and metastasis of a large number of cancers. The ability of ultrasonic excitation to induce thermal and mechanical effects has been used to release drugs from different carriers. However, the majority of these studies were performed with low frequency ultrasound (LFUS) at kHz frequencies. Clinical usage of LFUS excitations will be limited due to harmful biological effects. Herein, we report our results on the release of encapsulated contents from substrate lipopeptide incorporated echogenic liposomes triggered by recombinant human MMP-9. The contents release was further enhanced by the application of diagnostic frequency (3 MHz) ultrasound. The echogenic liposomes were successfully imaged employing a medical ultrasound transducer (4 – 15 MHz). The conditioned cell culture media from cancer cells (secreting MMP-9) released the encapsulated dye from the liposomes (30 – 50%) and this release is also increased (50 – 80%) by applying diagnostic frequency ultrasound (3 MHz) for 3 minutes. With further developments, these liposomes have the potential to serve as multimodal carriers for triggered release and simultaneous ultrasound imaging.

Introduction

Liposomes are nano to micrometer-sized vesicles with a hydrated lipid bilayer encapsulating an aqueous phase. Due to their structural similarity with biological cells, liposomes show attractive features as drug carriers (e.g., lesser toxicity, increased uptake and longer circulation time). Hence, liposomes have been extensively investigated for targeted drug-

delivery applications [70-73]. Currently, about 10 liposomal formulations are approved by the US Food and Drug Administration for human use. Conjugation with targeting ligands leads to active-targeting of the liposomes to the intended sites for drug-delivery and imaging [74, 75]. However, after reaching the intended sites, most of the liposomes release the contents passively and this process is often slow [76]. The rate of release from the liposomes can be increased by the application of triggers, e.g., temperature [77], pH [78], light [79], ultrasound [45], metal ions [80] and enzymes [81]. Recently, we have demonstrated enzymatic release of liposomal contents in the presence of recombinant as well as cancer cell secreted matrix metalloproteinase-9 (MMP-9) [82, 83].

MMP-2 and -9 are members of Zn^{2+} and Ca^{2+} dependent family of enzymes responsible for degradation of gelatin and collagen (IV and V) in the extracellular matrix [84]. MMPs play an important role in a variety of normal physiological processes e.g., embryonic development, tissue metamorphosis, angiogenesis, wound healing, ovulation etc. [85]. Increased expression levels of MMP-9 and MMP-2 correlate with arthritis, atherosclerosis, cancer and other diseases [86-89]. These two enzymes hydrolyze and weaken the fibrous caps of the plaques, leading to plaque rupture [90]. MMP-9 is also involved in progression and metastasis of many cancers and are being considered as biomarkers for various types of cancers [91]. Inhibitors of these enzymes are currently in clinical trials for adjuvant therapy of various cardiovascular diseases and cancers [92].

The ability of ultrasonic excitation to induce thermal and cavitational effects has been used to release drugs from different carriers such as polymeric assemblies, micelles, emulsions, microcapsules, microspheres and liposomes. However, majority of these studies were performed with low frequency ultrasound (LFUS) at kHz frequencies [93-95]. Although, inertial/transient cavitation thresholds are much lower at such frequencies [96, 97] favoring ultrasound mediated destruction and subsequent release from liposomes [98-100], clinical usage of similar excitations will be limited due to harmful biological effects. The release is

considerably diminished for MHz range excitation [101, 102]. Diagnostic frequency ultrasound has been used for drug delivery and imaging employing micron-sized bubbles [103-105] and microbubbles conjugated to liposomes.

Recently, a modified protocol for preparing acoustically reflective liposomes (echogenic liposomes or ELIPs) has been reported [106-108]. The preparation protocol ensures that the liposomes entrap air pockets, although exact location of the entrapped air has not yet been exactly ascertained [105, 108, 109]. It strengthens the mechanical coupling with ultrasound resulting in strong ultrasound echoes. Ultrasound excitation can also be used to destabilize the bilayer membrane and release of contents from liposomes. Since ELIPs retain all the desired properties of normal liposomes, they have been extensively investigated for simultaneous imaging and drug delivery applications employing diagnostic frequency ultrasound (1 – 10 MHz) [69, 109-111]. However, often the amount of contents released by ultrasound excitation of the ELIPs is not optimal, ranging from 20 – 50% [112]. Herein, we demonstrate that the combination of enzymatic triggering (by MMP-9) and ultrasound excitation leads to considerably higher amounts of contents release from echogenic liposomes. The echogenic liposomes were successfully imaged employing a medical ultrasound transducer (4 – 15 MHz). We also demonstrate that conditioned cell culture media from cancer cells (secreting MMP-9) released the encapsulated dye from the liposomes (30 – 50%) and this release is also increased (50 – 80%) by applying diagnostic frequency ultrasound (3 MHz) for 3 minutes.

Materials and Methods

Synthesis of lipopeptide (**LP4**)

The lipopeptide **LP4** was synthesized using a microwave assisted peptide synthesizer (Liberty, CEM Corporation, Matthews, SC) following a reported protocol [113]. Commercially available Fmoc-protected amino acids (0.1 mM) (Peptides International, KY, USA) were used in

the synthesis employing Fmoc-Gly-CLEAR acid resin (Peptides International, KY, USA) as the solid support. A mixture of 1-hydroxybenzotriazole (HOBT, AK Scientific, CA) and O-(benzotriazol-1-yl)-N,N,N',N'-tetramethyluronium hexafluorophosphate (HBTU, ChemPep, FL) was used as coupling agent in 5 fold excess. Coupling steps were performed with 20 W microwave power for 5 minutes at 50 °C except for arginine (25 °C for 25 minutes). Diisopropylethylamine was used as the activator base during the peptide coupling reactions. The Fmoc deprotection was carried out by 5% piperazine (TCI America) using N,N-dimethylformamide as the solvent (Macron Chemicals, NJ). The peptide was cleaved from resin using a mixture of trifluoroacetic acid (TCI America), triisopropyl silane and water (95:2.5:2.5) for three hours at room temperature with constant stirring. Subsequently, the reaction mixture was filtered and the filtrate was treated with cold ether to precipitate the crude peptide, dried and stored at −20 °C until use.

Purification of crude lipopeptide

Purification of the crude **LP4** was conducted by reverse phase high performance liquid chromatography (Shimadzu Scientific Instruments) using a diphenyl semipreparatory column (Grace Vydac, 300 Å pore diameter silica, 5 μm particle size, 10 x 250 mm) as the stationary phase. A linear gradient (0-70%) of acetonitrile in water was used at a flow rate of 8 mL/min over 45 minutes. Trifluoroacetic acid (25 mM) was added to both solvents and was monitored at 235 nm using a UV detector. After evaporating solvents from the purified product, the purity was determined using MALDI-TOF mass spectrometry with an AB 4800 MALDI TOF/TOF Mass Analyzer using α-cyano-4-hydroxy-cinnamic acid as the ionizing matrix. The dried powder was stored in freezer (−20 °C) until use.

Circular dichroism (CD) spectroscopy

CD spectra were recorded (to ascertain the triple helical structure of **LP4**) using a Jasco J-815 CD spectrometer with 1 mm path length quartz cuvette. The lipopeptide **LP4** (0.5 mg/mL) was dissolved in 4 mM phosphate buffer (pH = 4.0) and stored at 4°C overnight before recording the spectra. For each spectrum, 12 accumulations were carried out at scanning speed of 50 nm/min in order to obtain a good signal to noise ratio. For liposome-incorporated **LP4**, 1 mg/mL concentration was used and 36 accumulations were performed to reduce noise. The CD spectrum of MMP-9 was subtracted from CD spectrum of ELIPs treated with MMP-9. Melting temperature of **LP4** was calculated by plotting the intensity at 225 nm against temperature.

Preparation of dye encapsulated echogenic liposomes (ELIPs)

Stock solutions of 1-palmitoyl-2-oleoyl-*sn*-glycero-3-phosphocholine (POPC, Avanti Polar Lipids) was prepared (1 mg/mL) by dissolving in chloroform and stored in freezer. Solutions of POPC (2 mg) and **LP4** (2.6 mg) were mixed in the molar ratio of 70:30 respectively in a 10 mL round bottom flask. A thin film at the bottom of the flask was formed by evaporating the solvent at 40 °C using a rotary evaporator. In order to remove any residual solvents, the flask was placed under high vacuum overnight. Subsequently, the dried film was hydrated with 100 mM carboxyfluorescein (>90% fluorescence is quenched) in HEPES (2-[4-(2-hydroxyethyl)piperazin-1-yl]ethanesulfonic acid) buffer (25 mM, pH = 8) with added ions (Ca^{2+} and Zn^{2+}) and 2 mL of 0.64 M mannitol (final concentration 0.32 M) at 50 °C. Mannitol is a weak cryoprotectant; we have recently observed that finite amount of mannitol during preparation is critical for ensuring the echogenicity of ELIPs [108]. The lipids were hydrated for 3 hours and the resultant multilamellar vesicles were bath sonicated for 10 minutes. The liposomal solution was exposed to three freeze (–70 °C) and thaw cycles. Subsequently, the liposomes were extruded first through 800 nm and then 200 nm polycarbonate filters (Nuclepore, Whatman) 15 times at 60 °C using a mini-extruder (Avanti Polar Lipids). To remove

the unencapsulated dye, the liposomes were gel filtered using Sephadex G-100 column conditioned with HEPES buffer (25 mM, pH = 8). The osmolarity of the eluent buffer was adjusted (540 mOsm/kg with NaCl, 10 g in 1L, 0.17 M) to that of the liposomal solution to ensure the minimum leakage of dye from liposomes due to osmotic shock. A similar procedure was followed to prepare the liposomes without any encapsulated dye using HEPES buffer without carboxyfluorescein. ELIPs for CD spectroscopic studies were prepared by the same method using a 4 mM phosphate buffer (pH = 4.0).

Measurement of size distribution

Particle size distribution (PSD) of ELIPs was measured using a Dynamic Light Scattering (DLS) instrument (Malvern Zetasizer Nano-ZS90). DTS 0012 polystyrene latex disposable sizing cuvette (RI: 1.59) was used and the measurements were conducted at a scattering angle of 90°. Samples (0.1 mg/mL in HEPES buffer) were equilibrated for 120 seconds and 12 readings were then taken for a single sample at constant temperature (25 °C). Each batch of ELIPs was tested for polydispersity and each experiment repeated three times to ensure reproducibility of the results.

Transmission electron microscopy

The ELIPs samples were dispersed to 1 mg/mL concentration and dropped onto 300 mesh Formvar coated copper grids previously coated with 0.01% poly-L-lysine and allowed to stand for 1 min before wicking off with filter paper. After air drying for 2 minutes, the samples were negatively stained with 1% phosphotungstic acid for 1.5 minutes and subsequently wicked off with filter paper and allowed to dry before viewing. The samples were observed using a JEOL JEM-2100-LaB_6 transmission electron microscope operating at 200 kV.

Release studies with recombinant MMP-9

The release experiments were carried out using a microplate multidetection instrument (Spectramax-M5, Molecular devices) employing the liposomes prior to freeze drying at 25 °C. Release was monitored by recording the fluorescence emission intensity at 518 nm with excitation wavelength 480 nm. All experiments were conducted in triplicate. Each well contained 20 μL of 0.1 mg/mL ELIPs in HEPES buffer (25 mM, pH = 8.0, osmolarity 540 mOsm/kg adjusted with NaCl, 10 g in 1L, 0.17M) and 16 μL of 25 μM MMP-9 (final concentration: 2 μM). Release of dye was observed over 60 minutes. The emission intensity was recorded in one minute interval. After 1 h, 10 μL of Triton-X100 was added to disrupt all the liposomes and the emission intensity was measured (excitation: 480 nm). This fluorescence intensity was treated as total (100%) release. The percent release was calculated using the formula:

$$\text{Release (\%)} = \frac{\text{Observed intensity - Initial intensity}}{\text{Final intensity - Initial intensity}} \times 100$$

Measurement of echogenicity of ELIPs

For echogenicity experiments, the freeze-dried ELIPs sample was suspended in a solution of phosphate buffered saline (PBS) with 0.5% by weight of bovine serum albumin (BSA). We observed that the liposome solution prior to freeze-drying was not echogenic. Echogenicity of the freeze dried and then reconstituted ELIPs was investigated using an *in vitro* acoustic setup (Figure 1.1) which is capable of measuring non-linear response from contrast agents. The setup employs two single element spherically focused immersion transducers (Panametrics-NDT) confocally positioned at right angles. This type of transducer placement ensures the similarity of scattered signals to backscattered echoes [114] and also provides high spatial resolution [115]. Each transducer has an individual diameter of 1.27 cm and focal length of 3 cm. The sample is held in a rectangular chamber. Holes were drilled on adjacent walls for

insertion of transducers. Complete immersion of the transducers required 100 mL of solution. Appropriate amount of ELIPs was dissolved in 100 mL of PBS-BSA solution to yield a final lipid concentration of 10 μg/mL which is low enough to ensure absence of multiple scattering effects. The transmitting transducer has a nominal center frequency of 3.87 MHz with a –6 dB bandwidth of 86.4%. The receiving transducer has a center frequency of 5.54 MHz with an 85% bandwidth. The transmitting transducer was excited at 3.5 MHz with a 32 cycle sinusoidal wave. A 0.4 mm needle hydrophone (PZT-Z44-0400, Onda Corporation, CA, USA) was used to calibrate transducers. A programmable function generator was utilized (Model 33250A; Agilent, Santa Clara, CA) to generate the wave which was amplified using a power amplifier (Model A-300; ENI, Rochester, NY) and fed to the transmitting transducer. The scattered signal was received using the other transducer and a pulser/receiver (Model 5800; Panametrics-NDT, Waltham, MA) with a 20 dB gain. A digital oscilloscope (Model TDS2012; Tektronix, Beaverton, OR) was used to observe the signal in real-time. Scattered voltage-time responses were acquired from the oscilloscope using LabView (Version 6.0.3; National Instruments, Austin, TX) via a GPIB IEEE 488 cable and GPIB card and saved on a PC for post-experimental analysis using MATLAB (MathWorks, Natick, MA). Fast Fourier Transforms of 50 oscilloscope acquisitions were obtained and averaged in frequency domain which was then converted to dB scale using unit reference. Responses at fundamental, second and sub-harmonic frequencies were extracted from the resultant data set and plotted.

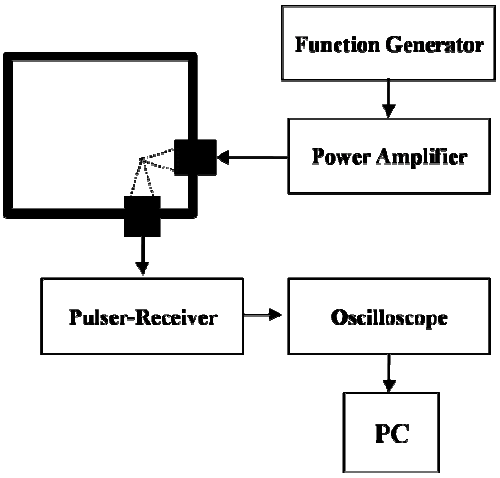

Figure 1.1: Schematic of the experimental setup for *in vitro* measurement of scattering

Culture of cancer cells and harvesting of conditioned media

All cell lines were obtained from American Type Culture Collection (Manassas, VA). PANC-1 (Human pancreatic cancer), PC-3 (Human prostate cancer), MCF-7 (Human breast cancer), 22Rv-1 (Human prostate cancer), HeLa (Human cervical cancer) and bEnd-3 (immortalized rat brain endothelial cells) were cultured in clear (without added phenol red) RPMI media supplemented with 5% antibiotics (penicillin, streptomycin), 10% (by volume) fetal bovine serum and grown in incubator at 37 °C in humidified atmosphere containing 5% CO_2. After three generations, confluent cells were centrifuged (200 g) and the supernatant media collected and frozen until use.

Ultrasound mediated release studies

The *in vitro* setup for ultrasound enhanced release studies employed a single element unfocused immersion transducer (Model IP301HP; Valpey Fisher Corporation, Hopkinton, MA). The active element of the transducer has a diameter of 0.3175 mm and a nominal center frequency of 3.5 MHz with a –6 dB bandwidth of 85%. An arbitrary function generator was used to generate a continuous sinusoidal wave with desired parameters (Model 33250A; Agilent,

Santa Clara, CA) which was then amplified with a power amplifier (Model A-150; ENI, Rochester, NY) and fed to the transducer. The release studies were carried out in a 48 well plate filled with 500 μL sample with a total lipid concentration of 0.02 mg/mL. The transducer face was always kept immersed in the sample volume at a distance of 20 mm from the base (Figure 1.2). The homogeneity of the sample was maintained using a small magnetic stirrer. The entire plate was kept on an ice bath to minimize the temperature changes. Most release studies were performed with 3 MHz continuous wave at 1 MPa pressure for an exposure period of 180 seconds. We note that although the current setup has often been used to subject biological cells or liposomes to ultrasound [67, 116-119], it allows reflections from air-water interface. This effect has been studied in detail recently [120, 121] to show that the reflection creates a standing wave pattern giving rise to a spatially varying acoustic field. Following these studies, we are currently developing a setup that would address this effect, and will be used to determine optimal ultrasound excitation parameters. For the limited goal of demonstrating ultrasound-mediated release here, current setup is adequate. Also note that less than 1% energy transfer due to stimulation from a transducer positioned in one well was measured at a neighboring well indicating negligible inter-well interference. All experiments were repeated three times to ensure the reproducibility of results obtained.

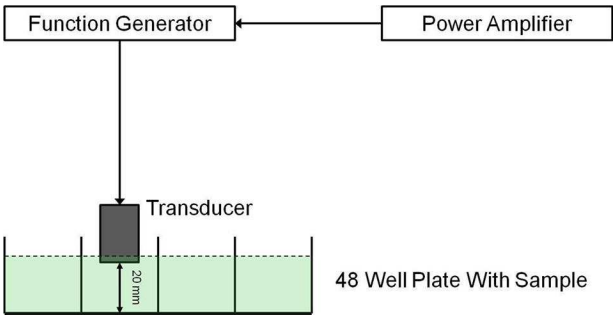

Figure 1.2: Schematic of the *in vitro* experimental setup for ultrasound mediated release studies

Ultrasound enhanced MMP-9 triggered release

This study was carried out in a 48 well plate, with 500 μL of 0.02 mg/mL of liposomes (prior to freeze drying) in each well using an ice bath. Three different procedures were followed for these experiments. In one set of experiments, we incubated 0.02 mg/mL of ELIPs with 2 μM MMP-9 for an hour and then applied the ultrasound (3 MHz, 1 MPa) for 180 seconds. In second set, we applied the ultrasound first and then allowed ELIPs to incubate with MMP-9. In third set we added MMP-9 to ELIPs and immediately applied the ultrasound to get the simultaneous exposure result. Control samples were also acquired for each of these set of experiments. All the experiments were conducted in triplicates in order to ensure repeatability of the results obtained.

For studies with conditioned media harvested from different metastatic cancer cell lines, we added 50 μL of media to 450 μL of ELIPs (lipid concentration: 0.02 mg/mL) and after one hour we applied the ultrasound. Two different negative control measurements were performed: one without the cell culture media (RPMI) and ultrasound and other with RPMI media as well as ultrasound whereas bEnd-3 cell media was treated as a positive control.

Ultrasonic imaging of the echogenic liposomes

The Terason t3200™ Diagnostic Ultrasound (MedCorp LLC., Tampa, FL) was utilized to image the reflection of the echogenic liposomes. A layer of Aquasonic® 100 (Parker Laboratories, Inc., Fairfield, New Jersey) ultrasound gel was applied to the 15L4 Linear (4.0-15.0 MHz) (MedCorp LLC., Tampa, FL) ultrasound transducer sound plate. The transducer with gel was placed over the parafilm covering the wells containing ELIPs (0.2 mg/mL in all four wells) in a 96-well plate. The ultrasound scan properties of the echogenic liposomes were set at 0.7 Mechanical Index (MI), 0.6 Thermal Index (TIS), Omni Beam activated, level C Image Map,

level 3 Persistence, high (H) frequency, level 3 TeraVision, level 51 2D Gain, level 60 Dynamic Range (DR), 3 cm scan depth, and 22 Hz frame rate. The images were labeled and saved.

Results and Discussion

Nonfibrillar collagens (types IV and V) are the principal substrates of MMP-9 [122]. The collagens contain high amounts of the amino acid triad Glycine-Proline-Hydroxyproline (GPO) and this contributes to the triple helical structure [123]. We have previously synthesized triple-helical substrate lipopeptides for MMP-9 and optimized the contents release from liposomes in the presence of this enzyme [82]. For these studies, we decided to synthesize the same lipopeptide [**LP4,** amino acid sequence: $CH_3(CH_2)_{16}$CONH-GPQ**GI**AGQR$(GPO)_4$GG-COOH, where MMP-9 cleavage site is between Glycine and Isoleucine] for preparing the ELIPs. The lipopeptide **LP4** was synthesized employing a microwave-assisted peptide synthesizer, purified by reverse-phase HPLC and the purity was confirmed by MALDI-TOF mass spectrometry (Calculated MH^+: 2333.26; Observed: 2333.28). Circular dichorism (CD) spectroscopic studies confirmed triple helical structure for **LP4** in phosphate buffer (pH = 4.0; Figure 1.3A). Poor solubility of the lipopeptide in buffer of higher pH prevented us from conducting these studies at physiological pH (7.4). Temperature-dependent CD spectra (5 – 60 ^oC) indicated the presence of an isosbestic point (Figure 3A) and the melting temperature was determined to be 49 ^oC (Figure 1.3B). This melting temperature is similar to that observed for human collagen (48 ^oC) [124]. The isosbestic point in Figure 1.3A indicates that the triple-helical lipopeptide is melting to monomeric species without going through any intermediates [125].

After confirming triple helical structure of lipopeptide **LP4** in solution, we prepared ELIPs incorporating 30 mol% of **LP4** and 70 mol% of POPC in phosphate buffer (pH = 8.0) employing a reported protocol [104, 105]. This liposomal composition was based on our previous mechanistic and optimization studies on MMP-9 triggered release of liposomal contents [82, 83]. We observed that **LP4** retains the triple helical structure when incorporated

into the liposomes (Figure 1.4, black trace). It is hypothesized that the hydrolysis of triple-helical substrate peptides by MMP-9 requires unwinding of the triple helix by the enzyme followed by hydrolysis [126]. We observed that upon incubation of these liposomes with 2 μM recombinant human MMP-9, the triple helicity decreased substantially (Figure 1.4, red trace). These results demonstrate that MMP-9 is able to unwind and cleave the triple helical **LP4** even when incorporated in the lipid bilayer of the ELIPs. We also observed that 2 μM of MMP-7, MMP-10 or trypsin released less than 5% of the encapsulated contents from the liposomes. This is likely due to the inability of these enzymes to unwind the triple helix [75, 127].

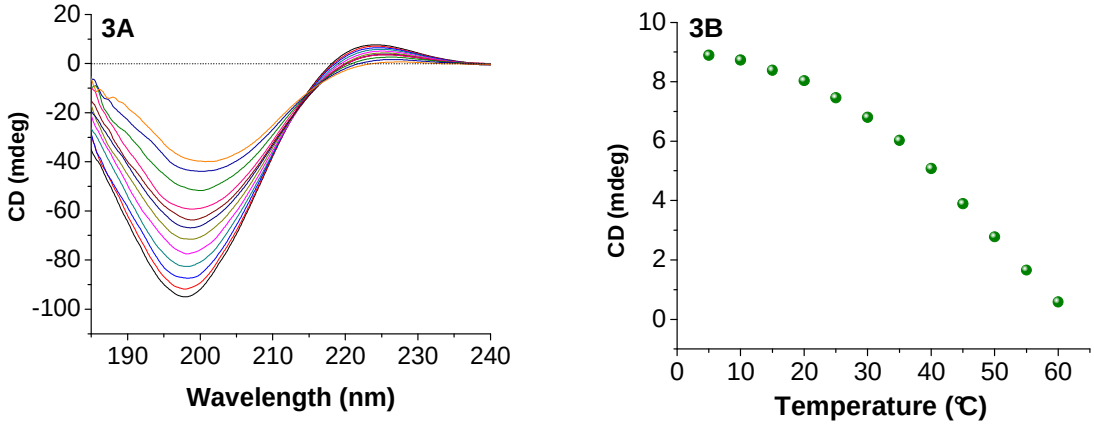

Figure 1.3. (**A**) Temperature dependent CD spectra (5-60 °C) of **LP4** (0.5 mg/mL) in 4 mM phosphate buffer (pH = 4). The presence of positive peak at 225 nm and negative peak at 198 nm indicates the triple helical nature of **LP4**. (**B**) The melting curve for **LP4** monitored at 225 nm is shown.

Next, we prepared ELIPs with carboxyfluorescein encapsulated and the liposomes were subsequently freeze-dried for long-term storage and shipment [128]. We determined the average diameters of the ELIPs before and after freeze-drying employing dynamic light scattering. We observed that average diameter of the liposomes in the reconstituted powder was larger (190 ± 35 nm; Figure 1.5D) compared to that prior to freeze drying (116 ± 22 nm, Figure 1.5C). The polydispersity index also increased to 0.85 from 0.3 – indicating a large distribution of size in the reconstituted liposomes [129]. Transmission electron microscopy corroborated these observations. TEM images show that the reconstituted ELIPs were heterogeneous (50 nm

– 1 μm) with median size between 100 – 200 nm (Figures 1.5A and B). During the freeze-drying and subsequent reconstitution steps, some of the liposomes fuse with each other – leading to a more heterogeneous size distribution. We have used mannitol [130] during the ELIPs preparation which plays a crucial role in ensuring echogenicity by aiding air entrapment [108]. Also note that the relatively high polydispersity indicates presence of larger liposomes (also seen in the inset of Figure 1.5D). These larger liposomes with air pockets of size around a micrometer are primarily responsible for the echogenicity of ELIPs. Consistent with this, we also observed that the liposome solution prior to freeze drying was not echogenic.

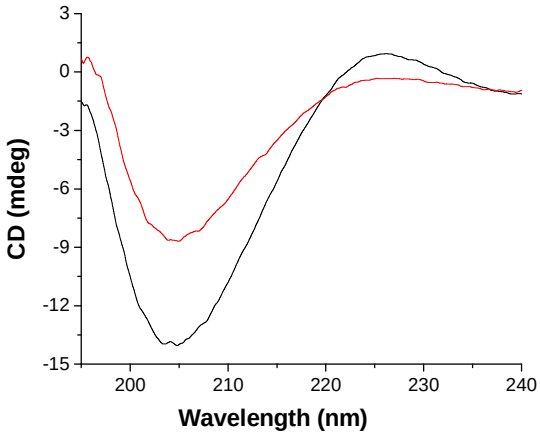

Figure 1.4. CD spectra of liposome-incorporated **LP4** is shown before (black trace) and after (red trace) incubation with 2 μM MMP-9 for an hour. These experiments were conducted in 25 mM phosphate buffer, pH = 8.0.

Echogenicity of the ELIPs (reconstituted from freeze dried powders) with and without encapsulated carboxyfluorescein was investigated using the acoustic setup for scattering measurements shown in Figure 1.1. We observed that the liposomes showed echogenicity only when freeze dried and subsequently reconstituted. However, this leads to some loss of the encapsulated dye. As mentioned above, the echogenicity is likely due to the presence of larger size liposomes with encapsulated gas in the reconstituted samples (see Figures 1.5B and 1.5D). The ELIPs were excited at an acoustic pressure amplitude of 500 kPa. Figure 1.6A shows the

FFT of the scattered response from suspension with and without any ELIPs. At an acoustic pressure of 500 kPa, we observed distinct peaks at both fundamental frequency (i.e., at excitation frequency of 3.5 MHz) and second-harmonic frequency (i.e., at twice the excitation frequency, 7 MHz) in presence of the ELIPs. However, no distinct subharmonic peak (i.e. response at half the excitation frequency, 1.75 MHz) was observed. The nominal central frequency (5.54 MHz) of the receiving transducer is rather high compared to the subharmonic frequency (1.75 MHz). However, using a receiving transducer with a lower central frequency (2.25 MHz) did not change the result. We conclude that these ELIPs do not generate any significant subharmonic response at this excitation frequency. Figure 1.6B shows the experimentally measured echogenic response from the ELIPs (the scattered fundamental and second-harmonic components). Control measurements are acquired without any ELIPs in the sample solution. Each set of experiments was repeated five times. The mean of the five different runs is plotted along with the corresponding standard deviation. We also imaged the ELIPs (in a well plate) employing a Terason t3200 ultrasonic medical imaging system using a 4 – 15 MHz transducer (Figure 1.6C, D).

We observed that both ELIP formulations with and without encapsulated dye show echogenicity with nearly 20 dB enhancement of the fundamental response when reconstituted in PBS-BSA. The preparation procedure includes addition of mannitol, a weak cryoprotectant. It has been hypothesized that lyophilization in presence of mannitol creates defects in the bilayer that serves as nucleation sites for air entrapment [106, 107, 110, 131]. The presence of air creates a mismatch in acoustic impedance rendering the liposomes echogenic i.e., capable of reflecting ultrasound waves [132, 133]. It has been reported that these air pockets are created during the rehydration step in the PBS-BSA/PBS solution [132]. Creation of air pockets is facilitated by the use of mannitol during the lyophilization [106, 110, 132]. Mannitol thus plays a critical role in the echogenicity of the ELIPs. Recently, we have shown that a small but finite amount of mannitol is required for echogenicity [108]. Although echogenicity of the ELIPs have been

attributed to the presence of these air pockets, the exact location of these air pockets still remains uncertain [134, 135]. Hypothesized structure of ELIPs considers existence of trapped air within the bilayer in between hydrophobic tails of the lipid molecules [109, 136]. Air can also be trapped as a small lipid monolayer coated bubble freely floating within the aqueous core of the liposomes [107, 109]. Recently, TEM image have shown the existence of such individual lipid coated bubbles [137]. The lipid coating in both situations—in the bilayer or for individual bubbles—can render the air pocket stable against Laplace pressure driven dissolution by drastically decreasing the effective surface tension at the air-liquid interface [138-140]. The lipid shell also modifies the echogenicity of the air pocket and thereby of the emulsion [115, 141, 142]. Notably, there is no difference in the echogenicity of the ELIPs due to dye-loading. The ELIPs also show non-linear response with around 10 dB enhancement for second-harmonic response.

We conducted the enzymatic release studies employing an optimized concentration of freshly-prepared liposomes (0.01 mg/mL of total lipid). We used the self-quenching property of the encapsulated dye (carboxyfluorescein) in determining the contents release from the liposomes [83]. In order to determine if the presence of the entrapped air pockets in the echogenic emulsion has any effect in the fluorescence of the dye, we recorded the emission spectra of carboxyfluorescein (5 μM in 25 mM HEPES buffer, pH = 8.0) in the presence of ELIPs (without any encapsulated dye) and regular liposomes. We observed that these emission intensities were same, indicating that the entrapped air in the ELIPs is not affecting the emission from carboxyfluorescein (Appendix A, Table A1).

In the absence of any added enzyme, less than 10% of the encapsulated dye was released in 60 minutes (Figure 1.7, magenta spheres). Upon incubation with 1 μM of recombinant human MMP-9, we observed 25% release of the encapsulated dye in 20 minutes (Figure 1.7A, blue spheres). After this time, no further release was observed from the liposomes (Figure 1.7A, blue spheres). Increasing the concentration of MMP-9 to 2 μM leads to 62% release in 50

minutes (Figure 1.7A, green spheres). These release profiles can be fitted with a single exponential rate equation (Figure 1.7A, red lines through the observed data points) with rate constants of (12.9 $\pm$ 0.4) x 10^{-2} s^{-1} (1 μM MMP-9) and (15.1 $\pm$ 0.1) x 10^{-2} s^{-1} (2 μM MMP-9).

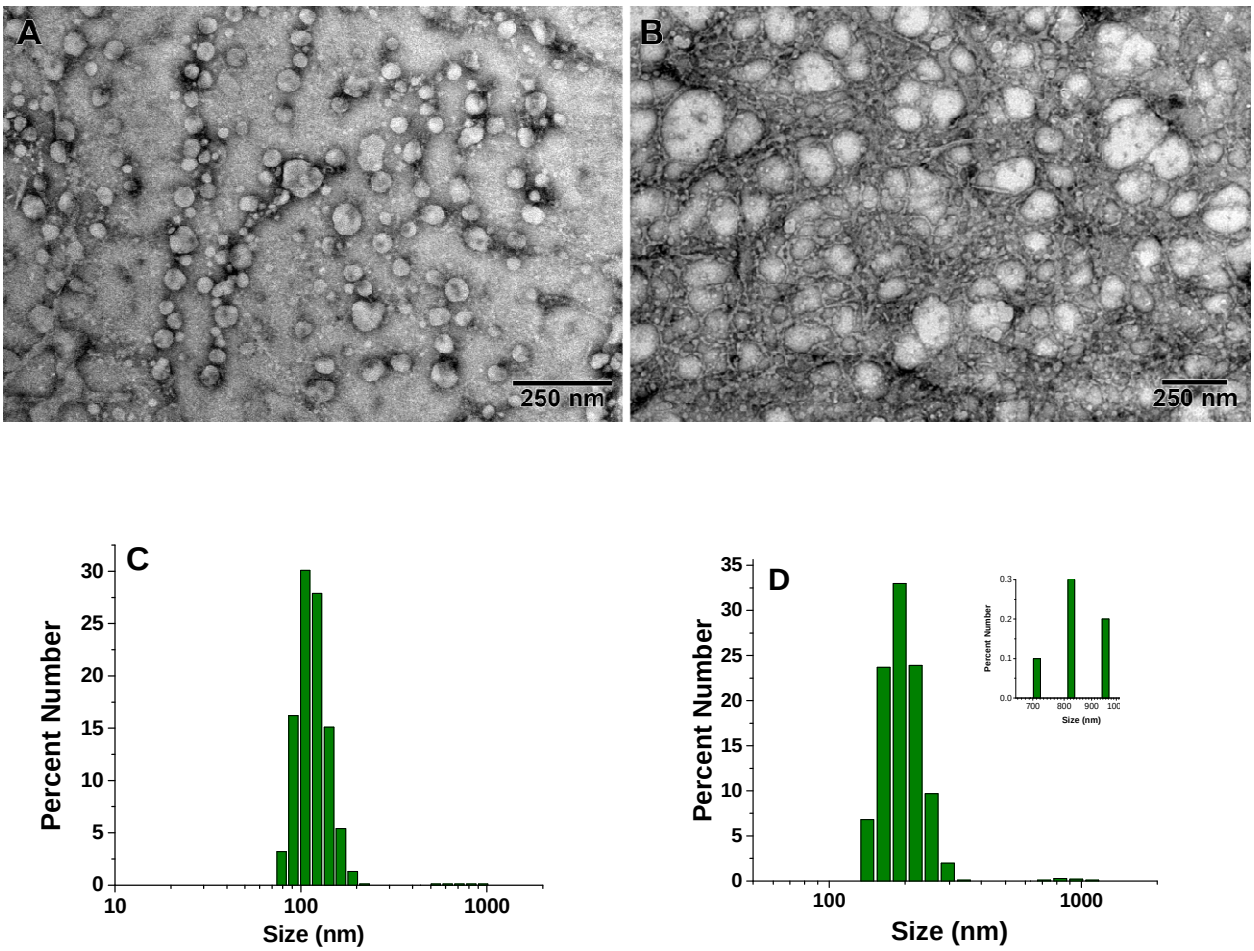

Figure 1.5. TEM images (**A**: before freeze drying **B**: after freeze drying) and DLS size distributions (by number) of carboxyfluorescein encapsulated ELIPs (**C**: before freeze drying; **D**: after freeze drying). The inset plot of panel **D** shows the presence of liposomes in the size range 700 – 1100 nm. The TEM images of the samples were obtained using a LaB_6 emitter at low magnifications and with the beam spread to reduce the amount of electron beam interaction per unit area and hence beam damage to sample.

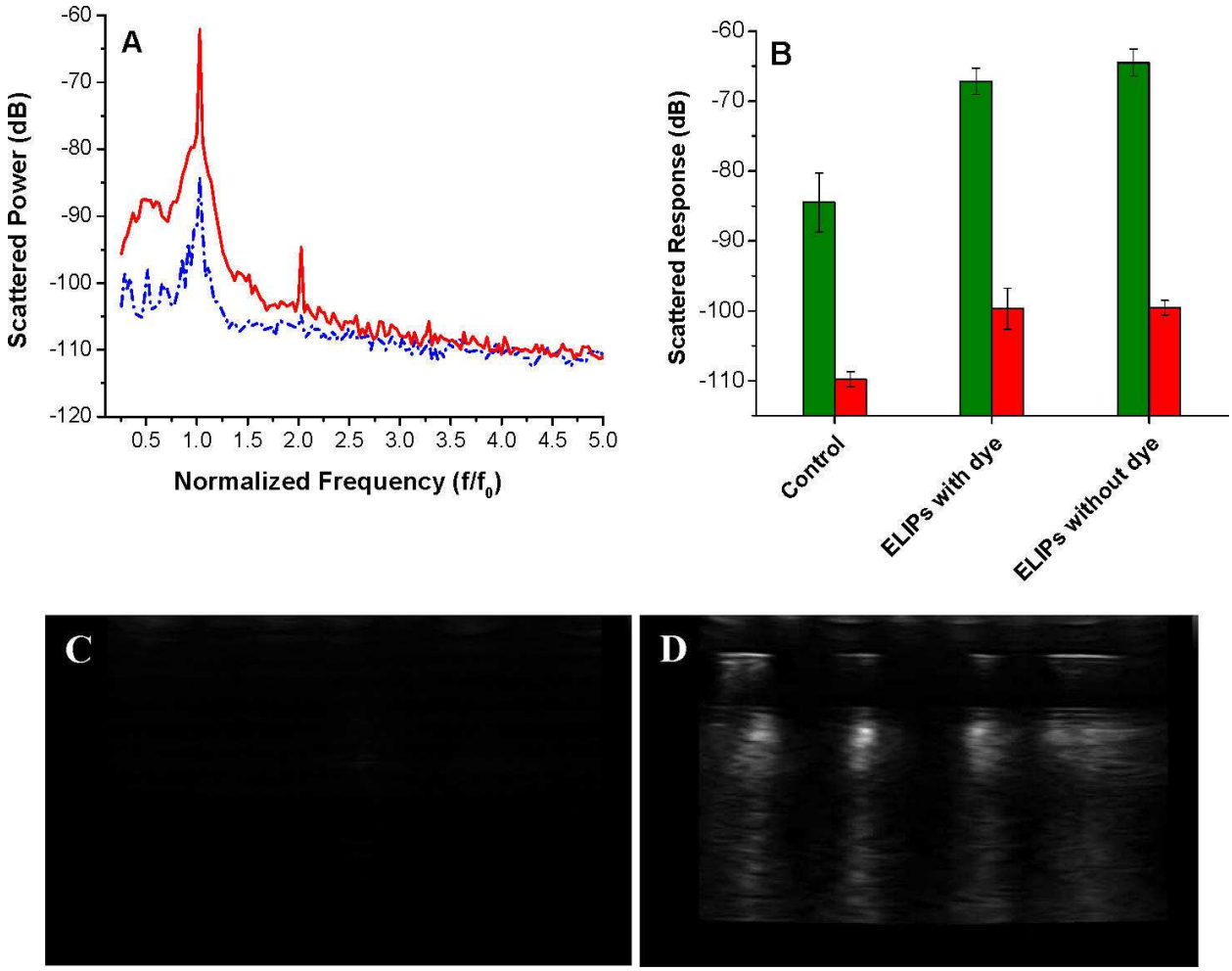

Figure 1.6. (A) FFT of the scattered signal from a suspension with (red trace) and without (blue trace) liposomes at an acoustic pressure of 500 kPa. (**B**) Fundamental (green columns) and second harmonic (red columns) of ultrasound scattered response from ELIPs prepared with or without dye-loading and reconstituted in PBS and PBS-BSA solutions. (**C**, **D**): Ultrasound images (5 – 10 MHz transducer) of 4 wells of a 96-well plate containing buffer (**C**) and echogenic liposomes (0.2 mg/mL in each well) incorporating **LP4** peptide and encapsulating the dye carboxyfluorescein (**D**).

MMP-9 cleaves the triple helical peptide exposed on the liposome surface, leading to destabilization of the lipid bilayer and release of the encapsulated content [47]. As the bilayer "heals" itself, the release from the liposomes slows down. We also observed that the recombinant MMP-9 used in these studies undergoes self-hydrolysis and resulting in the formation of catalytically inactive enzyme. The reduction in the concentration of the active enzyme will also contribute to reducing the rate of release from the liposomes. It should be

noted that for healthy individuals, the serum concentration of MMP-9 is less than 10 nM. For gastric, colorectal and pancreatic cancer patients the serum concentration of MMP-9 can be as high as 1 μM [74]. We also observed that exposing the liposomes to diagnostic frequency ultrasound (3 MHz, 1 MPa) for 3 minutes led to around 25% release of the encapsulated dye (Figure 1.7B); ultrasound destabilizes the ELIPs[143].

The lipopeptide **LP4** adopts triple helical conformation in the liposomes (Figure 1.4). The fibronectin domain of MMP-9 unwinds the triple helix and subsequently, the catalytic domain hydrolyzes the peptide bond [144]. We hypothesized that enzymes incapable of unwinding the triple helix should not release the encapsulated dye from the liposomes. In accordance with this, we observed that MMP-7, MMP-10 and trypsin (2 μM each) failed to release the encapsulated dye from the liposomes (data not shown).

After ensuring release by MMP-9 and diagnostic frequency ultrasound separately, we proceeded to determine the combined effect of these two triggers on contents release from the ELIPs. In this endeavor, we first incubated the ELIPs with MMP-9 (2 μM) for an hour and observed 62% release of the encapsulated dye. Subsequent application of ultrasound (3 MHz, 3 minutes) increased the release to 71% (Table 1.1). As MMP-9 releases the encapsulated dye by disturbing the lipid bilayer of the liposomes, it is likely that the entrapped air is also escaping – making the resultant liposomes less responsive to ultrasound trigger. When we applied the ultrasound first for 3 minutes, we observed 15% release of the contents from the liposomes. This indicates that a majority of the liposomes are not releasing the contents in the presence of ultrasound alone. However, upon subsequent treatment with MMP-9 (2 μM) for an hour, the release increased to 65%. When we incubated the liposomes with MMP-9 (2 μM) and applied ultrasound at the same time, the release decreased to 30%. A probable reason for this may be the local increase in temperature during the ultrasonic excitation [145]. The local heating will deactivate MMP-9, leading to a decrease in the contents release from the liposomes. The control

in Table 1 represents release when the transducer was inserted in the liposomal solution without sending any ultrasound waves (for 3 minutes).

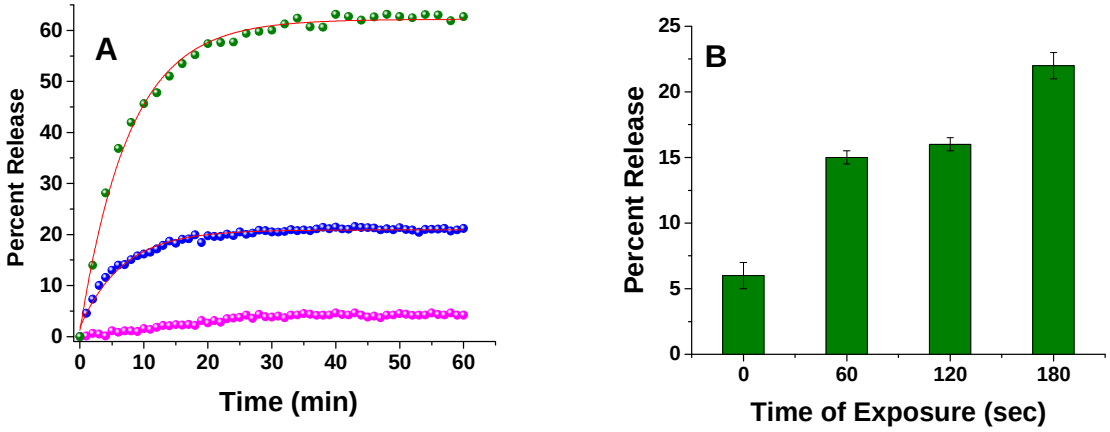

Figure 1.7. (**A**) MMP-9 triggered release profile for encapsulated carboxyfluorescein from ELIPs after incubation for an hour with 1 μM (blue spheres) and 2 μM (green spheres) recombinant MMP-9. The magenta spheres indicate the release from the liposomes in the absence of any added enzyme. The red lines indicate the fitted curves through these data points using a single exponential rate equation. (**B**) High frequency ultrasound (3 MHz, continuous wave, 1 MPa) triggered release from ELIPs with varying exposure time.

Table 1.1: Ultrasound (US) enhanced recombinant MMP-9 triggered contents release from ELIPs.

Conditions	**Release (% ± SD) with MMP-9**	**Release (% ± SD) with US**	**Total Release (% ± SD)**
MMP-9 followed by US	62 ± 10	9 ± 1	71 ± 5
US followed by MMP-9	50 ± 12	15 ± 4	65 ± 10
Simultaneous			30 ± 2
Control (no US)			4 ± 4

Various cancer cells are known to secrete varying amounts of MMP-9 in the extracellular matrix [146]. We decided to determine if the conditioned media from cancer cells can release

the encapsulated dye from the ELIPs and if this release can be further enhanced by the application of diagnostic frequency ultrasound. In this endeavor, we cultured the cells HeLa (cervical cancer), PC-3 (prostate cancer), 22Rv1 (prostate cancer), MCF-7 (breast cancer) and PANC-1 (pancreatic cancer) in dye-free RPMI. After reaching confluency, the cells were pelleted and the media was harvested. The immortalized mouse brain endothelial cell line bEnd-3 (which does not secrete MMP-9) was taken as control [147]. Based on our results with recombinant MMP-9, we incubated the ELIPs with the conditioned media for an hour, followed by the application of ultrasound pulses (3 MHz) for 3 minutes.

We observed that the culture media (RPMI containing 10% by volume of fetal bovine serum) released 16% of the liposome encapsulated dye (Figure 1.8A). As cells become confluent and consume fetal bovine serum, the conditioned media from bEnd-3 cells showed less release (<5%) compared to fresh RPMI (Figure 1.8A). The release also decreases slightly over time. Since the release was very low (< 5%), we did not conduct any further studies to determine the reasons for this time-dependent decrease. The conditioned media from the cancer cells released varying amounts of encapsulated dye (16 – 50%, Figure 1.8A). We observed that the release was highest in the presence of the conditioned media from the PC-3 cells (47%, Figure 1.8A and 1.8B). The time course of the dye release in the presence of conditioned media from PC-3 cells can be fitted with a single exponential rate equation with rate constant of $(57.4 \pm 1.6) \times 10^{-2}\ s^{-1}$. However, we observed that the amount of contents release does not correlate with the total amount of MMP-9 present in the conditioned media (as determined by ELISA). ELISA determines the total amount of MMP-9, which includes both catalytically active and inactive enzymes. It is also possible that besides MMP-9, other triple helicase secreted in the conditioned media (i.e., MMP-2, MMP-14, ADAM-10 etc.) are contributing to the release of the dye [87, 148]. However, we were pleased to find that upon application of ultrasound for 3 minutes, the amounts of dye release increased to 25 – 75% (Figure 1.8A). Currently we are

testing the effects of ultrasound frequency, incorporation of PEG-lipid and cholesterol on the contents release from these liposomes and these results will be reported later.

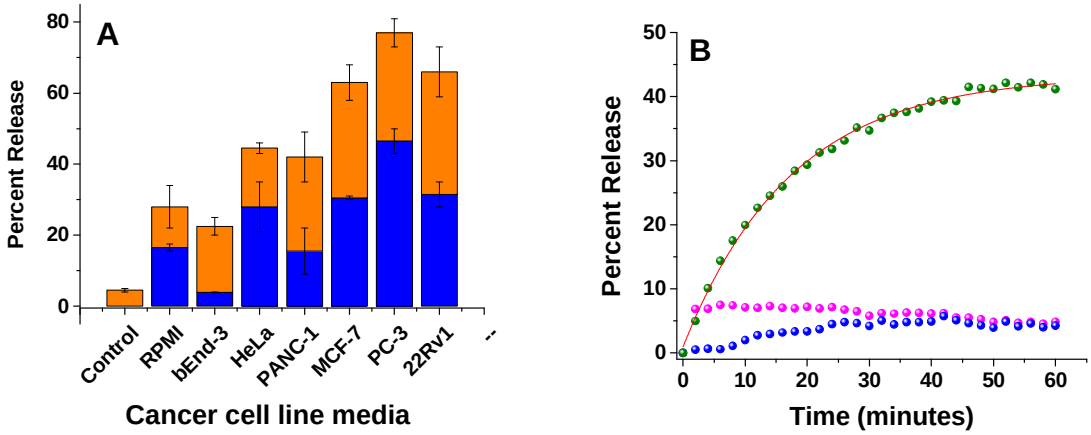

Figure 1.8. (**A**) Release of liposomal contents in presence of conditioned cell culture media from metastatic cancer cells (blue bars) and upon subsequent application of 3 minutes of 3 MHz ultrasound pulse (orange bars) are shown. Control represent release in absence of media as well as ultrasound (**B**) The kinetic profiles of the contents release in the presence of conditioned media of PC-3 (Green spheres) and bEnd-3 (Magenta spheres) cells and in the absence of any media i.e. Control (Blue spheres) are shown. The red line shows the fitted curve using a single exponential rate equation.

Conclusion

We have demonstrated that echogenic liposomes can be prepared incorporating a substrate lipopeptide for MMP-9 in the lipid bilayer. The liposomes retain echogenicity after encapsulation of a hydrophilic dye and can be imaged by ultrasound. The encapsulated contents from the liposomes are released in presence of recombinant as well as cancer cell secreted MMP-9. The contents release can be further increased by the application of diagnostic frequency ultrasound pulses. This study demonstrates that diagnostic frequency ultrasound can be used simultaneously with enzymes as an additional method to trigger contents release from suitably constructed liposomes. We employed continuous excitations for the release study, which deliver more energy than a pulsed excitation used in ultrasound imaging. Future studies are required systematically varying the intensity, frequency and duty cycles of the ultrasound

stimulation to determine the optimum excitation parameters. With further developments, these liposomes have the potential to serve as multimodal carriers for triggered release and simultaneous ultrasound imaging.

CHAPTER II. POLYMER COATED ECHOGENIC LIPID NANOPARTICLES WITH DUAL RELEASE TRIGGERS

Abstract

Although lipid nanoparticles are promising drug delivery vehicles, passive release of encapsulated contents at the target site is often slow. Herein, we report contents release from targeted, polymer coated, echogenic lipid nanoparticles in the cell cytoplasm by redox trigger and simultaneously enhanced by diagnostic frequency ultrasound. The lipid nanoparticles were polymerized on the external leaflet using a disulfide cross-linker. In the presence of cytosolic concentrations of glutathione, the lipid nanoparticles released 76% of encapsulated contents. Plasma concentrations of glutathione failed to release the encapsulated contents. Application of 3 MHz ultrasound for 2 minutes simultaneously with the reducing agent enhanced the release to 96%. Folic acid conjugated, doxorubicin loaded nanoparticles showed enhanced uptake and higher cytotoxicity in cancer cells overexpressing the folate receptor (compared to the control). With further developments, these lipid nanoparticles have the potential to be used as multimodal nanocarriers for simultaneous targeted drug delivery and ultrasound imaging.

Introduction

Targeted drug delivery remains one of the major challenges in current pharmaceutical research. Upon injection, drugs get distributed in the body according to their pharmacokinetic and pharmacodynamics properties, resulting in low therapeutic concentrations at the target site and unwanted side effects. The drug biodistribution can be suitably altered and side effects can be minimized by employing targeted delivery systems. A wide variety of drug carriers and passive and active targeting strategies have been reported in the literature [149]. However, upon reaching the intended site, the rate of drug release from the carriers is often very slow. For example, one of the marketed liposomal doxorubicin formulations (Doxil®) is passively targeted

to the tumors employing the enhanced permeation and retention (EPR) effect [150]. Because of its long circulation time and slow drug release kinetics, several side effects of Doxil® are reported (e.g., hand-foot syndrome, neutropenia, anemia and thrombocytopenia) [151]. Stimuli responsive drug delivery vehicles are highly attractive because of local control over payload release and consequently, reduced systemic toxicity. Both biological/endogenous/local (e.g., enzymes [82, 152], redox [49], pH [153]) and non-biological/exogenous/remote (e.g., temperature [154], light [155], ultrasound [156]) triggers have been used as stimuli to release the payload of these drug carriers. A combination of a biological and an external trigger can give dual levels of control for drug release at the targeted site. Incorporation of concurrent contrast imaging capability renders multimodal characteristics to the drug carrier. However, there are only a few reports of such multimodal nanocarriers responding to multiple triggering stimuli with simultaneous imaging capability [157].

Ultrasound has been extensively used as a tool for different applications using different carriers such as polymers [158], micelles [159], emulsions [160], microcapsules [161], microspheres [162] and liposomes [106]. Most of these reported applications use low frequency ultrasound (LFUS) [95, 98-101, 163-166]. Although application of kHz frequency ultrasound leads to more release compared to MHz frequency, it has very limited clinical applications due to the associated harmful biological effects [101]. There are only a few reports of MHz frequency ultrasound utilized to release drugs from liposomes [112, 156, 167-169] and microbubbles conjugated to liposomes [170].

Acoustically reflective lipid nanoparticles/liposomes (echogenic liposomes or ELIPs) have been developed as stimuli responsive drug carriers [107, 171]. The ELIPs are prepared in presence of a cryoprotectant (e.g., mannitol) that helps in entrapping air pockets within the liposomes and thereby, making them responsive to acoustic excitation. Ever since the first report [172] of acoustically reflective liposomes, questions are raised on the presence and the exact location of entrapped air, especially when the diameters of the vesicles are small (< 1 μm).

Consequently, different terms are currently used for this system, e.g., lipid nanoparticles, lipid dispersions, bubble liposomes [67, 106, 116], acoustically reflective liposomes [173] and echogenic liposomes [174]. Although termed differently, these systems are fundamentally acoustically reflective lipid nanoparticles (ARLINs) as these are made of phospholipids and are in nanometer dimensions. Thus, we will refer to these lipid particles as ARLINs in this manuscript. Although the exact location of the entrapped air in ARLINs remains uncertain [107, 109, 137, 175] their echogenic properties have been well established through comprehensive acoustic experiments [105, 175, 176]. The ARLINS are being studied as novel ultrasound imaging contrast agents for atherosclerotic plaques and cancerous tumors [105]. Extensive ultrasound mediated drug release studies [45, 109, 112] with ARLINs have established their potential as simultaneous drug delivery and ultrasound imaging agents.

The lipid-based drug delivery systems offer excellent biocompatible vehicles for both hydrophilic and lipophilic drugs. However, in the biological system, they get destabilized due to interactions with plasma proteins and biomembranes, resulting in leakage of the encapsulated drugs in the circulation (before reaching the intended site) [177]. This could result in only a small fraction of drug actually reaching the targeted site. Polymerization of the lipid bilayer improves stability but their clinical usage is limited because of poor biocompatibility.

The tripeptide glutathione (L-γ-glutamyl-L-cysteinylglycine, GSH) functions as an important free radical scavenger and protects cells from harmful effects of reactive oxygen species, toxins, drugs and many mutagens. It is one of the most abundant organic reducing agents present in human body. GSH level is elevated in various human cancer tissues (such as breast [178, 179], ovary [178], colon [180], lung [181], bone marrow [182], and larynx [183]) compared to normal tissues. It has been implicated in drug resistance and in tumor growth [184]. The disulfide functional group has gained attention in the preparation of stimuli-responsive drug carriers because of its stability in mildly oxidizing environments (of atmospheric oxygen and blood stream [185]) and it's lability in the presence of reducing agents. Due to the large redox potential

difference between the extracellular matrix (thiol concentration: 10 – 40 μM) and the cytosol of cancer cells (thiol concentration: 0.5 – 10 mM because of the presence of GSH), [186] the reversible disulfide thiol conversion is being widely used for cytosolic drug delivery [60, 187-189].

Herein, we have prepared folate conjugated, disulfide-cross-linked polymer-coated acoustically reflective lipid nanoparticles for cytosolic drug delivery. When exposed to mM concentration of reducing agents, these polymer-coated lipid nanoparticles release their contents and this release is further enhanced by applying diagnostic frequency ultrasound (3 MHz, 0.5 MPa, CW) for 2 minutes. We have also imaged these lipid nanoparticles by using diagnostic frequency ultrasound. With further developments, these polymerized lipid nanocarriers hold promise as a vehicle for ultrasound image guided, targeted cytosolic drug delivery. To the best of our knowledge, there are no reports of using polymer-coated acoustically reflective lipid nanoparticles for simultaneous targeted drug delivery and ultrasound imaging.

Materials and Methods

Preparation and polymerization of ARLINs

The gallate derivative with three propargyl groups coupled to 1-palmitoyl-2-oleoyl-*sn*-glycerol-3-phosphoethanolamine (POPE-G) was synthesized following a published procedure [190]. Stock solution of 1-palmitoyl-2-oleoyl-*sn*-glycero-3-phosphocholine (POPC, Avanti Polar Lipids) was prepared (1 mg/mL) by dissolving the lipid powder in chloroform and methanol (9:1) and stored in freezer (-20°C). Solutions of POPC (3 mg), POPE-G (3.9 mg) and 1,2-dipalmitoyl-*sn*-glycero-3-phosphoethanolamine-N-(lissamine rhodamine B sulfonyl) ammonium salt (DPPE-LR, 0.045 mg) were mixed in the molar ratio of 50:49:1 respectively in a 10 mL round bottom flask. The mixture was swirled to ensure proper mixing of components. Solvent was evaporated using a rotary evaporator and the flask was placed under vacuum overnight to remove any residual solvent traces. Next day, the dried film was hydrated for 3 h with 3 mL of 10 μM calcein dissolved in 10 mM HEPES buffer (pH adjusted to 7.4) and 3 mL of

0.64 M mannitol (final concentration 0.32 M). The lipid dispersion was then bath sonicated for 10 minutes with constant swirling and exposed to 3 freeze (-70°C) and thaw (23°C) cycles to enhance calcein encapsulation. Sequential extrusion was performed using a mini-extruder (Avanti Polar Lipids) using 800 nm, 200 nm polycarbonate filters (Nuclepore, Whatman) in succession. For cancer cells uptake studies, ARLINs were prepared using the same protocol except that the concentration of calcein used was 3 mM. Two different batches were prepared, one with and other without (1 mole%, 0.1 mg) of 1,2-distearoyl-*sn*-glycero-3-phosphoethanolamine-N-[folate(polyethylene glycol)-2000] (ammonium salt).

For polymerization, the reported procedure [190] was modified in order to make it suitable for our experiments. To the above 6 mL solution, the cross linker CL, 150 μL of 0.04 M aqueous solution), Cu-complex (150 μL of 0.053 M aqueous solution prepared by mixing 3 mL of $CuCl_2$, 71.7 mg, 0.53 mmol) solution, 3 mL of PMDETA solution (442 μL, 2.1 mmol)) and sodium ascorbate (150 μL of 27 mg/mL solution, 1.4 μmol) were added together. Mixture was divided into 6 closed vials and stirred slowly at room temperature for 24 h. After 24 h, the mixture was passed through a Sephadex-G100 gel (GE healthcare) filtration column in order to remove unencapsulated dye and other compounds from the ARLINs. Mannitol was added to the ARLINs solution to 0.32 M concentration, the solution was frozen and subsequently, the ARLINs were placed in a lyophilizer. The freeze dried powder was stored in a refrigerator and reconstituted just before use.

Preparation of doxorubicin loaded ARLINs

To encapsulate doxorubicin into the lipid nanoparticles, the reported pH gradient loading method was employed [191] with some modifications. Briefly, the lipid film was hydrated with 400 mM citrate buffer (pH 4.0) and after bath sonication and freeze thaw cycles, the external pH of buffer increased to 7.4 by addition of dilute sodium hydroxide. To this lipid dispersion, 0.2 mg of doxorubicin/mg of lipid was added and the dispersion was stirred for 30 minutes at room temperature. The lipid dispersion was then passed through a Sephadex-G100

gel filtration column to remove unencapsulated doxorubicin. Encapsulation efficiency was determined by recording the absorbance of doxorubicin at 475 nm before and after gel filtration. These lipid nanoparticles were then polymerized using the same procedure described earlier. After polymerization, the doxorubicin content was determined by plotting the absorbance onto the calibration curve established at 475 nm.

Measurement of size distribution, zeta potential and mobility

The size distribution, zeta potential and mobility of the ARLINs were measured by Malvern Zetasizer Nano-ZS90 using dynamic light scattering (DLS) method before and after lyophilization. Polystyrene latex disposable cuvettes (DTS 0012 for Size and DTS 1061 for zeta potential and mobility) were used and scattering measurement was performed at 90° angle. Each sample (0.1 mg/mL in 10 mM HEPES buffer pH 7.4) was equilibrated for 60 seconds and 10 readings were taken for each sample of ARLINs at room temperature. All the batches were tested and each sample was tested 5 times to ensure reproducibility and to calculate the standard deviation.

Transmission electron microscopy

The samples were observed using a JEOL JEM-2100-LaB_6 transmission electron microscope operating at 200 kV at low magnifications and with the beam spread, which is not converged, to reduce the amount of electron beam interaction per unit area and hence beam damage to sample if it were to occur. Lyophilized ARLINs sample reconstituted in 10 mM HEPES buffer pH 7.4 to obtain 1 mg/mL concentration and dropped onto 300 mesh Formvar coated copper grids previously coated with 0.01% poly-L-lysine and allowed to stand for a minute before wicking off with filter paper. After air drying for 2 minutes, the sample was negatively stained with 1% phosphotungstic acid for 1.5 minutes and subsequently wicked off with filter paper and allowed to dry before viewing.

Atomic force microscopy

The sample (freshly reconstituted in 10 mM HEPES buffer pH 7.4) was dropped onto a mica sheet and air dried for performing the AFM experiments. For performing AFM imaging, a Multimode™ atomic force microscope with Nanoscope III a controller and J type piezo scanner from Veeco Metrology Group, Santa Barbara, CA was used. Antimony (n) doped Si tip was used for obtaining images in Tapping Mode™ under laboratory conditions. Images were taken before and after treatment with 5 mM GSH.

Measurement of echogenicity of ARLINs

Echogenicity of the ARLINs was measured *in vitro* using the acoustic setup to measure scattered response discussed in our previous publications [175] (Figure 2.1A). The setup consisted of two single element focused immersion transducers (Panametrics-NDT) confocally positioned at right angles by inserting them through holes drilled on the adjacent walls of a rectangular polycarbonate chamber that held our sample volume. Each transducer had an individual diameter of 1.27 cm with a focal length of 3 cm. The transmitting and receiving transducers had nominal central frequencies of 3.87 MHz and 5.54 MHz and -6 dB bandwidths of 86.4% and 85% respectively. A programmable function generator (Model 3325A; Agilent Santa Clara, CA) was used to generate a 32 cycle sinusoidal wave at 3.5 MHz frequency which was then amplified using a power amplifier (Model A-300; ENI, Rochester, NY) before being fed to the transmitting transducer. The output of the transducer was calibrated using a needle hydrophone (PZT-Z44-0400, Onda Corporation, CA). All scattering experiments were performed at an acoustic pressure of 500 kPa. The scattered signal was received through a pulser/receiver (Model 5800; Panametrics-NDT, Waltham, MA) with a 20 dB gain. The received signal was observed in real-time utilizing a digital oscilloscope (Model TDS2012; Tektronix, Beaverton, OR). Scattered voltage-time responses were saved on a desktop computer for post-experimental analysis using LabView (Version 6.0.3; National Instruments, Austin, TX) connected to the oscilloscope via a GPIB IEEE 488 cable and GPIB card. The voltage-time

responses were analyzed using a Matlab® code (MathWorks, Natick, MA) by taking Fast Fourier Transforms of 50 oscilloscope acquisitions which were averaged and converted to dB scale with unit reference before extracting the responses at desired frequencies (fundamental, second and sub-harmonics). Each experiment was repeated five times and the average responses with corresponding standard deviation errors were plotted.

Phosphate buffered saline (PBS) solution mixed with 0.5% by weight of bovine serum albumin (BSA) were prepared and kept refrigerated for a minimum of 48 hours before using them to reconstitute the freeze dried ARLINs. Correct amounts of ARLINs were weighed and dissolved in 100 mL of PBS-BSA solution and poured into the sample chamber to carry out the scattering measurements. At the lipid concentration 5 μg/mL, it was sufficiently diluted so that multiple scattering could be safely neglected.

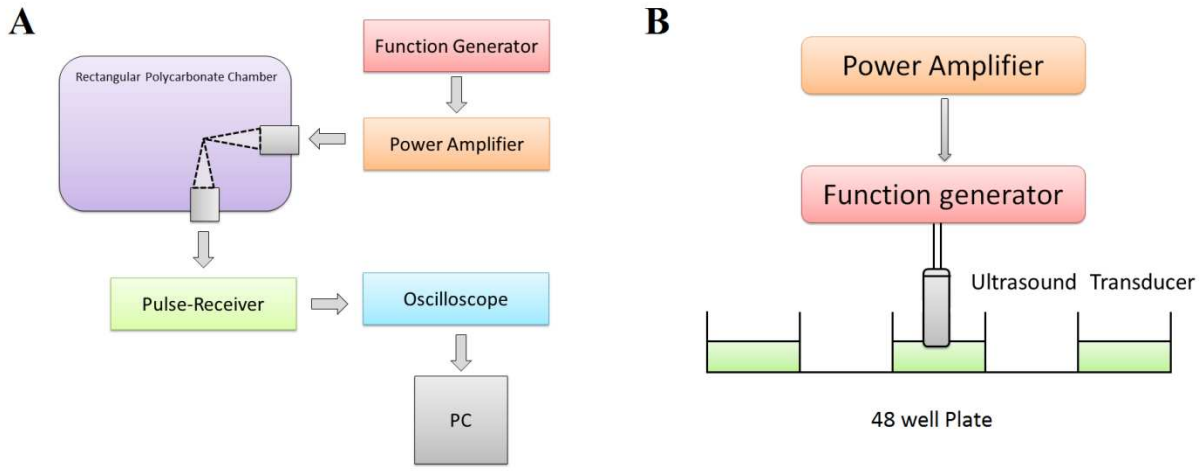

Figure 2.1. (**A**) Schematic of the experimental setup for *in vitro* measurement of scattering. (**B**) Schematic of the *in vitro* experimental setup for ultrasound mediated release studies.

Ultrasonic imaging of ARLINs

Terason t3200™ Diagnostic Ultrasound (MedCorp LLC., Tampa, FL) was used to image reconstituted ARLINs. A layer of Aquasonic® 100 (Parker Laboratories, Inc., Fairfield, New Jersey) ultrasound gel was applied to the 15L4 Linear (4.0-15.0 MHz) (MedCorp LLC., Tampa, FL) ultrasound transducer sound plate. The transducer with gel was placed over the parafilm

covering the wells containing the ARLINs in a 96-well plate. The ultrasound scan properties of the ARLINs were set at 0.7 Mechanical Index (MI), 0.6 Thermal Index (TIS), Omni Beam activated, level C Image Map, level 3 Persistence, high (H) frequency, level 3 TeraVision, level 51 2D Gain, level 60 Dynamic Range (DR), 3 cm scan depth, and 22 Hz frame rate. The images were labeled and saved.

Ultrasound mediated release studies

For ultrasound mediated release studies with ARLINs, we used a setup similar to the one described in our previous publication [175] (Figure 2.1B). A single element unfocused immersion transducer (Model IP301HP; Valpey Fisher Corporation, Hopkinton, MA) was used to excite the ARLINs suspension. Frequency (3 MHz) continuous sinusoidal waves utilized for the release studies were generated using the waveform generator (Model 33250A; Agilent, Santa Clara, CA) and amplified using a power amplifier (Model A-150; ENI, Rochester, NY) before being input to the transducer. The transducer output was calibrated using a needle hydrophone (PZT-Z44-0400, Onda Corporation, CA). All of our release studies with ultrasonic excitation were carried out at a pressure of 0.5 MPa with a 2 minute exposure time. The release studies were performed in 48 well plates with a 500 μL sample volume and a lipid concentration of 0.02 mg/mL. The entire plate was placed on constant temperature water bath to minimize temperature fluctuations and homogeneity of the sample was ensured by placing small magnetic stirrers within each well during the course of the experiment. Although this setup allows reflection of ultrasound wave from the air-water interface thereby giving rise to standing wave patterns [121, 192] the setup was found adequate for the present study to demonstrate the validity of the proof of concept. Also as mentioned in our previous publication we observed negligible (less than 1%) energy transfer to neighboring wells during stimulation indicating almost no inter-well interference. All experiments were performed three times and in triplicates each time to ensure reproducibility of results and calculate standard deviations.

Redox triggered release studies

Release studies were carried out using a fluorescence microplate multidetection instrument (Spectramax-M5, Molecular devices) using calcein and $CoCl_2$ quenching method. Since sub-self-quenching concentration (10 μM) of calcein was used, we could quench external fluorescence by adding $CoCl_2$. $CoCl_2$ quenches fluorescence of unencapsulated calcein outside the ARLINs, so the fluorescence signal observed is from the encapsulated dye only. For the release studies, 0.02 mg/mL ARLINs were taken into 96 well plate and external calcein was quenched with 10 mM $CoCl_2$. Dithiothreotol (DTT), Glutathione (GSH) and Cysteine (CYS) were added in specific concentration to determine the release of calcein. Fluorescence was monitored at 515 nm (excitation 495 nm) for an hour and subsequently, the ARLINs were disrupted using triton-X100 to record background fluorescence (if any). Initial fluorescence intensity was treated as 100% and percent decrease in fluorescence intensity was treated as percent release accordingly.

$$Percent\ Release = \frac{Intial\ Fluorescence - Final\ Fluorescence}{Intial\ Fluorescence} \times 100$$

Ultrasound enhanced thiol triggered release

For these experiments, a 48 well plate was used, in which 0.02 mg/mL of freeze dried ARLINs were suspended in 10 mM HEPES buffer (pH 7.4). Two different set ups were employed to study the combined effects of reducing agents and ultrasound on release. In the first set up, ARLINs were incubated with 5 mM reducing agent and after 60 minutes, the solution was exposed to ultrasound (3 MHz, 0.53 MPa) for 2 minutes. In the second set up, we applied ultrasound immediately after the addition of the reducing agent. Control samples were kept and release was checked for each experiment. Care was taken to keep two sample wells as far as possible to minimize the effect of ultrasound in other wells.

Cell culture and ARLINs uptake studies

For cancer cell uptake studies, MCF-7 (human breast adenocarcinoma) and HeLa (human cervical carcinoma) were cultured in clear (without added Phenol red) RPMI media supplemented with 10 % fetal bovine serum and 1% antibiotics. The culture flasks were incubated at 37 °C in humidified atmosphere containing 5% CO_2. When cells became 90% confluent, they were suspended using trypsin-versene. The suspended cells then cultured onto sterile 6 well plates until 90% confluent.

For uptake studies with calcein encapsulation, the media was removed and MCF-7 cells were gently washed with HBBS (Hank's Balanced Salt Solution) 2-3 times to completely remove any media. Subsequently, the ARLINs suspended in media (0.2 mg/mL) were incubated with the cells for 30 minutes. After specific time intervals, ARLINs solution was removed from wells and cells were again rinsed with HBSS to remove ARLINs on the surface of cells. Hoechst-33342 stain (1 mg/mL, 1:1000 dilution) was used to stain nuclei of cells. Finally, fresh media was added to cells and were observed under fluorescent microscope at different time points (10, 20, 30 min.) A similar procedure was followed for the uptake studies with doxorubicin loaded ARLINs (targeted, non-targeted) using the HeLa cells.

Percent uptake of ARLINs by HeLa cells was calculated by measuring fluorescence of MCF-7 cells lysed with 5% triton. For this cells were seeded onto 96 well plate and once confluent, incubated with ARLINS loaded with 50 mM calcein for 6 h at two different concentrations - 40 μg/mL and 20 μg/mL. After incubation, cells were washed with HBSS thrice and lysed using 5% triton-X100. Fluorescence was measured (Ex: 485 nm Em: 515 nm) and then compared with fluorescence of respective ARLINs solution lysed using 5% triton. Percent uptake was calculated for Folate targeted and non-targeted ARLINs for both concentrations.

Cell viability assay

The cytotoxicity of targeted and non-targeted ARLINs was determined by AlamarBlue® assay, measuring the fluorescence of resorufin (red) formed by reduction of resazurin (blue) in

the cytosol of viable cells (metabolically active) [193]. Briefly, HeLa cells were transferred to flat, clear bottomed 96-well tissue culture plates (Corning) at a density of 2 x10^4 per well 24 hours prior to the assay (or 70-80% confluency). The culture medium in each well was carefully removed and replaced with doxorubicin loaded folate conjugated ARLINs, doxorubicin loaded non-targeted ARLINS and doxorubicin solution mixed with media. After incubation at 37 °C for 6 h, 12 h and 24 h, the cells were washed three times with sterile HBSS and incubated in fresh culture medium. At this point, 20 μL of AlamarBlue® was added to each well and the fluorescence readings (Ex: 560 nm Em: 590 nm) were taken after 3 h of incubation at 37°C. Average readings were then compared with control and plotted on the graph.

Results and Discussion

The gallate-derived polymerizable lipid (POPE-G) and the diazide cross-linker (CL) were synthesized in our laboratory. The lissamine rhodamine lipid (DPPE-LR) and the DSPE-PEG-2000-Folate are commercially available (Figure 2.2). We prepared the ARLINs incorporating 50 mol% POPC, 49 mol% POPE-G and 1% DPPE-LR in 10 mM HEPES buffer (pH 7.4). Nanoparticles were polymerized in the presence of added diazide CL, $CuSO_4$, ascorbic acid and subsequently freeze dried in presence of a weak cryoprotectant mannitol. Based on a literature report, we anticipate that the disulfide cross-links were formed only on the outside surface of the lipid nanoparticles[190] (Figure 2.2). Being a weak cryoprotectant, mannitol does not provide effective protection during lyophilization which leads to defects in the polymer coated lipid shell. It has been hypothesized that these defects are responsible for the entrapment of air within the lipid nanoparticles during the rehydration/reconstitution stage [105, 132]. This entrapped air (which gives rise to mismatch of acoustic impedance) is critical for the echogenicity of these lipid structures. We have recently reported that a finite amount of mannitol is necessary during lyophilization for making them echogenic [175]. We also observed that these lipid nanoparticles were echogenic only when lyophilized and reconstituted; prior to freeze drying these were not echogenic i.e., did not respond to ultrasonic excitation. Hence, the polymerized ARLINs studied

here were prepared using the freeze-drying technique mentioned above and tested for echogenicity.

We determined the size distribution of ARLINs before and after lyophilization using a dynamic light scattering (DLS) instrument. We observed that the number average diameter after lyophilization increased (117 ± 11 nm, Figure 1.3A) compared to the average diameter before lyophilization (78 ± 14 nm, Figure 1.3B). Polydispersity index was also found to increase from 0.37 ± 0.04 to 0.71 ± 0.05, indicating a more heterogeneous distribution of sizes in the lyophilized sample. This was confirmed in subsequent transmission electron microscopic images obtained for lyophilized ARLINs (Figure 1.4B). Note that, due to the modified preparation protocol, the ARLINs indeed entrapped air as verified by TEM images (Figure 1.4A) and gave rise to a more polydispersed suspension with a larger average diameter. We also studied the effect of addition of GSH on the morphology and size distribution of ARLINs employing an atomic force microscope (AFM). We observed that, before treatment ARLINs look spherical with average size about 100-200 nm (Figure 1.5A); but upon addition of 5 mM GSH, the particles fuse with each other and their size distribution becomes more heterogeneous (Figure 1.5B).

We also characterized these particles for their physical properties. We determined zeta potential and mobility of empty and doxorubicin loaded ARLINs using dynamic light scattering method on Zetasizer instrument (Table 2.1). During gel filtration with Sephadex column, lipid particles can get adsorbed and thus their stability and physical characteristics can get changed. To check this, we studied these particles before and after passing through Sephadex column for their size, zeta potential, mobility and stability. We observed that gel filtration did not the stability of ARLINs as they leaked less than 5% when incubated for an hour. We also noticed that gel filtration also don't affect the physical characteristics of particles like size, zeta potential and mobility (Table 2.1).

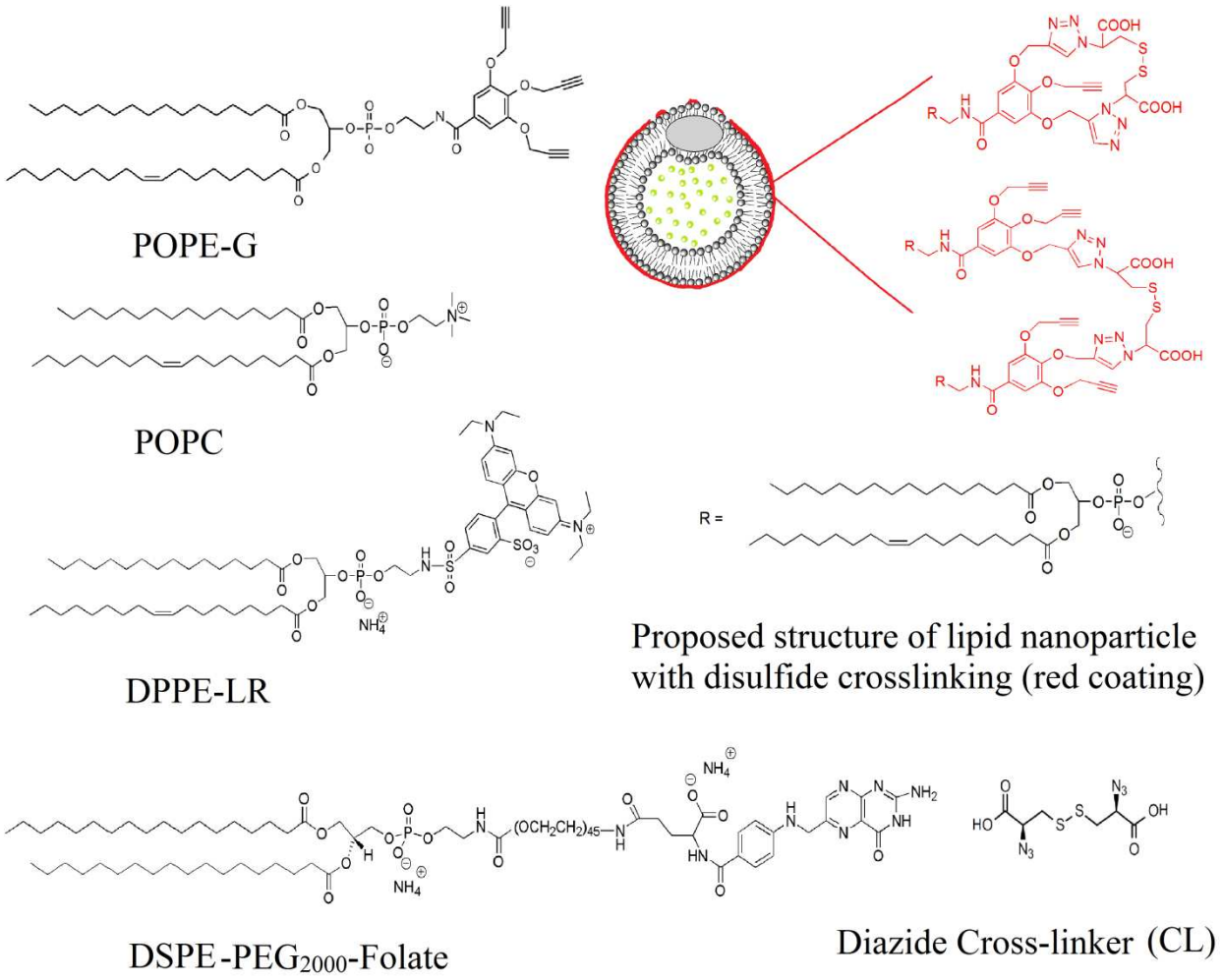

Figure 2.2. Lipids used in preparation of lipid nanoparticles and proposed structure of lipid nanoparticle with disulfide polymer coating (red coating around nanoparticle) after polymerization by diazide cross-linker CL.

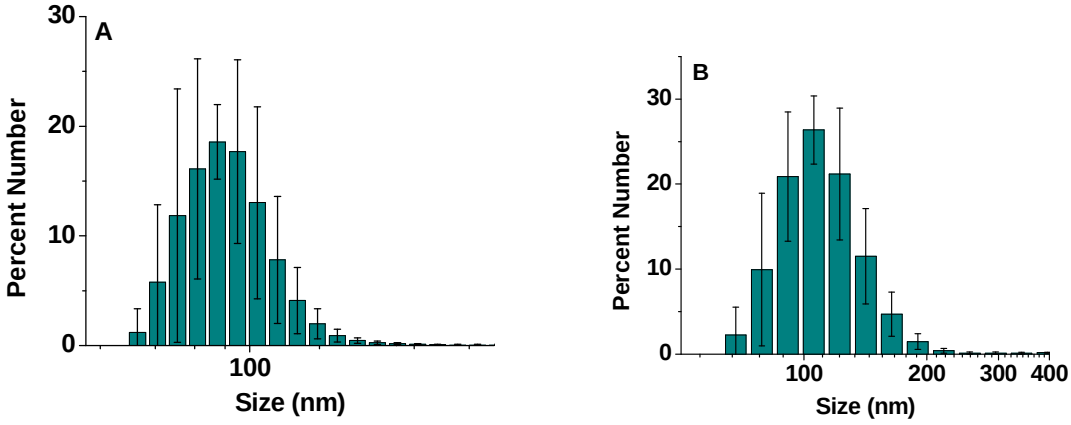

Figure 2.3. Size distribution analysis of nanoparticles by dynamic light scattering method. (**A**) Size distribution by number before lyophilization (**B**) Size distribution by number after lyophilization. (n=5)

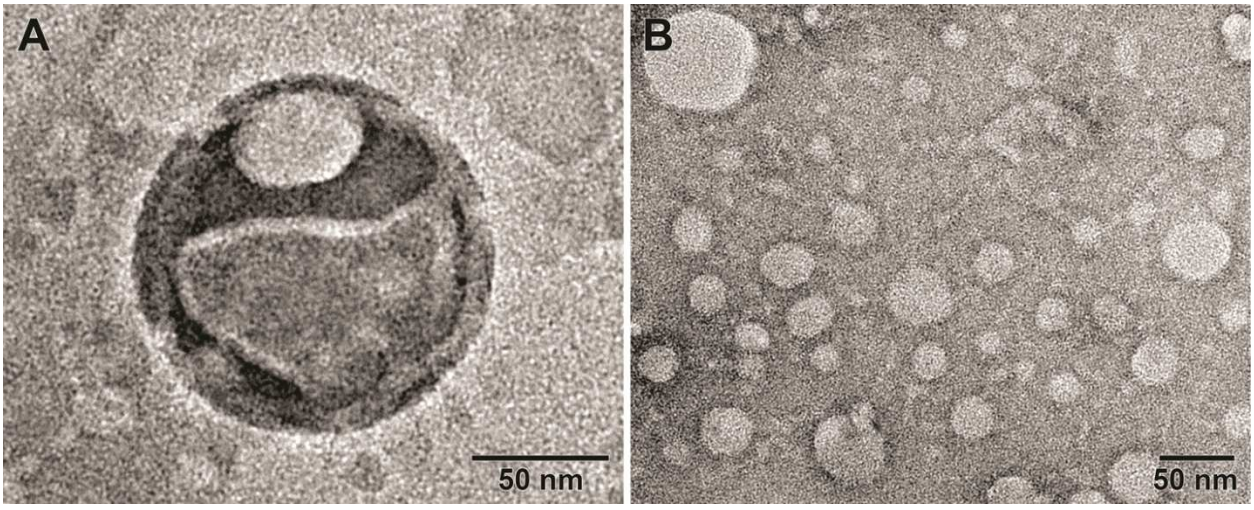

Figure 2.4. Transmission Electron Microscopic images of negatively stained ARLINs with 1% phosphotungstic acid, using a JEOL JEM-2100-LaB_6 transmission electron microscope operating at 200 kV. The beam is spread and not converged, to reduce the amount of electron beam interaction per unit area and to minimize beam damage to sample. (**A**) ARLINs after lyophilization showing presence of air bubble entrapped in the shell. (**B**) Heterogeneous size distribution of ARLINs after lyophilization.

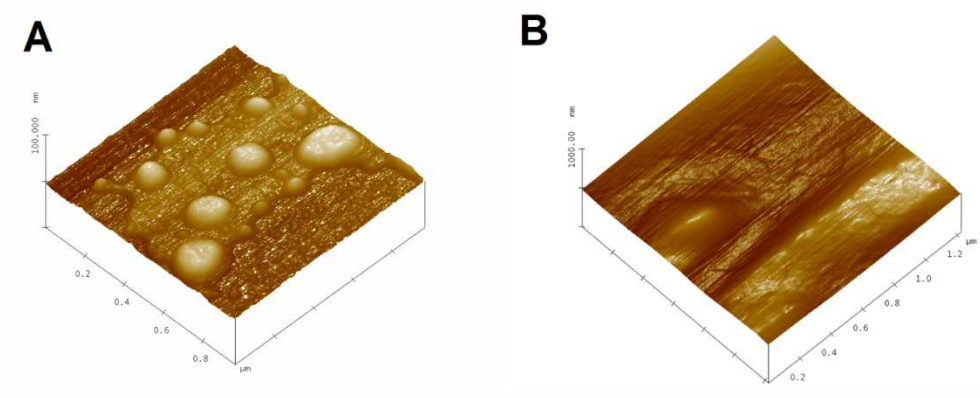

Figure 2.5. MultiMode™ atomic force microscopic images of ARLINs before (**A**) and after (**B**) treatment with 5 mM GSH.

Table 2.1. Zeta potential and mobility of empty and doxorubicin loaded ARLINs determined using dynamic light scattering method (Zetasizer).

N=5	Zeta Potential (mV)		Mobility (µmcm/Vs)	
	Empty ARLINs	Dox-loaded ARLINs	Empty ARLINs	Dox-loaded ARLINs
Avg	-16.28	-17.8	-1.27	-1.39
SD	0.38	1.31	0.03	0.10

Table 2.2: Effect of gel filtration on physical properties of ARLINs determined using dynamic light scattering method (Zetasizer).

N=5	Size (nm)		Zeta (mV)		Mobility (µmcm/Vs)	
	Before*	After*	Before*	After*	Before*	After*
Avg	147	158.3	-18.02	-17.8	-1.4	-1.54
SD	12.7	8.1	0.55	1.3	0.04	0.07

Similar to other literature reports [172, 194], we observed by TEM the presence of air bubble either inside the aqueous interior or in the shell of the ARLINs (Figure 2..4A). The ARLINs prepared following freeze-drying/reconstitution in presence of mannitol also showed significant echogenicity, incontrovertibly indicating air entrapment. Figure 2.6 shows the scattered response from a suspension of ARLINs under ultrasonic excitation for two different frequency components viz. fundamental (at frequency of excitation 3.5 MHz), second harmonic (at twice the excitation frequency 7 MHz). The control data indicates the response without any ARLINs in suspension. There was an enhancement in response for both components which demonstrates the echogenic nature of the ARLINs. The fundamental response shows around 20 dB enhancement for the lipid concentration of 5 µg/mL at an acoustic pressure of 500 kPa. The nonlinear response from the ARLINs is much weaker with only 8 dB enhancement for the second harmonic component. Note that normal ELIPs[175] and our previously-reported lipopeptide conjugated ELIPs generated larger (33 and 25 dB respectively) enhancement of the

fundamental response at 10 μg/mL (double the concentration accounts for 3 dB discrepancy) lipid concentration and 500 kPa. The weaker response here may be attributed to the change in the lipid composition and increased strength of lipid shell due to polymerization. Note that as reported previously [169, 175] with other ELIPs, scattered responses from lipopeptide incorporated ELIPs do not show any distinct peak at the subharmonic frequency (at half the excitation frequency or 1.75 MHz). Echogenicity was also confirmed by ultrasound imaging with a Terason t3200 ultrasonic medical imaging system using a 4–15 MHz transducer. Reconstituted ARLINs reflected ultrasound indicating the presence of entrapped air inside (Figure 1.7B) whereas control samples (no ARLINs) were dark due to no reflection (Figure 1.7A).

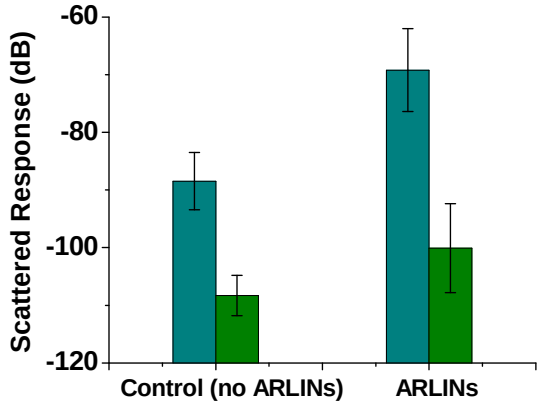

Figure 2.6. *In vitro* ultrasound scattering: fundamental (dark cyan) and second harmonic (green) responses from ARLINs. (n=5)

We encapsulated the dye calcein in the aqueous interior of the ARLINs and added cobalt (II) chloride ($CoCl_2$) in the outside buffer. Most of the triggered release reports from drug carriers containing disulfide bonds employ either dithiothreitol (DTT [195]) or cysteine (CYS [196]) as the reducing agent. Hence, we decided to perform the release studies using DTT, CYS as well as the physiologically more relevant reducing agent glutathione (GSH). Upon addition of the reducing agent, as the encapsulated calcein is released, its emission intensity is quenched by the $CoCl_2$ in the external media.

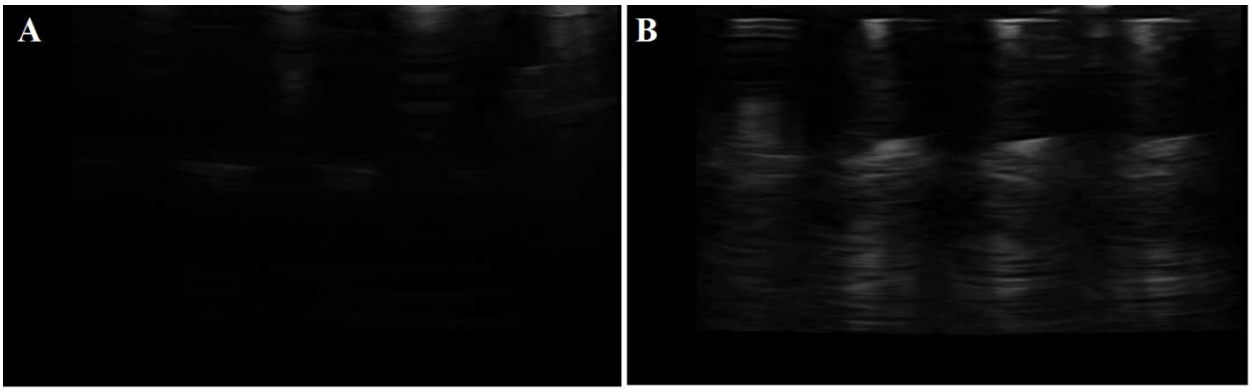

Figure 2.7. Ultrasound imaging of ARLINs reconstituted in 10 mM HEPES buffer pH 7.4, using a Terason t3200 ultrasonic medical imaging system using a 12–15 MHz transducer. (**A**) Control- 10 mM HEPES buffer pH 7.4 (**B**) ARLINs sample- 0.1 mg/mL.

We studied the release of encapsulated calcein from the ARLINs using 10 μM to 10 mM concentrations of reducing agents. The range was selected based on the concentrations of reducing agents in the extracellular matrix/blood plasma (10 μM) and cancer cell cytosol (10 mM). The disulfide bonds on the external surface of the ARLINs were cleaved (disulfide to thiol exchange) by the added reducing agents. This process creates sufficient disturbance to make nanoparticles unstable and leaky. We observed that the percent release was directly proportional to the concentration of reducing agents (Figure 1.8A). The maximum release of around 90% was observed with 10 mM concentration of either GSH or DTT. DTT has a very low redox potential (E_o = – 0.332 V at pH 7.0) and it rapidly reduces the disulfide bonds [197] as compared to glutathione (E_o = + 0.062 V) and cysteine (E_o = + 0.025 V) [198, 199]. In fact, DTT reduces the bonds so rapidly that we were unable to obtain a reliable release profile from the ARLINs. However, the release profiles employing GSH and CYS were slow enough to be easily analyzed (Figure 1.9). Given the relative concentrations of reducible disulfide bonds and reducing agents, we expected the overall kinetic profile to be single exponential in nature. The latter was found to be the case for the release of the encapsulated content from photocleavable as well as enzyme (MMP-9) cleavable liposomes [152], albeit in both these cases the single exponential phases proceeded with a finite lag phase. No lag phase was noticeable during the

GSH and CYS dependent cleavage of these ARLINs. However, in attempting to analyze the data of Figure 1.9, we realized that the release profile did not confirm to the single exponential rate equation. The data could only be fitted by the single exponential plus steady-state equation in the following format (Equation 1).

$$\text{Release} = F_1(1-e^{-k_1 t}) + k_2 t + offset \quad \text{..... (Equation 1)}$$

Where k_1 and k_2 are the rate constants of exponential and steady-state phases. The solid lines in Figure 1.9 are the best fitted curves of the data. We determined the magnitudes of k_1 to be 0.21 $\pm$ 0.03 min^{-1} (for CYS mediated release) and 0.23 $\pm$ 0.02 min^{-1} (for GSH mediated release); the values for k_2 being equal to 0.18 + 0.01 (for CYS mediated release) and 0.25 $\pm$ 0.01 min^{-1} (for GSH mediated release).

The question arose as to why, unlike other formulations [82], the thiol mediated cleavage and content release from disulfide linked ARLINs exhibited the single exponential (burst) phase followed by the steady-state phase. In contemplating the mechanistic origin of such profile (Figure 1.9), we realized that due to initial high concentration of GSH and CYS, they would rapidly reduce a major fraction of the disulfide bonds of the ARLINs. Subsequently, the reducing agent (e.g., CYS or GSH) as well as the reduced thiol groups on the ARLINs surface would trigger the sulfhydryl-disulfide exchange reaction in a steady-state fashion. Such situation is unlikely to prevail either with photo- or MMP-9 cleavable drug carriers, and thus the release profiles are devoid of the steady-state phase. We are currently assessing the molecular mechanism underlying the release of contents under different experimental conditions to validate or refute our working hypothesis, and we will report our findings subsequently.
We observed minimal leakage (less than 5% over 12 hours at room temperature in pH 7.4 buffer) from the ARLINs in the absence of any added reducing agent (Figure 1.8A). With 10 μM concentration of the reducing agents, the release was less than 5% – indicating the relative stability of ARLINs in extracellular environments/blood stream. This is likely due to the

polymerized external leaflet of the ARLINs. We note that the extracellular environment of tumors is more reducing compared normal cells (because of cell deaths, necrosis) and this can lead to release of some of the encapsulated contents from the ARLINs.

DTT is a chelating agent and forms complexes with many transition metals ions[176]. We added 10 mM $CoCl_2$ in the buffer to quench the fluorescence emission from the calcein released from the ARLINs. It is likely that a considerable amount of DTT is consumed in forming complexes with the added Co^{2+} ions. This will likely contribute to lesser release from the ARLINs in presence of 5 mM DTT as compared to 5 mM GSH. We also observed and confirmed that that DTT results in the highest amount of complex formation and precipitation followed by CYS. The formation of colored complex and precipitate were minimal with GSH.

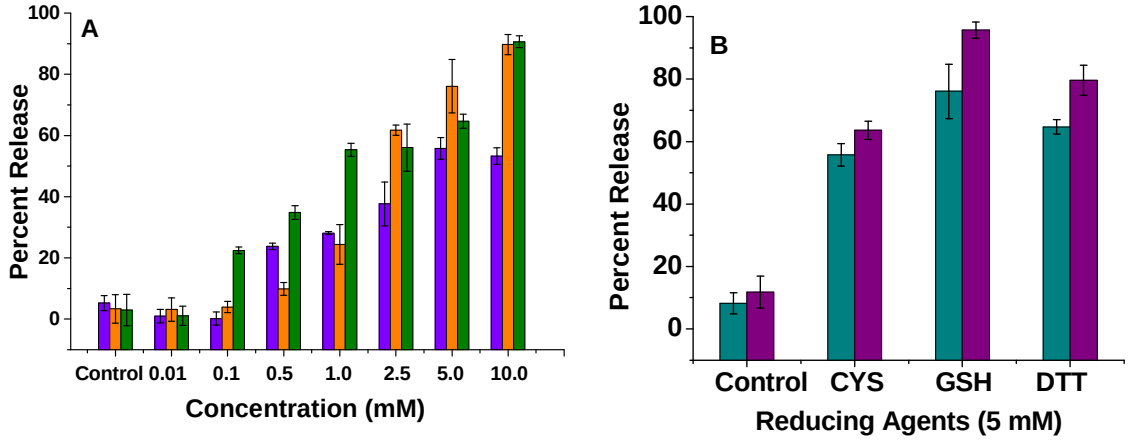

Figure 2.8. (**A**) Thiol triggered release of calcein from polymer coated ARLINs with increasing concentration of reducing agents CYS (violet), GSH (orange) and DTT (green). (**B**) Ultrasound enhancement of redox triggered release from ARLINs. The dark cyan columns indicate release with reducing agents at 5 mM concentration and violet columns indicate release with simultaneous application of two triggers - reducing agent (5 mM) and ultrasound (CW excitation at 3 MHz, 0.5 MPa for 2 minutes). (n=5)

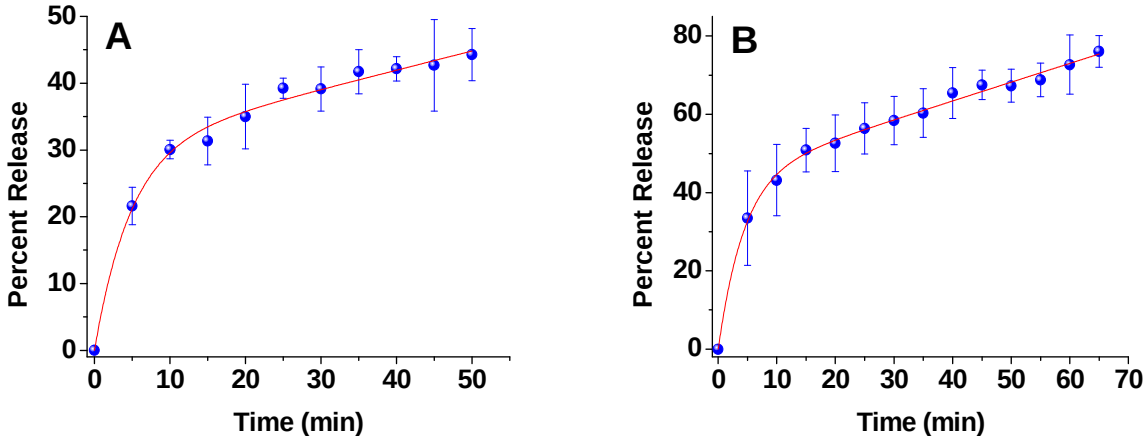

Figure 2.9. Release profiles of calcein from ARLINs in presence of 5 mM CYS (**A**) 5 mM GSH (**B**). The red lines indicate the fitted curves for the observed data using the equation 1. (n=3)

It was evident from the *in vitro* scattering experiments, TEM images and ultrasound imaging, that these lipid nanoparticles were echogenic and contains entrapped air inside. After ensuring release with reducing agents, we proceeded to determine whether the ARLINs release calcein in response to an ultrasound trigger. In this endeavor, reconstituted ARLINs along with $CoCl_2$ were taken in the wells of a 48 well plate and excited with continuous wave ultrasound. We observed that in absence of any reducing agents, ultrasound alone failed to release calcein from ARLINs. Less than 5% release was observed in both control and test samples after application of continuous wave ultrasonic excitation (3 MHz frequency, 0.5 MPa acoustic pressure for 2 minutes). Increasing the intensity of ultrasound to higher values had no significant effect on the results. Subsequently, we added 5 mM reducing agents to ARLINs and applied ultrasound concurrently to observe the combined effects of both triggers on the release. With simultaneous application of both triggers, 8-20% enhancement in release was observed as compared to release with reducing agents alone. ARLINs treated with GSH showed the highest additional enhancement (20%) with ultrasound trigger whereas CYS treated sample showed only 8% additional ultrasound induced enhancement under the same excitation conditions. We

note that GSH is more effective in reducing the disulfide groups on ARLIN surface and release more contents compared to CYS (Figure 2.9).

In another set of experiments, ultrasonic excitation was initiated an hour after incubating ARLINs with the reducing agents (5 mM). No significant change in calcein release was observed. We hypothesize that upon incubating ARLINs with reducing agents for an hour, the lipid shell of nanoparticle becomes leaky, allowing the entrapped air to escape and thereby, diminishing their acoustic reflectivity.

These observations suggest that polymerization on the external surface makes lipid shell stronger and less responsive to disturbance created by ultrasound excitation of air entrapped inside. Hence, ultrasound alone fails to create a sufficient disturbance or defects in the polymer-coated lipid shell in order to release calcein from its aqueous core. But once reducing agents are added, the effects of polymerization are reversed, making ARLINs sensitive to ultrasound and release the contents. This further corroborates our hypothesis that cross-linking/polymerization using reversible disulfide bonds leads to stronger and more stable ARLINs without compromising release efficacy at targeted sites (reducing environment of cell cytosol). This hypothesis was also supported by the release data obtained upon application of low frequency ultrasound (CW, 22.5 kHz, 4 W, usually used to disrupt cells) to non-polymerized and polymerized ARLINS (Figure 2.10). The obtained results clearly show that at each time interval, the release was less with polymer coated ARLINs compared to non-polymerized ARLINs.

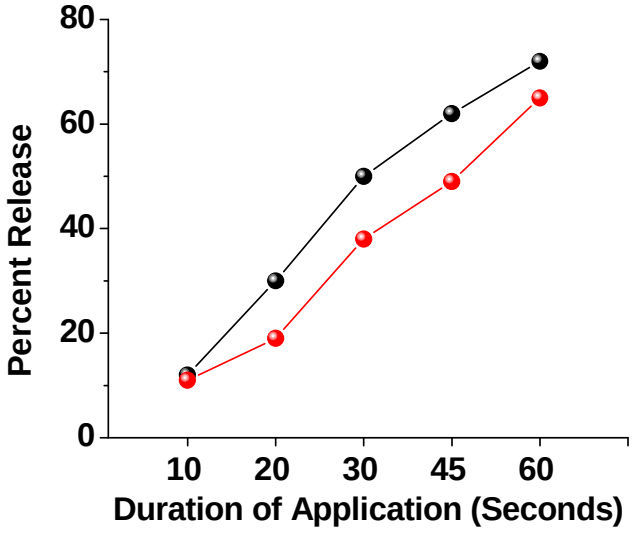

Figure 2.10. Low frequency ultrasound (CW, 22.5 kHz, 4W) triggered release from ARLINs prior to polymerization (black spheres) and after polymerization (red spheres).

Subsequently, we proceeded to demonstrate the effectiveness of our ARLINs in releasing the encapsulated contents in the cytosol of cancer cells. In this endeavor, we used folic acid as the targeting group for the ARLINs. Folic acid is a vitamin B family member which plays an important role in cell survival by participating in the biosynthesis of nucleic acids and amino acids [200]. Due to the faster growth rate, cancer cells need more folic acid compared to normal cells. As a result, cancer cells express higher number of folic acid receptors on the surface compared to normal cells. Folate receptors actively internalize bound folic acid or folate conjugated entities via receptor mediated endocytosis [201, 202]. Folate conjugation to anti-cancer drugs or delivery vehicles improves drug selectivity for cancer cells overexpressing the folate receptor on the surface [75, 203-207].

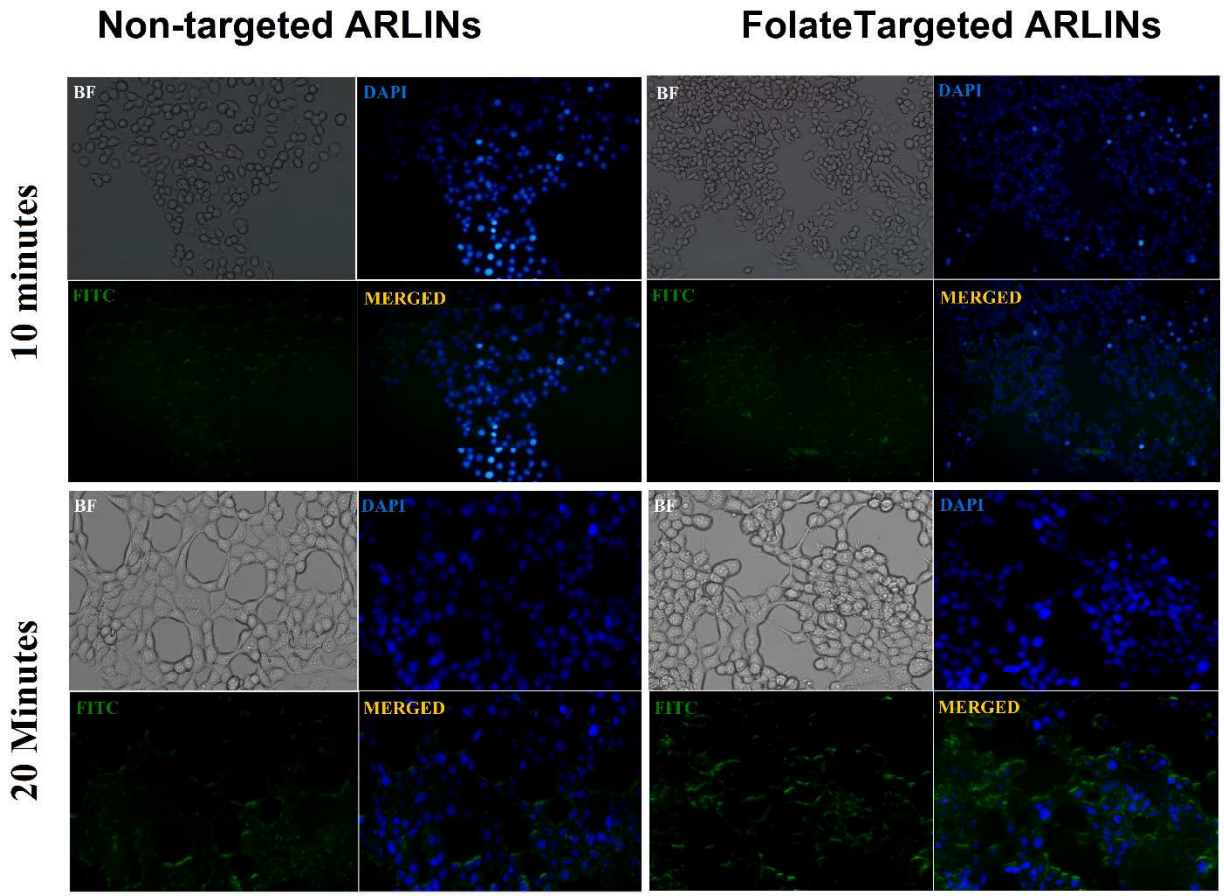

Figure 2.11. Fluorescence microscopic images of ARLINs uptake by folate receptor overexpressing MCF-7 cancer cell line (20x magnification).

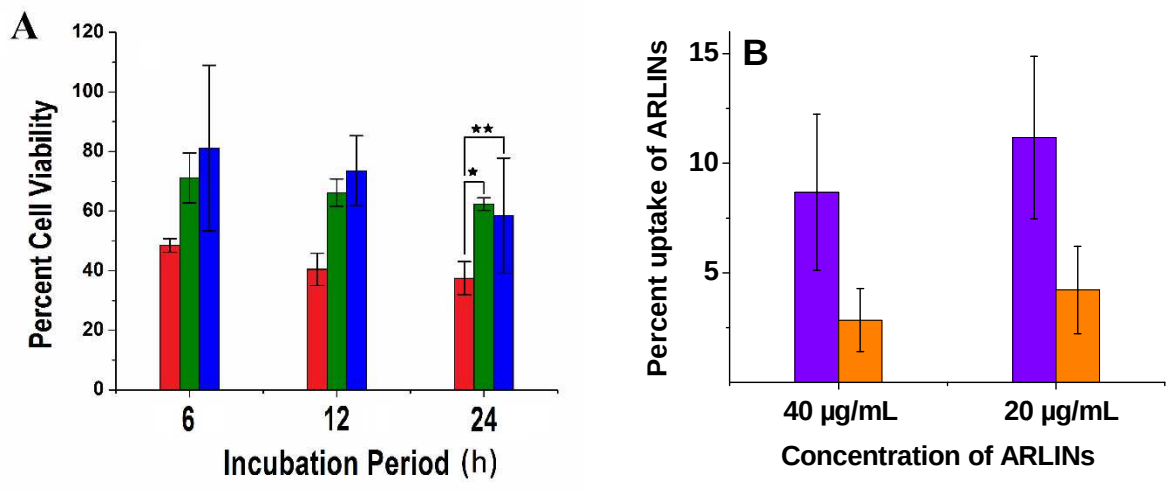

Figure 2.12. (A) Cell viability studies with HeLa cells: Folate conjugated doxorubicin loaded ARLINs (red), non-targeted doxorubicin loaded ARLINs (green) and free doxorubicin (blue).

Doxorubicin final concentration used was 50 µg/mL in all the samples. (n=6) *P<0.001 **P<0.05 (B) Percent uptake of ARLINs by MCF-7 cells after incubation for 6 h.

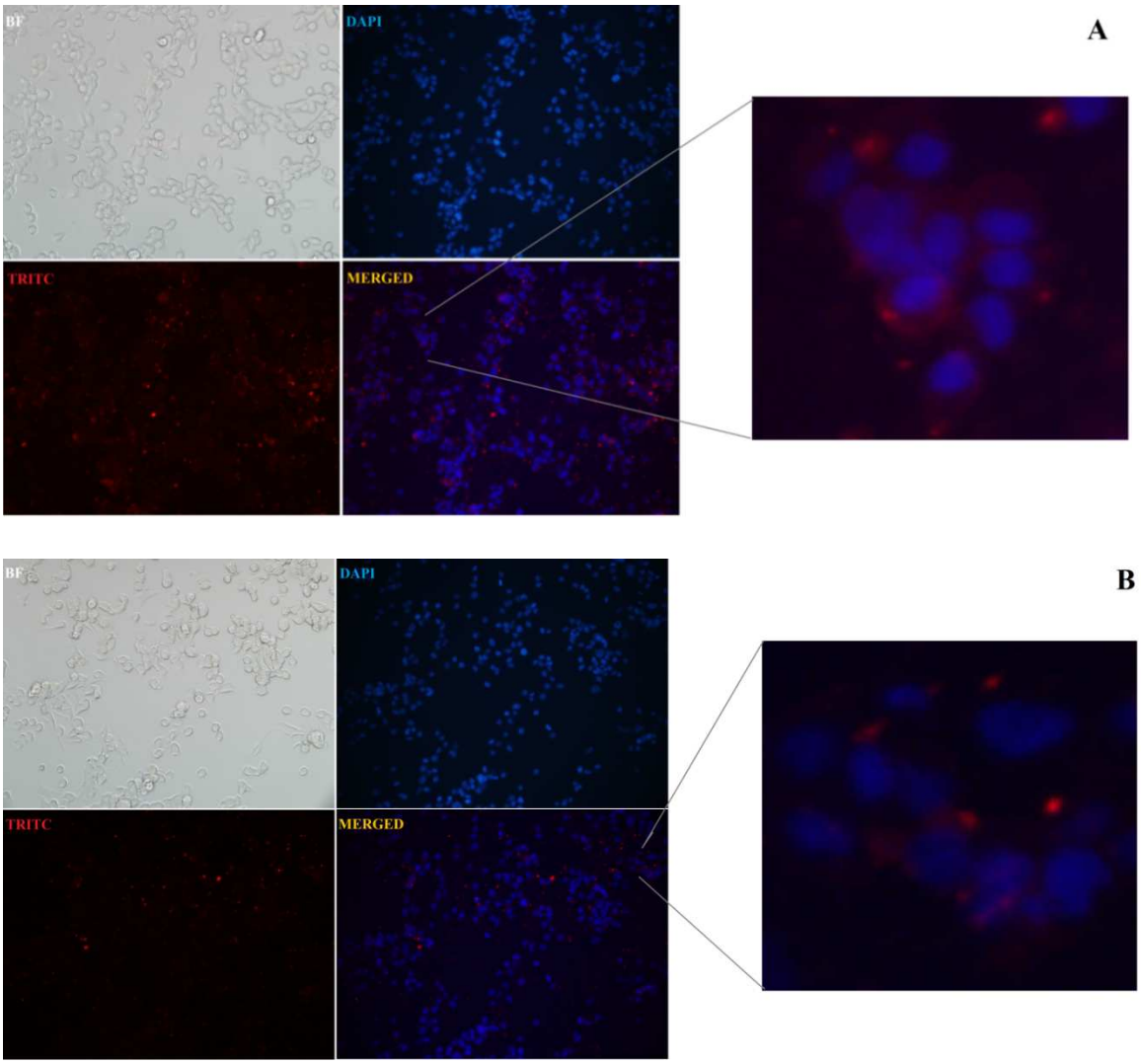

Figure 2.13. Fluorescence microscopic images for the uptake of doxorubicin loaded ARLINs by folate receptor overexpressing HeLa cells. (**A**) Folate conjugated doxorubicin loaded ARLINs (**B**) non-targeted doxorubicin loaded ARLINs. (20x magnification).

For the cellular studies, we incorporated the DPPE-PEG_{2000}-Folate lipid (Figure 2.2, 1 mol%) in the ARLINs and studied their uptake by folate overexpressing breast cancer cell line-MCF-7. For these experiments, the non-targeted ARLINs were used as the controls. MCF-7 is a breast cancer cell line known to overexpress folate receptors and has been used to demonstrate

enhanced uptake of folate conjugated drug delivery systems [208-212]. We observed significantly higher uptake of folate-lipid incorporated ARLINs in the MCF-7 cells compared to the non-targeted ARLINs. There was a significant difference in calcein fluorescence observed in fluorescence microscopic images (at 10 and 20 minutes) of folate conjugated ARLINs compared to the non-targeted ARLINs (Figure 2.11). We also observed that maximum uptake of the folate incorporated ARLINs in the MCF-7 cells takes place after 20 minutes of incubation. We further determined the percent of ARLINs uptake by the cells. For that cells were incubated with 40 μg/mL and 20 μg/mL of ARLINs encapsulating 50 mM calcein for 6 h. Cell and ARLINs were disrupted using 5% Triton-X100 solution and fluorescence was measured and percent uptake was calculated accordingly. Complying with fluorescence microscopic images, we noticed that folate targeted ARLINs were taken up by MCF-7 cells in higher amount compared to non-targeted ARLINs. Uptake was slow and it took around 6 h incubation to get around 10% of uptake with folate targeted ARLINs (Figure 2.12B). We also observed that uptake was concentration dependent, percent uptake increased with decrease in concentration but the total uptake increases with increase in concentration of ARLINs. When concentration was reduced from 40 μg/mL to 20 μg/mL, uptake was almost doubled with non-targeted ARLINs.

Subsequently, we encapsulated the anticancer drug doxorubicin in the folate-PEG lipid incorporated ARLINs by pH gradient method (80-90% encapsulation efficiency). Although some leakage of doxorubicin was observed during polymerization, we found that cell viability decreases to 37% when folate conjugated doxorubicin encapsulated ARLINs were incubated with HeLa cells (human cervical carcinoma overexpressing folate receptors) for 24 h. The cell viability was significantly lower for folate conjugated ARLINs compared to non-targeted ARLINs ($p<0.001$) and free doxorubicin ($p<0.05$), indicating that folate conjugation enhances the uptake in the HeLa cells (Figure 2.12). This was further confirmed by capturing fluorescence images of HeLa cells incubated with doxorubicin-ARLINs. The images clearly show enhanced uptake of doxorubicin-loaded-ARLINs into the cytosol of the HeLa cells (Figure 2.13).

Conclusion

We have successfully demonstrated the preparation of polymer coated ARLINs. These lipid nanoparticles were stable in the extracellular oxidizing environment but released their contents efficiently in the reducing environment of cell cytosol. The ARLINs were also found to be echogenic with a 20 dB enhancement in fundamental scattered response with 3.5 MHz excitation at 500 kPa acoustic pressure for a lipid concentration of 5 μg/mL. Although, the ARLINs failed to show significant release under diagnostic frequency ultrasonic excitation alone, the release was enhanced by simultaneous application of ultrasound and redox triggers. Doxorubicin loaded ARLINs showed enhanced uptake and cytotoxicity when conjugated to folic acid and thus can be used for targeted drug delivery for cancer cells overexpressing folate receptors on their surface. We have employed continuous wave ultrasound excitation for release studies, which sends more energy than pulsed ultrasound. Future studies are needed to optimize the ultrasound parameters such as frequency, intensity and duty cycles to establish optimum parameters maximum possible release. The current study however successfully validates the proof of concept and with further developments and modifications, these polymer-coated ARLINs have the potential to be used as multimodal nanocarriers for targeted drug delivery and simultaneous ultrasound imaging.

CHAPTER III. pH-TRIGGERED ECHOGENICITY AND CONTENTS RELEASE FROM LIPOSOMES

Abstract

Liposomes are representative lipid nanoparticles, and are widely used for delivering anticancer drugs, DNA fragments or siRNA to cancer cells. Upon targeting, various internal and external triggers have been used to increase the rate of contents release from the liposomes. Amongst the internal triggers, the decrease in pH within the cellular lysosomes has been successfully used to enhance the rate of contents release. However, imparting pH-sensitivity to liposomes requires the synthesis of specialized lipids whose structures are substantially modified at reduced pH. Herein, we report an alternative strategy to render liposomes pH-sensitive by encapsulating a precursor which generates gas bubbles *in situ* in response to acidic pH. The disturbance created by the escaping gas bubbles leads to the rapid release of the encapsulated contents from the liposomes. Atomic force microscopic studies indicate that the liposomal structure is destroyed at reduced pH. The gas bubbles also render the liposomes echogenic – allowing ultrasound imaging. In order to demonstrate the applicability of this strategy, we have successfully targeted doxorubicin-encapsulated liposomes to the pancreatic ductal carcinoma cells overexpressing the folate receptor on the surface. In response to the decreased pH in the lysosomes, the encapsulated anticancer drug is efficiently released. Contents release from these liposomes is further enhanced by the application of (1 MHz) continuous wave ultrasound, resulting in substantially reduced viability for the pancreatic cancer cells (14%).

Introduction

Amongst the lipid nanoparticles, liposomes are widely studied as drug delivery vehicles [213-215]. Liposomes protect the encapsulated drugs from getting metabolized in the circulation

prior to reaching the target. The US Food and Drug Administration has approved liposome-based formulations for the treatment of several types of cancers [216]. However, upon targeting, the passive release of the encapsulated drugs from the liposomes is often slow[76]. Reorganization of the lipid domains has been used as a trigger to enhance, and to control the rate and extent of contents release from liposomes [47, 83]. Amongst the various triggers, the decrease in pH in the lysosomes have been widely used as a successful strategy to efficiently release the encapsulated liposomal contents [217, 218]. However, imparting pH-sensitivity to liposomes requires the synthesis of specialized lipids whose structures are substantially modified at reduced pH, either due to hydrolysis or due to changes in the protonation states of the lipid head groups [217, 219-221].

Stabilized gas bubbles are widely used as contrast enhancing agents for ultrasound imaging of perfused tissues [222]. There are many reports of ultrasound mediated drug release from nanoparticles, liposomes and other carriers [45, 223-227]. Majority of these studies were conducted employing KHz frequency ultrasound [93, 94, 228]. Although ultrasound in KHz frequency efficiently releases the drugs from the carriers (due to cavitation and high local temperatures), the harmful biological effects associated with low-frequency ultrasound limits the usefulness of such strategies [229]. To make liposomes responsive to high-frequency ultrasound, they need to be coupled with gas pockets. Echogenic liposomes (ELIPs) entrap small amounts air along with hydrophilic drug in its aqueous interior and are currently being developed as drug delivery vehicles for ultrasound triggered drug release and simultaneous imaging [172, 230]. Although there is uncertainty about the exact location and size of the entrapped air bubbles in ELIPs, their acoustic characterization has been reported extensively in literature [105, 175, 231, 232].

We are developing targeted, multimodal liposomes for triggered release of encapsulated contents, and simultaneous ultrasound imaging. Furthermore, we are interested in enhancing

the contents release from the liposomes employing diagnostic frequency (MHz) ultrasound. We have recently demonstrated ultrasound enhanced, extracellular release of liposomal contents mediated by the cancer cell secreted enzyme matrix metalloproteinase-9 (MMP-9) [169]. Herein, we report a strategy to render liposomes pH-sensitive by encapsulating ammonium bicarbonate which generates gas bubbles *in situ* in response to acidic pH [233]. Our strategy does not require the use of pH-sensitive lipids in the liposomal formulations. We hypothesize that at reduced pH, the hydronium ions diffuse into the aqueous interior of the liposomes, produce carbon dioxide bubbles and thereby, "turning on" the echogenicity. We have successfully imaged the liposomes employing a medical ultrasound scanner. As more bubbles are generated, the liposomal bilayer is disturbed, leading to the release of encapsulated contents. We observed that the release was further enhanced by the application of ultrasound with a frequency 1 MHz. To the best of our knowledge there are no reports in the literature of ultrasound enhanced triggered release from pH tunable echogenic liposomes.

Materials and Methods

Preparation of liposomes

Liposomes were prepared with POPC (1-palmitoyl-2-oleoyl-*sn*-glycero-3-phosphocholine; Avanti Polar Lipids) lipid solution using traditional lipid film formation, hydration and sonication method. The lipid solution (4 mL of 1 mg/mL) was placed in a rotary evaporator for approximately 10 minutes to allow for the lipid film to form, and then placed under a vacuum overnight to remove traces of chloroform. Subsequently, 4 mL of 100 mM carboxyfluorescein solution was added, along with ammonium bicarbonate (0.4 M) and allowed to hydrate for three hours. The lipid dispersion was then sonicated for ten minutes to form liposomes. The liposomes were then exposed to three freeze (-70 °C) and thaw (23 °C) cycles to ensure dye encapsulation inside the aqueous interior of the liposomes. After the freeze-thaw cycles, an extrusion apparatus (Avanti Polar Lipids) was used to extrude the liposomes through

800 nm, then 200 nm polycarbonate membrane filters. The liposomes were then placed in a Sephadex-G100 gel filtration column preconditioned with HEPES buffer (pH 7.4, osmolarity adjusted to liposomal levels) to separate unencapsulated contents from the liposomes. Liposome fractions were collected and used for subsequent studies.

For cellular uptake studies, the lipids used were POPC (99 mol%) and 1,2-distearoyl-*sn*-glycero-3-phosphoethanolamine-N-[folate(polyethylene glycol)-5000] (ammonium salt; Avanti Polar Lipids) (1 mol%). The same procedure as described in the previous paragraph was followed for preparing these liposomes.

Preparation of doxorubicin loaded liposomes

Doxorubicin (Bridge Bioservices) was encapsulated by the traditional passive entrapment method. Briefly, the lipid film was hydrated with 400 mM ammonium bicarbonate and 0.2 mg of doxorubicin per mg of lipid for 3 hours. After bath sonication for 10 min and freeze thaw cycles liposomes were passed though Sephadex column to remove unencapsulated doxorubicin. Encapsulation efficiency was determined by recording the absorbance of doxorubicin at 475 nm before and after gel filtration. The doxorubicin content was determined by plotting the absorbance onto the calibration curve established at 475 nm.

Size distribution analysis (Dynamic light scattering)

Dynamic light scattering method (NanoZS 90 Zetasizer, Malvern Instrument) was used to study size distribution of the liposomes. For these experiments, 0.1 mg/mL of liposomal solution was taken in DTS 0012 polystyrene disposable sizing cuvette. The measurements were performed at a scattering angle of 90°. Samples were equilibrated for 60 seconds and ten readings were taken for a single sample at a constant temperature (25 °C). Each batch of liposomes was studied for size distribution and each experiment was repeated three times for consistency.

Transmission electron microscopy

The samples were observed using a JEOL JEM 2000 transmission electron microscope operating 100 kV and at low magnifications with the beam spread, which is not converged, to reduce the amount of electron beam interaction per unit area and hence beam damage to sample if it were to occur. The liposomal samples were dispersed to 1 mg/mL and dropped onto a 300 mesh Formvar coated copper grids previously coated with 0.01% poly-L-lysine and allowed to stand for one minute before wicking off with filter paper. Then it was allowed air dry for two minutes and after that it was negatively stained with 1% phosphotungstic acid for 90 seconds and subsequently wicked with filter paper and then allowed to dry before being beamed.

Atomic force microscopy

The liposomal sample was placed onto a mica sheet and air dried. For performing AFM imaging, a MultimodeTM atomic force microscope with Nanoscope III controller and J type piezo scanner (Veeco Metrology Group, Santa Barbara, CA) was used. Antimony (n) doped Si tip was used for obtaining images in Tapping ModeTM under laboratory conditions. Images of liposomes were taken before and after incubating in pH 6.0 buffer for an hour to study the effect of bubbles generated on the morphology of the liposomes. Images were captured, processed and labeled properly.

Ultrasound imaging of liposomes

A Terason t3200 diagnostic ultrasound (MediCorp LLC) instrument was utilized to image liposomal solution incubated in different pH buffers. A layer of Aquasonic 100 (Parker Laboratories) ultrasound gel was applied on 15L4 linear ultrasound transducer (4-15 megahertz MediCorp LLC). The gel was placed over parafilm covering 96 well plates containing 200 μL of liposomal solution in each well. The ultrasound scan properties were fixed at 0.7 mechanical index (MI) and 0.6 thermal index,(omni Mean activated, level C image map, level C persistence,

high frequency, level three TeraVision, level 51 2D gain, level 60 dynamic range, 3 cm scan depth, and 22 Hz frame rate). The images were taken for liposomes (0.05 mg/mL) incubated in different pH buffers [7.4 (control), 7, 6, 5] at different time intervals and saved. Images were further analyzed using ImageJ software (version 1.45s, NIH, USA) to calculate mean and maximum grey scale values for each pH for a specific concentration of liposomes.

pH triggered release

The release studies were carried out on a spectrophotometer (Spectramax M5, Molecular Devices) by exciting at 460 nm and monitoring the emission at 497 nm using a 96 well plate. In each well, 20 μL of the liposomal solution (0.02 mg/mL) was incubated with phosphate buffer saline solutions with pH adjusted to 7.4 (control), 6.0 and 5.0. The release was monitored for two hours and reading was taken at 30 second intervals. Each sample was taken in triplicates and each study was repeated three times in order to check the repeatability of the results. Release was calculated using formula:

$$\text{Release (\%)} = \frac{\text{Observed intensity - Initial intensity}}{\text{Final intensity - Initial intensity}} \times 100$$

Ultrasound enhanced pH triggered release

For the release experiments, Sonitron 1000® (Richmar) ultrasound instrument was employed. Carboxyfluorescein encapsulated liposomes (0.02 mg/mL) were incubated in 48 well plate with HEPES 25 mM buffers with different pH 7.4 (control), 6, and 5. Ultrasound probe tip was immersed into the solution and ultrasound was applied at different time points after incubation for different time intervals to check the release. Ultrasound parameters were optimized and employed to enhance contents release from liposomes (frequency 1 MHz, 100% Duty cycles, 2 W/cm^2, 5 minutes of application time). Release was monitored on Spectramax (Molecular devices) spectrofluorimeter (λ_{ex} = 460 nm; λ_{em} = 497 nm) after ultrasound

application for of 2 hours. Percent release was calculated using formula mentioned in the previous section.

Effect of temperature on ultrasound triggered release

Application of ultrasound leads to cavitation and thermal effects, and are often responsible for release from liposomes. To determine individual contribution of these two phenomena in release of contents, we carried out two different experiments. In one set up, we conducted release studies at room temperature (25 °C) and temperature of solution was noted before and after ultrasound application. In another experiment, we kept the plate on ice bath to decrease the temperature (below 10 °C) and noted the temperature before and after application of ultrasound. Although set up used to carry out this study allows reflection of ultrasound waves from air –water interface which gives rise to standing wave pattern, we see that the set-up is adequate for the present study for demonstration of proof of concept. Also, as mentioned in our previous publications, we noticed negligible (less than 1%) energy transfer to adjacent wells during stimulation indicating almost no interwell interferences [120, 121]. All experiments were performed thrice and in triplicates each time to ensure reproducibility of results and calculate standard deviations.

Cell culture and liposomal uptake studies

For liposomal uptake studies, HeLa (cervical cancer) and PANC-1 (Pancreatic epithelioid carcinoma) was cultured in clear (without added Phenol red) RPMI media supplemented with 10 % fetal bovine serum and 1% antibiotics. Culture flasks were incubated at 37 °C in humidified atmosphere containing 5% CO_2. When 90% confluent; the cells were suspended using trypsin-versene reagent. The suspended cells were then cultured onto sterile 6 well culture plate until 90% confluent.

Once confluent, the media was removed and cells were gently washed with HBSS (HyClone®, Thermo Scientific, UT) 5-6 times to completely remove any media left. Subsequently, liposomes were suspended in HBBS (0.2 mg/mL) and were incubated with the cells for 30 minutes. HOESCHT 33342 dye (Enzo Life Sciences) in 1 in 1000 dilution was added to stain the nuclei of the cells. After specific time intervals, the liposomal solution was removed from wells and the cells were again washed with HBSS to remove any liposomes on the surface of cells. Cells were then observed under fluorescence microscope at different time points for liposomal uptake. All images were obtained with Olympus IX81® motorized inverted microscope, viewed using 20X and 40X objectives and captured using CellSens Standard software (version 1.6). A similar procedure was followed for doxorubicin-encapsulated liposomal uptake by HeLa cells.

Cell viability studies

For cell viability studies, $5x10^5$ seeded cells onto the 400 nm pore sized transwell inserts (Thincert-6 well, Greiner bio-one) and bottom of 6 well plates. Once confluent cells in the upper compartment (Figure 3.11A-8) were exposed to different combinations treatments involving doxorubicin liposomes (targeted and non-targeted), bicarbonate liposomes without doxorubicin, free doxorubicin and ultrasound. Cells were kept in incubator for 6 hours and then live-dead staining (Enzo life sciences) was performed. Cells in the upper and bottom compartment were incubated with live-dead stain for 15 minutes, washed thrice with HBSS and then observed under fluorescence microscope using filters (FITC for live cells and rhodamine for dead cells). Images were taken and merged using ImageJ software. Percent killing was calculated by measuring green (live) and red (dead) fluorescence of three images of each sample using ImageJ software (http://rsbweb.nig.gov).

Migration assay

For migration assay $5x10^5$ cells/well in serum free media were seeded on the top of 8 μm pore sized cell culture inserts, with serum containing media in the lower chamber of 6 well plates. To determine %relative migration, cells were seeded onto membrane without any treatment. Once cells get attached (around 6-8 hrs), cells were exposed to ultrasound treatment and incubated overnight. After overnight incubation at 37°C, media was removed and cells were washed with HBSS thrice. Non-migrated cells on the filter were removed with sterile cotton swab and migrated cells were quantified by 10% of the total volume of Alamar blue. The assay measures the fluorescence of resorufin (red) formed by reduction of resazurin (blue) in the cytosol of viable cells (metabolically active). Percent relative migration was calculated using following formula:

Percent relative migration = Fluorescence intensity of treated sample*100/Fluorescence intensity of control sample.

Results and Discussion

Preparation of liposomes encapsulating ammonium bicarbonate and demonstration of pH-tunable echogenicity: In order to demonstrate tunable echogenicity, we prepared the liposomes from 1-palmitoyl-2-oleoyl-*sn*-glycero-3-phosphocholine (POPC), encapsulating 400 mM ammonium bicarbonate along with the self-quenching dye carboxyfluorescein (100 mM). We reasoned that for multilamellar liposomes, the outside hydronium ions need to diffuse through several lipid bilayers to generate sufficient amounts of CO_2 gas inside the liposomes. The presence of several lipid bilayers is also expected to decrease the efficiency of contents release in response to escaping gas bubbles and ultrasonic excitation. Hence, we decided to formulate unilamellar liposomes with a narrow size distribution by sonicating and sequentially extruding (through 800 nm and 200 nm polycarbonate membrane filters) the initially formed

multilamellar vesicles. We observed (by dynamic light scattering) that the average hydrodynamic diameter of the liposomes is 110 ± 15 nm with polydispersity index of 0.05 (Figure 3.1A). These results were corroborated by transmission electron microscopic imaging of the liposomes (Figure 3.1B).

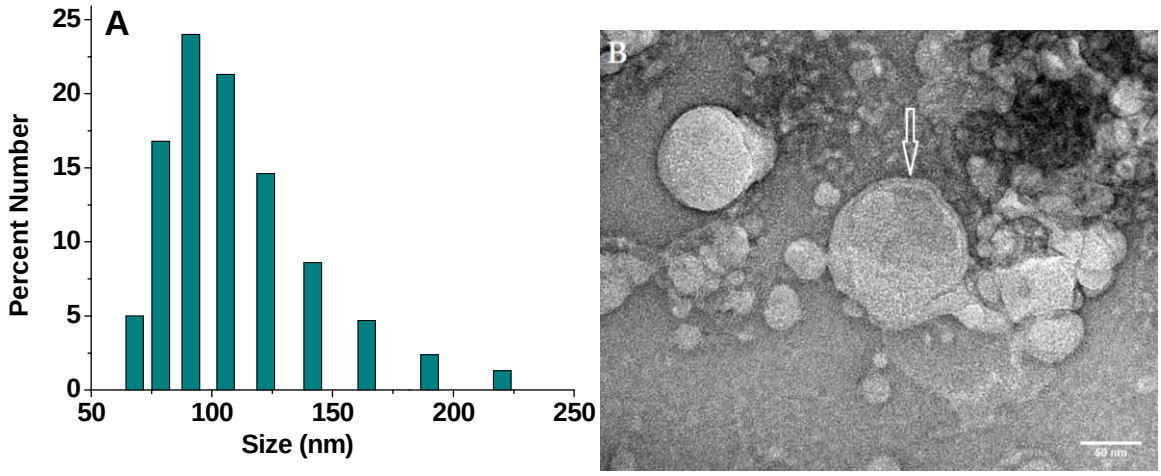

Figure 3.1. (**A**) Representative particle size distribution (by number) of the liposomes using dynamic light scattering instrument. (**B**) Transmission electron microscopic image (JEOL JEM 2100 LaB_6 200 kV) of pH tunable echogenic POPC liposomes using negative staining by 1% phosphotungstic acid. The beam is spread and not converged, to reduce the amount of electron beam interaction per unit area and to minimize beam damage to liposomal sample. The white arrow (Panel **B**) indicates the unilamellar bilayer structure of liposome.

In order to demonstrate the tunable echogenicity, we added the liposomes to buffers of different pH (7.4 – 5.0), and recorded the images using a Terason t3200 high-frequency (12 – 14 MHz) diagnostic ultrasound transducer. We observed that there was a lag time before the liposomes became echogenic and the duration of this lag phase decreased with the reduction in pH. For example, the liposomes in pH 7.4 buffer did not show any ultrasound contrast in 10 minutes. The liposomes at pH 6.0 became weakly echogenic in 5 minutes, but the liposomes in pH 5.0 were fairly echogenic within 3 minutes. The ultrasound images of the liposomes in buffers of different pH after 5 minutes are shown in Figure 3.2.

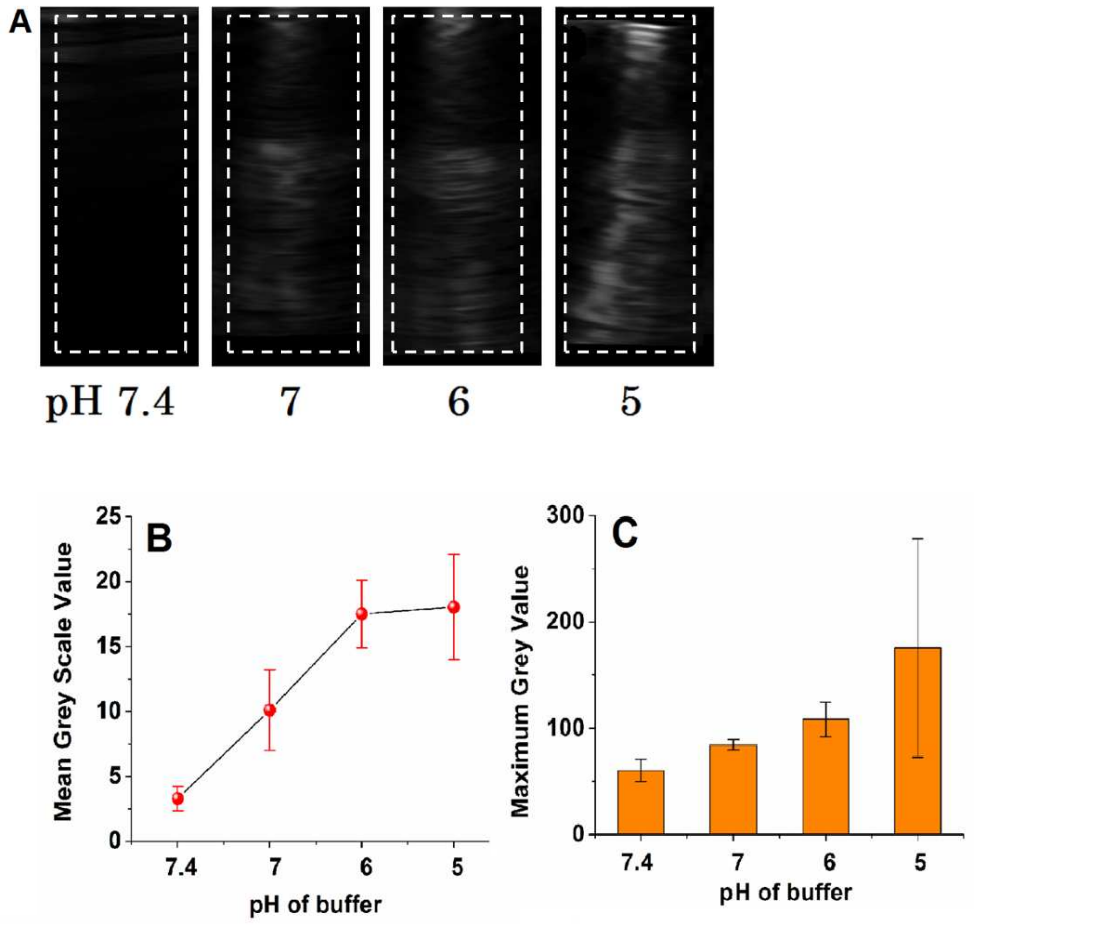

Figure 3.2. (A) pH-Dependent diagnostic ultrasound imaging of POPC liposomes encapsulating 400 mM ammonium bicarbonate. Dotted white lines represent the regions of interest (ROI) used to calculate the grey scale values. (**B**) Mean grey scale values (**C**) maximum gray scale values of ultrasound images shown in (**A**) as a function of pH (n = 3).

We anticipated that the concentration of hydronium ions in the external buffer will affect the rate of diffusion inside the liposomes and the subsequent generation of CO_2 bubbles. As the encapsulated ammonium bicarbonate is depleted, the generations of CO_2 gas slows down and finally stops. Consistent with this hypothesis, we observed that the liposomes in pH 5.0 buffer are not echogenic after 20 minutes (Figure 3.3). However, we note that the diameters of the gas bubbles inside the liposomes are likely to be small (in nm) and they may not reflect the ultrasound very well [234]. It is likely that the nanobubbles coalesce in the lipid bilayer of the liposomes, generating larger bubbles, and reflecting ultrasound. POPC lipid has a gel low transition temperature (–2 ^{o}C) and the liposomal bilayer is in the fluid phase under the

experimental conditions (20 ^{o}C) [235]. The loose lipid packing and fluidity of the POPC bilayer accommodate the coalescence and size increase of the gas bubbles.

We analyzed the ultrasound images of Figure 3.2A using the ImageJ software (http://rsbweb.nih.gov) to calculate mean and maximum grey scale values of region of interest (ROI, shown in Figure 3.2A). As expected, the mean and maximum grey scale values increase with decrease in pH. We observed that the highest grey scale value was observed at pH 5.0, and it does not increase any more below this pH (data not shown). We also observed time-dependent decrease in echogenicity of these liposomes at pH 5.0 (Figure 3.3). These results demonstrated that the liposomes are programmed to reflect ultrasound only after reaching the acidic microenvironment of cancer cells.

pH-Triggered release of liposomal contents and mechanistic studies: Having demonstrated pH-tunable echogenicity, we decided to determine if the escaping gas bubbles are sufficiently disturbing the lipid bilayer to release the encapsulated contents from the liposomes. In this endeavor, we incubated the POPC liposomes (encapsulating carboxyfluorescein and 400 mM ammonium bicarbonate) in buffers of different pH (7.4 – 5.0), and monitored the emission intensity of carboxyfluorescein. However, the emission intensity of carboxyfluorescein is quenched as the pH is lowered [236]. In order to correct for this decrease in emission intensity, we measured the absorption spectra of carboxyfluorescein as a function of pH and determined the isosbestic point to be 460 nm. Subsequently, the dye solution was prepared in buffers of pH 7.4, 6.0 and 5.0, excited at 460 nm, and the emission spectra were recorded. We observed that the emission spectra produced an isosbestic point at 497 nm. We then monitored the emission of the dye at 497 nm (excitation: 460 nm) for 2 hours. Correction factors were calculated at each pH as a function of time, and all emission intensities were appropriately corrected for calculating the percent release (Appendix B).

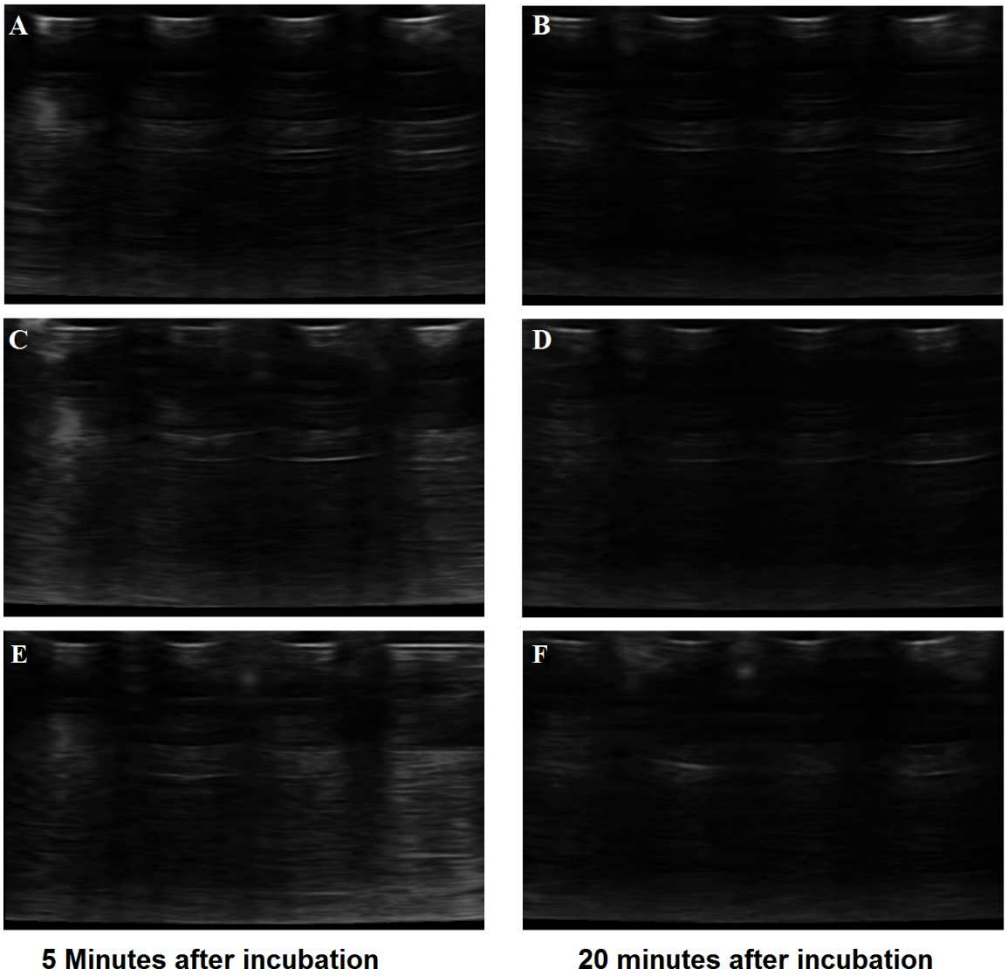

Figure 3.3. Diagnostic ultrasound Imaging of POPC liposomes encapsulating 400 mM ammonium bicabonate as function of frequency and incubation time in pH 5 buffer. The images were acquired employing high Frequency (12-15 MHz; **A**, **B**), medium frequency (8-12 MHz; **C**, **D**), and low frequency (4-8 MHz; **E**, **F**) ultrasound.

When the liposomes were incubated in acidic buffers, there was a time lag before dye release (Figure 3.4). However, the liposomes continued to leak the contents for considerably long time (2 – 3 hours). This indicates that the disturbances created in the lipid bilayers by the escaping gas bubbles are either not sealed, or take a long time to heal.

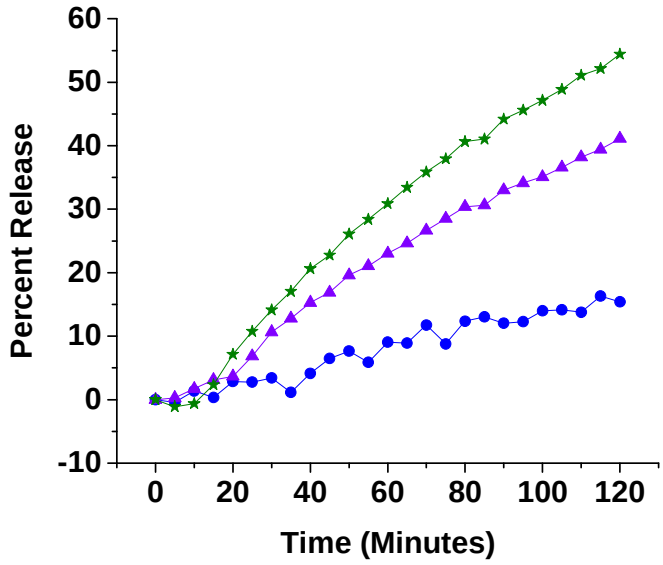

Figure 3.4. Representative release profile of carboxyfluorescein from POPC liposomes encapsulating 400 mM ammonium bicarbonate, incubated in buffers of pH 7.4 (blue circles), pH 6.0 (purple triangles), and pH 5.0 (green stars). The lines are generated by connecting the observed data points.

While the liposomes at pH 7.4 (control) released only 15% of the encapsulated dye in 2 hours, at pH 5, the release increased to 55% (Figure 3.5A). When we encapsulated sodium bicarbonate in the liposomes (instead of ammonium bicarbonate), the amount of contents release decreased. In 2 hours, we observed that the sodium bicarbonate encapsulated liposomes released 40% of the encapsulated dye (at pH = 5.0; Appendix B, Figures B2 and B3). For both of these liposomal formulations, the rate of contents release decreases considerably after 2 hours. In 3 hours at pH 5.0, the ammonium bicarbonate encapsulated liposomes released 75% of the contents and the sodium bicarbonate encapsulated liposomes released 44% of the contents (Figure 3.5A). Decreasing the amount of encapsulated ammonium bicarbonate (from 400 mM to 200 mM) also reduces the amount of contents release from the liposomes (Figure 3.5B).

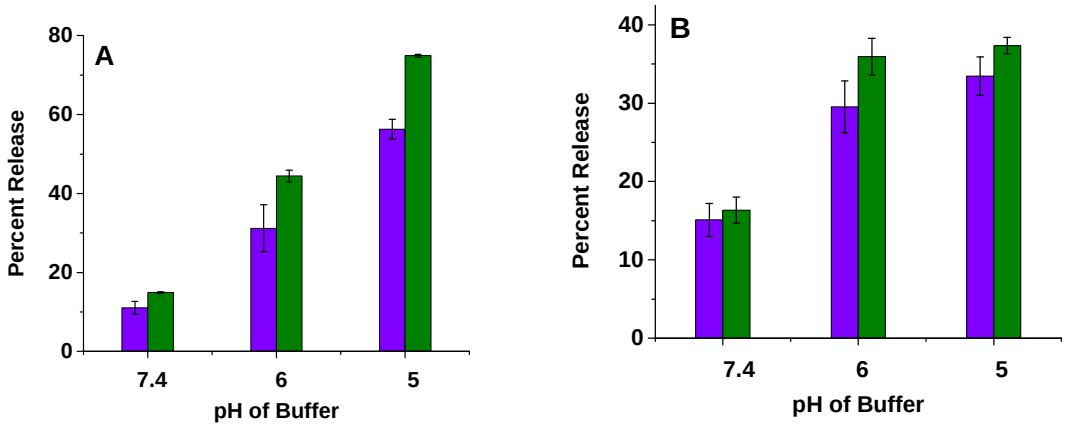

Figure 3.5. Contents release from POPC liposomes as a function of pH encapsulating (**A**) 400 mM ammonium bicarbonate and (**B**) 200 mM ammonium bicarbonate after 2 hours (violet bars) and after 3 hours (olive bars) (n = 3).

The acidic decomposition of ammonium bicarbonate generates NH_3 and CO_2, while sodium bicarbonate produces the sodium salt of the buffer, H_2O and CO_2. The ammonia gas will react with the hydronium ions in the liposome interior, leading to a reduction in pH. The resultant pH-gradient will facilitate the diffusion of more hydronium ions into the liposomal lumen, and generating more CO_2 gas and ammonia. Amount of generated gas decreases by reducing the concentration of encapsulated ammonium bicarbonate, leading to a reduction in contents release from the liposomes (Figure 3.5B). As an additional control, we prepared the POPC liposomes without encapsulating any gas precursor, and studied the contents release as a function of pH. We observed minimal release (< 10%) of the encapsulated carboxyfluorescein at pH 7.4 and 6.0. However, at pH 5.0, about 20% of the dye was released in 2 hours (Figure B4, Appendix B).

In these liposome formulations, we have used POPC as the bilayer forming lipid. The POPC molecules contain the saturated palmitoyl and the unsaturated oleoyl groups. Due to the presence of an alkene in the Z-configuration, this lipid does not form a tight bilayer and the gel transition temperature is also low (– 2 ^{o}C) [235]. In order to determine if the packing of the lipids in the liposomal bilayer and the gel transition temperature affect the contents release, we prepared two batches of DSPC liposomes encapsulating ammonium and sodium bicarbonate

respectively (400 mM each). The DSPC molecules contain two saturated stearoyl groups; hence it forms tight bilayer and has a melting temperature of 56 ^{o}C [237]. We anticipated that the tight packing of the lipid molecules in the bilayer will hinder the coalescence of the generated CO_2 bubbles. In addition, the rate of diffusion of hydronium ions across the lipid bilayer will be slower compared to the POPC bilayer. We observed that both ammonium bicarbonate and sodium bicarbonate encapsulated DSPC liposomes released less than 5% of contents after incubation for 2 hours at pH = 5.0 (Appendix B, Table B1).

We employed tapping mode atomic force microscopic imaging to determine if the escaping gas bubbles at pH 5.0 cause any structural changes (shape and surface morphology) to the ammonium bicarbonate encapsulated POPC liposomes. After preparation, the ammonium bicarbonate encapsulated liposomes (pH = 7.4 buffer) were found to be spherical with average diameter of about 100 nm (Figure 3.6A). However, after incubating in pH 5.0 buffer for an hour, the liposomes were observed to be fused and the majority of the structures showed irregular shapes with sizes up to 800 nm (Figure 3.6B). These results demonstrate that the escaping gas bubbles caused permanent changes to the morphology of these liposomes, leading to the leakage of encapsulated contents.

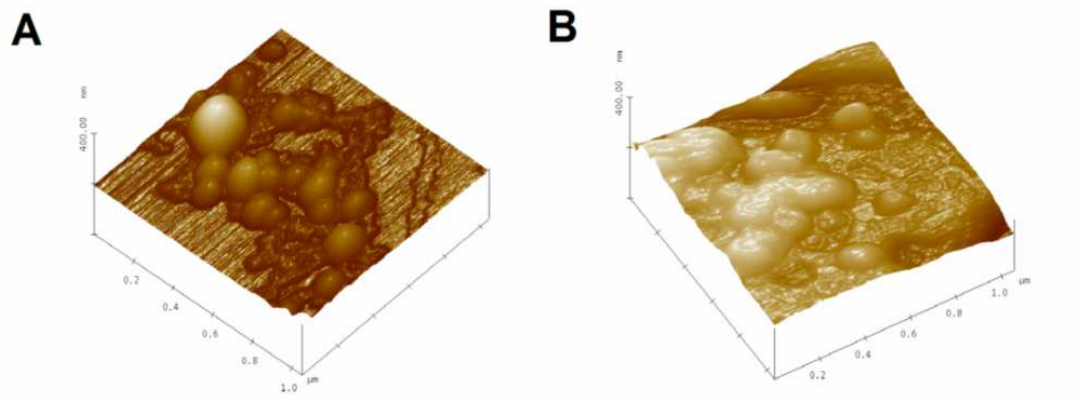

Figure 3.6. Atomic force microscopic images of 400 mM ammonium bicarbonate pH tunable echogenic POPC liposomes (**A**) before incubation (**B**) after incubation in pH 5.0 buffer for an hour.

Triggered release of liposomal contents with pH and ultrasound: We reasoned that the released gas bubbles inside the liposomes will allow for an additional control on contents release employing high-frequency ultrasound. In order to test this hypothesis, we incubated the ammonium bicarbonate encapsulated POPC liposomes in pH 5.0 buffer and after 5 minutes, and exposed them to continuous wave ultrasound (1 MHz, 2 W/cm^2) for 5 minutes. We observed that 80% of the encapsulated contents were released from the liposomes in 2 hours (compared to 55% release in the absence of ultrasound; Figure 3.7A). Decreasing the concentration of encapsulated ammonium bicarbonate (from 400 mM to 200 mM) reduced the amount of contents release upon application of ultrasound to 45% (Figure 3.7B). We also observed that the applied ultrasound exerted maximum effect when applied within 5 – 15 min of incubation of the liposomes with the pH 5.0 buffer (Figure 3.7B). It is likely that the generated CO_2 bubbles escape from the liposomes within 15 minutes, and after that liposomes become less responsive to ultrasound. During the imaging studies, we have also observed a decrease in the echogenicity of the liposomes after 15 minutes of incubation in the pH 5 buffer (Figure 3.3).

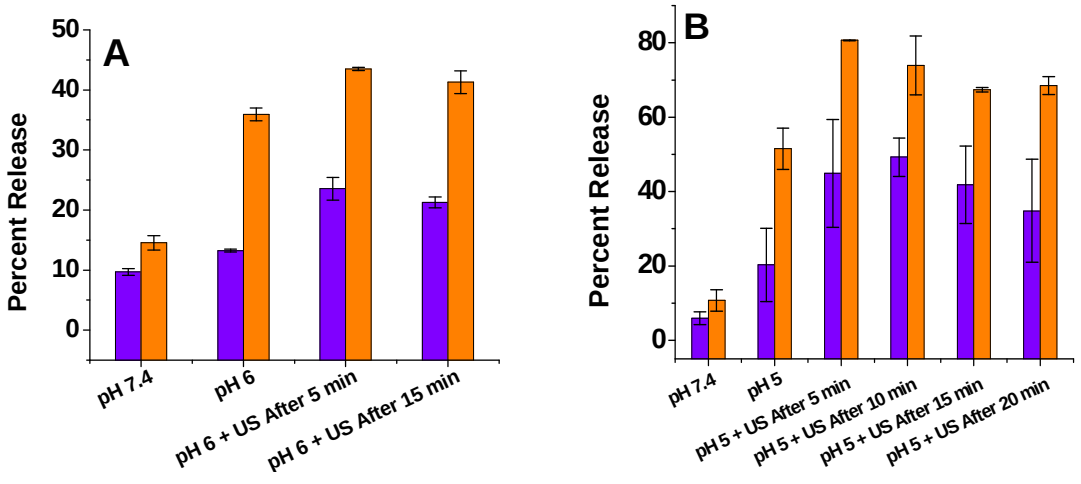

Figure 3.7. Ultrasound (1 MHz, CW, 2 W/cm^2, 5 min) enhanced, pH-triggered release from POPC liposomes encapsulating 400 mM ammonium bicarbonate (**A**), and 200 mM ammonium bicarbonate encapsulated liposomes (**B**). Violet bars: release after 20 min with ultrasound application; Orange bars: release after 2 h with ultrasound application (n = 3).

When the ammonium bicarbonate encapsulated POPC liposomes (400 mM) were incubated in pH 6.0 buffer, we observed that the application of ultrasound enhanced the release by 10%. Contrary to the pH 5.0 experimental results, this enhancement in contents release was not strongly dependent on the time when the ultrasound was applied (Figure 3.8). At pH 6.0, the concentration of hydronium ions is 10 times less compared to that at pH 5. This contributes to a slow generation of gas bubbles inside the liposomes and it takes longer time to consume the encapsulated ammonium bicarbonate. These two factors are likely contributing to the results observed with ultrasound at pH 6.0. If the concentration of ammonium bicarbonate is reduced to 200 mM, application of ultrasound did not induce any significant increase in contents release from the liposomes (< 5%).

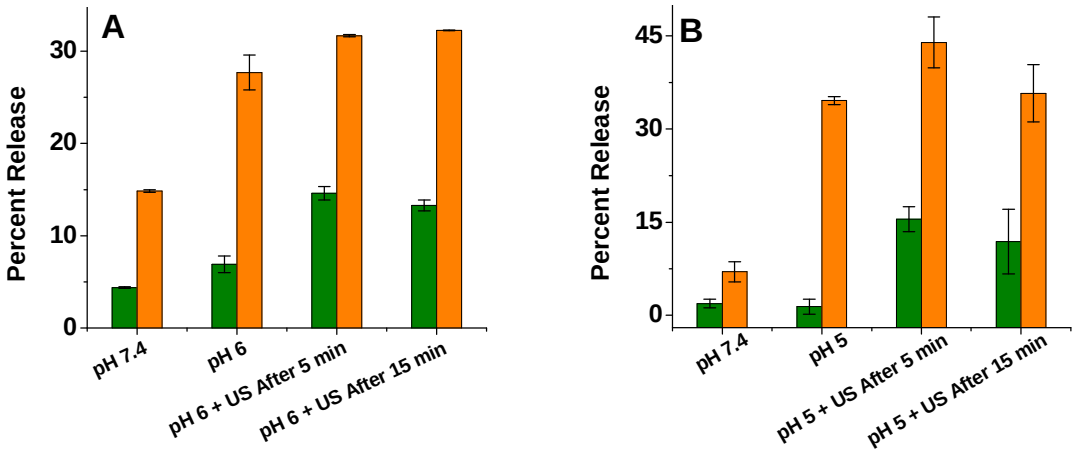

Figure 3.8. Ultrasound (1 MHz, CW, 2 W/cm^2, 5 min) enhanced pH triggered release from POPC liposomes encapsulating 200 mM ammonium bicarbonate at pH = 6.0 (**A**) and pH = 5.0 (**B**). Green bars: release after 20 min with ultrasound application, Orange bars: release after 2 h with ultrasound application (n = 3).

We observed that the application of ultrasound increased the temperature of the liposome solutions from 25 ^{o}C to 30 ^{o}C. In order to determine if this temperature change is influencing the contents release from liposomes, we repeated the studies (in pH 5.0 buffer) in a large ice bath. The temperature of the ice bath was maintained below 10 ^{o}C throughout the experiments. The results from these two experiments were identical – indicating that the

temperature increase was not influencing the contents release from our pH-sensitive liposomes [238].

Internalization studies with pancreatic cancer cells: Having optimized the ultrasound enhanced release from the pH-sensitive liposomes, we proceeded to demonstrate the effectiveness of the strategy in cellular studies. In order to demonstrate efficient cellular internalization, we prepared liposomes incorporating 1 mol% of 1,2-distearoyl-*sn*-glycero-3-phosphoethanolamine-N-[folate(polyethylene glycol)-5000] (ammonium salt, commercially available from Avanti Polar Lipids) and POPC encapsulating 100 mM carboxyfluorescein. We selected the folate receptor overexpressing pancreatic ductal carcinoma cells (PANC-1) for our cellular studies [239]. It should be noted that pancreatic cancer is one of the leading causes of cancer-related deaths in both men and women in the U.S., with a 5-year survival rate of less than 5% [240, 241]. According to The American Cancer Society, 38,460 pancreatic cancer related death (nearly equally split between men and women) occurred in US in 2013.

After incubating with the liposomes, we imaged the cells employing a fluorescence microscope. We noticed that liposomes incorporating 1 mol% of the folate lipid were taken up by cells more effectively by the PANC-1 cells compared to the liposomes without the folate lipid (Figure 3.9). If the cells have a higher expression of the folate receptor, the rate of internalization was faster. For example, the breast cancer cell line MCF-7 internalized the folate lipid containing liposomes faster compared to the PANC-1 cells (Appendix B: Figure B5).

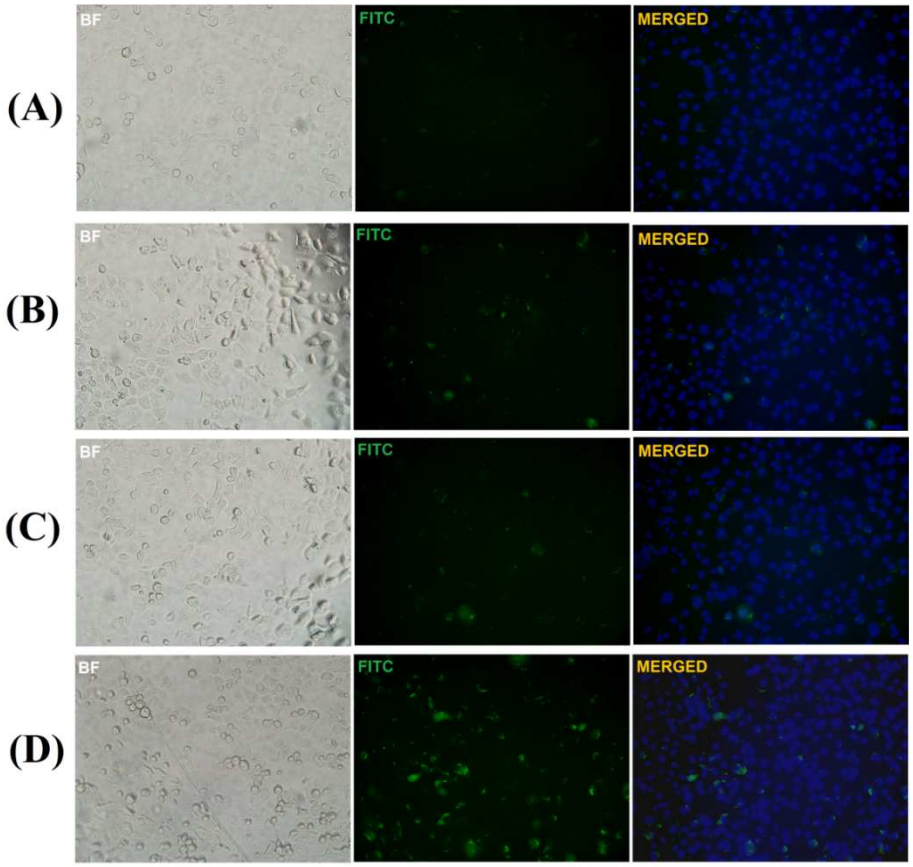

Figure 3.9. Fluorescence microscopic images for the uptake of pH-tunable, echogenic POPC liposomes by folate receptor overexpressing PANC-1 cancer cells. (**A**) Non-targeted liposomes after 3 hours of incubation (magnification: 20X). (**B**) Non targeted liposomes after 6 hours of incubation (magnification: 20X). (**C**) Folate-targeted liposomes after 3 hours of incubation (magnification: 20X). (**D**) Folate-targeted liposomes after 6 hours incubation (magnification: 20X).

Intracellular release of liposomal contents in response to reduced pH and application of ultrasound: After confirming cellular internalization, we encapsulated the anticancer drug doxorubicin in the POPC liposomes and studied its release in the cytosol of the PANC-1 cells (in the absence and presence of applied diagnostic frequency ultrasound). Although gemcitabine is the standard chemotherapeutic drug for pancreatic cancer, doxorubicin is currently being tested as a possible adjuvant therapy [242-244]. We noted, *a priori*, that some literature reports question the safety of ultrasound for the healthy tissues surrounding a tumor [63]. To determine

if the ultrasound has any deleterious effects for the normal cells, we seeded the PANC-1 cells onto the transwell inserts consisting of two chambers. In this experimental design, the PANC-1 cells in the upper chamber represent the tumor tissue and receive direct exposure to the liposomes as well as applied ultrasound. The cells in the lower chamber represent the neighboring tissue which may be indirectly exposed to the treatment (Figure 3.10A). The pore size for the transmembrane was 400 nm and the average diameter of the liposomes was 110 nm. Hence, we expected that some of the liposomes as well as the ultrasound waves will pass through the membrane and reach the lower chamber.

Upon reaching confluency, we exposed the cells in the upper chamber to various combinations of targeted/non-targeted doxorubicin-encapsulated liposomes and ultrasound (applied between 15-20 minutes of incubation) (Figure 3.10A). Subsequently, we placed the cells in an incubator for 6 hours and stained to visualize the live and the dead cells. We observed that indirect exposure to any of the treatments did not cause cell death in the lower chamber (Figure 10A and B). On the other hand, direct exposure to folate targeted or non-targeted, pH-tunable, doxorubicin-encapsulated liposomes and ultrasound led to significant cell death in the upper chamber (Figure 3.10A and B).

We observed that the folate-targeted, doxorubicin and ammonium bicarbonate encapsulated POPC liposomes (Figure 3.10A-1) were more toxic (14% cell viability) compared to the corresponding liposomes without bicarbonate encapsulation (cell viability 25%) (Figure 3.10A-5). It is reported that the cavitation force of exploding CO_2 bubbles in the lysosomes mechanically disrupt the membranes, leading to the release of lysosomal proteolytic enzymes in the cytosol, and cell death [233, 238]. Contrary this report, we observed less than 5% cell death in the presence of liposomes encapsulating only ammonium bicarbonate (i.e., without doxorubicin, Figure 3.10A-4). These results indicate that in our experiments, cavitation induced by CO_2 bubbles enhance the toxicity of the liposomal formulations.

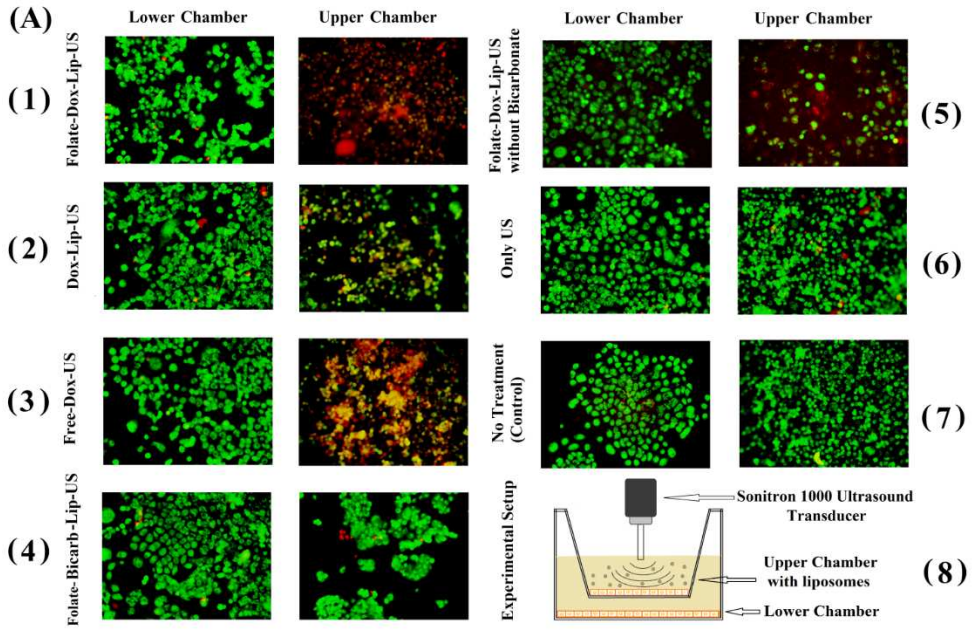

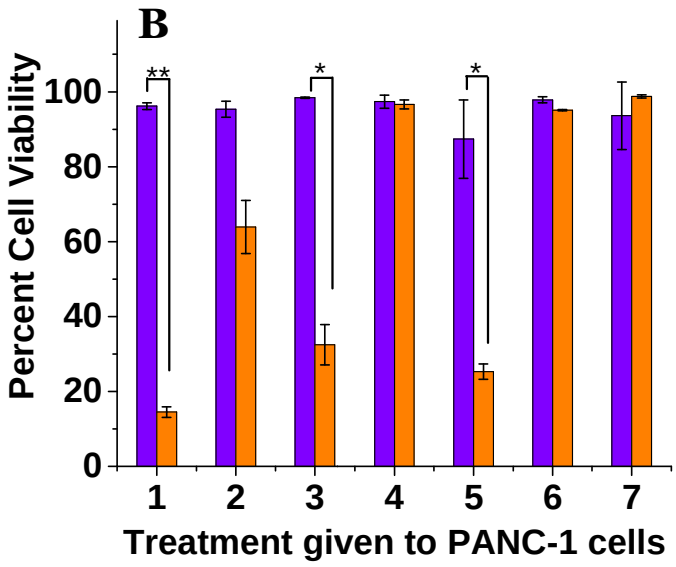

Figure 3.10. (**A**) PANC-1 cell viability studies using live (green) and dead (red) cell staining of different treatment groups (n = 3). Upper chamber cells received direct whereas the lower chamber cells received indirect exposure to POPC liposomes and ultrasound. (**B**) Cell viability of upper chamber (orange bars) and lower chamber (violet bars). (**1**) Folate targeted doxorubicin liposomes (encapsulating ammonium bicarbonate) + ultrasound; (**2**) non-targeted doxorubicin liposomes (encapsulating ammonium bicarbonate) + ultrasound; (**3**) free doxorubicin + ultrasound; (**4**) folate targeted liposomes (encapsulating ammonium bicarbonate but no doxorubicin) + ultrasound; (**5**) folate targeted doxorubicin liposomes (no ammonium bicarbonate encapsulation) + ultrasound; (**6**) ultrasound only; (**7**) no treatment (control). (**8**)

Schematic representation of the experimental set up. Doxorubicin final concentration used was 25 μg/mL. (* $P < 0.05$, ** $P < 0.01$, n=4)

Interestingly, the free doxorubicin was more effective compared to liposomal doxorubicin (without folate) in inducing cell death (Figure 3.10A-2 and 3). It is likely that sonoporation by the ultrasound is contributing to this effect. In the absence of any microbubbles, the pores formed in the cell membranes by the applied ultrasound are likely to be small and transient. Possibly, the sizes of these transient pores are large enough to allow doxorubicin molecules to cross the cell membranes [245]. These observations are consistent with literature reports demonstrating higher uptake of smaller particles compared to larger ones upon sonoporation [246]. We observed that under our experimental conditions, direct or indirect exposure to the ultrasound does not induce cell death (Figure 3.10A-6).

PANC-1 is a metastatic pancreatic cancer cell line known to secrete the enzymes matrix metalloproteinase (MMP) – 2 and – 9 in the extracellular matrix [247]. These two proteolytic enzymes are responsible for the hydrolysis of extracellular matrix, leading to the migration and metastasis of cancer cells [248]. Ultrasound treatment can loosen the extracellular material surrounding a tumor, resulting in dissemination of cancer cells into the blood stream. This leads to increased migration and metastasis of the cancer cells when exposed to ultrasound [249]. In order to determine if our experimental conditions are contributing to such effects, we conducted migration assays of the PANC-1 cells in the presence of applied ultrasound. In this endeavor, we seeded the PANC-1 cells onto 8 μm transwell insert. After 6 hours, we exposed the cells to ultrasound (1 MHz, 5 minutes), incubated overnight and determined the migration of the cells. We observed that there was no significant difference ($P > 0.01$, $n = 5$) in migration ability of the ultrasound exposed cells compared to the control samples (no ultrasound exposure). This confirms that within our experimental parameters, the migration of the PANC-1 cells remains unaffected by the applied ultrasound.

Conclusion

We have successfully demonstrated the proof-of-concept for a new strategy to release liposomal contents in response to reduced pH. In our design, the liposomes encapsulate the gas precursor ammonium bicarbonate, and do not incorporate pH-sensitive lipids in the bilayer. When incubated in buffers of acidic pH, CO_2 gas bubbles are generated and thus, induces echogenicity to the liposomes. The escaping gas bubbles cause structural changes to the liposomes, and release the encapsulated contents (up to 56%). The contents release is further enhanced by the simultaneous application of diagnostic frequency ultrasound (1 MHz, 5 min; 80% release). The fluidity of the liposomal membranes plays a crucial role in the contents release. By incorporating a folate lipid in the bilayer, we have successfully targeted the liposomes to pancreatic cancer cells overexpressing the folate receptor on the surface. Liposome-encapsulated doxorubicin is efficiently released in the cancer cells, and the release is enhanced by the simultaneous application of diagnostic frequency ultrasound. While ultrasound was innocuous, the combination of doxorubicin release from the liposomes and ultrasound reduced the viability of pancreatic cancer cells to 14%. With further developments, these liposomes have potential to be an excellent option for ultrasound image guided, targeted drug delivery at tumor sites.

CHAPTER IV. MULTIFUNCTIONAL POLYMERSOMES FOR CYTOSOLIC DELIVERY OF GEMCITABINE AND DOXORUBICIN TO CANCER CELLS

Abstract

Although liposomes are widely used as carriers of drugs and imaging agents, they suffer from a lack of stability and the slow release of the encapsulated contents at the targeted site. Polymersomes (vesicles of amphiphilic polymers) are considerably more stable compared to liposomes; however, they also demonstrate a slow release for the encapsulated contents, limiting their efficacy as a drug-delivery tool. As a solution, we prepared and characterized echogenic polymersomes which are programmed to release the encapsulated drugs rapidly when incubated with cytosolic concentrations of glutathione. These vesicles encapsulated air bubbles inside and efficiently reflected diagnostic frequency ultrasound. Folate-targeted polymersomes showed an enhanced uptake by breast- and pancreatic-cancer cells in a monolayer as well as in three-dimensional spheroid cultures. Polymersomes encapsulated with the anticancer drugs gemcitabine and doxorubicin showed significant cytotoxicity to these cells. With further improvements, these vesicles hold the promise to serve as multifunctional nanocarriers, offering a triggered release as well as diagnostic ultrasound imaging.

Introduction

Gemcitabine, a fluorinated nucleoside analog (2′,2′-difluorodeoxycytidine), has emerged as an effective anticancer drug against various malignancies [250] and is currently used in both palliative and adjuvant therapy following surgery for pancreatic cancer. However, the drug is not devoid of limitations. For example, it shows systemic toxicity [251] and has a very short half-life, ranging from 8 to17 minutes. In addition, it undergoes rapid conversion to an inactive metabolite in the blood stream [252]. Gemcitabine is a prodrug that requires cellular uptake by

the hENT1 receptors on the cancer-cell surface. Unfortunately, a majority of patients (more than 65%) lack this receptor, further limiting the usefulness of the free drug [253].

In order to overcome these limitations, gemcitabine has been delivered by employing various carriers, e.g., theranostic nanoparticles [254], targeted liposomes [255], micelles [256], and microbubbles [257]. Recent clinical studies demonstrate that gemcitabine, in combination with other antineoplastic agents, is more effective for treating pancreatic cancer [258-262]. For example, due to the non-overlapping toxicity profiles, gemcitabine's efficacy is synergistically enhanced in the presence of the anticancer drug doxorubicin [263-265]. However, this drug combination also has severe side effects [266-268]. Consequently, there is an urgent and unmet need to deliver these drugs to tumor tissues using a drug-delivery vehicle. There is only one report of simultaneous delivery for these two drugs as polymer conjugates [269]. To date, there are no reports about the targeted delivery of this drug combination to pancreatic-cancer cells employing any other drug carrier.

Currently, several liposomal drug formulations are approved by the U.S. Food and Drug Administration to treat cancer. Although these formulations show improved efficacy and safety, most of them still lead to severe side effects [24]. With these formulations, the presence of polyethylene-glycol (PEG) lipids renders the long-circulating property, and facilitates the accumulation of liposomes in the tumor tissues due to the enhanced permeation and retention effect [270]. Upon reaching the intended sites, the encapsulated contents are released passively, and this process is often slow [271]. In addition, anti-phospholipid antibodies cause other complications, such as pulmonary hypertension, due to pseudo-allergic reactions [272]. Thus, tunable release, specifically at the target site, would be desirable for a greater therapeutic impact for the drug formulation without compromising its safety profile. Several research groups, including ours, have successfully demonstrated that the integration of targeting and triggering strategies considerably improves the anti-tumor efficacy of liposomal formulations [68, 169].

Polymersomes are vesicles prepared from synthetic, amphiphilic-block copolymers [273]. They have several advantages over liposomes, including enhanced stability, longer circulation times, mechanical robustness, and the ability to carry large quantities of hydrophobic and hydrophilic drug molecules [274]. Due to the polymers' higher molecular weights, polymersomes' bilayer membranes are generally thicker, stronger, and hence, inherently more stable than conventional liposomes and micelles. The hydrophilic block of the copolymers is usually polyethyleneglycol, imparting the long-circulating property to the resultant polymersomes [275].

The enhanced stability of the polymersomes also has disadvantages; the release of encapsulated drugs is rather slow [276, 277]. Because of robustness, the polymersomes require a stimulus to sufficiently disturb the compact bilayer and to release the encapsulated contents. There are a few reports of targeting [278-282] and content release from polymersomes that employ either internal (pH [283], glucose [284], or cysteine [285]) or external triggers (light [286], heat [287], or magnetic field [288]).

In the pursuit of designing stimuli-response polymersomes for simultaneously delivering gemcitabine and doxorubicin to cancer cells, we noted that the concentration of thiol-based reducing agents increases from 10-40 μM in the blood to 1-10 mM in the cell cytosol [185, 186]. We are using this differential reducing-agent concentration to cause permanent structural changes in the amphiphilic-block copolymers. We demonstrate that the disturbance created compromises the vesicular structure of the polymersomes, resulting in a rapid release of the encapsulated anticancer drugs. In order to impart multimodal characteristics, we have encapsulated air bubbles as ultrasound contrast agents. In our design, targeting groups (folate-conjugated lipids) on the outside surface of the polymer vesicles ensure the targeting and subsequent facile entry inside the cancer cells. We note that, currently, there are no reports of

air-encapsulated, echogenic polymersomes, although the corresponding liposomal counterparts are well documented and characterized [68, 169, 175].

Materials and Methods

Synthesis and characterization of polymers

To synthesize the polymers, first, methoxy-PEG (MW: 1900) was reacted with succinic anhydride in dichloromethane solvent in the presence of triethylamine. The carboxy-terminated PEG thus obtained was subjected to further conjugation with cystamine dihydrochloride in the presence of EDC (ethyl-3-(3-dimethylaminopropyl)-carbodiimide). Finally, polylactic acid (MW: 3600) was prepared by ring-opening polymerization of lactide at the amine terminal of PEG using tin (II) bis(2-ethylhexanoate) as the catalyst under the refluxing condition (Scheme 1) [289]. For the detailed procedure, see the Appendix D.

Gel-permeation chromatography

To determine the weight average molecular weights of polymers and disulfide degradation by glutathione, gel-permeation chromatography (Agilent) was performed. THF (tetrahydrofuran) was used to dissolve the polystyrene standards (Supelco) and the polymers. Analysis was done with an Ultrahydrogel 250 (7.8 mm × 300 mm) column with THF as the mobile phase at a flow rate of 0.6 mL/min. Run time was kept at 30 minutes with refractive-index (RI) detection at room temperature. For each analysis, 50 μL of a sample (1 mg/mL) were injected. The calibration curve for standards was established, and retention times for polymers were extrapolated on the curve to obtain the average molecular weights. To check the sensitivity toward glutathione, the polymers were injected before and after incubation with 5 mM of glutathione for an hour. Changes for the retention times of polymer peaks were noted and compared.

Differential scanning calorimetry

To determine the melting points of the synthesized polymers, a Nano DSC instrument (TA Instruments) was used. The polymer solution (1 mg/mL) of a 10-mM phosphate buffer (pH 7.0) was used as the sample, and heated from 0 °C to 80 °C at the rate of 1 °C per minute. The phosphate buffer (pH 7.0) was taken as the control. The heating and cooling cycles were repeated twice to ensure reproducibility and reversibility of melting. The collected data were analyzed using Nanoanalyze software (version 4.2.2) provided by the vendor.

Preparation of polymersomes

Calcein encapsulation

Initially, we prepared polymersomes with the thin-film hydration-sonication and solvent-exchange methods [273]. We observed that the solvent-exchange method produced a narrower-size distribution of polymersomes, and showed higher encapsulation efficiency. Briefly, polymers were dissolved in THF (5 mg/mL) and slowly added to a calcein solution (10 μM) in a 10 mM HEPES buffer (pH 7.4) with constant stirring. After stirring for an hour, THF was removed under reduced pressure using a rotary evaporator. The solution was then sonicated for 60 minutes using a bath sonicator (Aquasonic, Model 250D) at room temperature. The polymersomes were then extruded at 70 °C through polycabonate membrane filters with a pore size of 1000 nm.

Doxorubicin-gemcitabine encapsulation

Doxorubicin (Bridge Bioservices) and gemcitabine (Matrix Scientific) were encapsulated into the polymersomes with the pH gradient method [290]. The polymersomes were prepared with the solvent-exchange method as described earlier, encapsulating a citrate buffer with a pH of 4.0. Subsequently, the pH of the external buffer was adjusted to 7.0 by adding sodium bicarbonate powder. The polymersomes were then incubated with a mixture (1:1) of gemcitabine

and doxorubicin at a 0.2 mg/mL concentration for an hour at 60 °C. Unencapsulated drugs were removed by passing the polymersomes through a Sephadex™ G-100 (GE Healthcare) size exclusion column. The encapsulation efficiency was established by measuring the absorbance at 276 nm (for gemcitabine) and 480 nm (for doxorubicin) before and after gel filtration.

Simultaneous determination of doxorubicin and gemcitabine

We used the dual-wavelength UV spectrophotometric method to simultaneously estimate the concentrations of encapsulated doxorubicin and gemcitabine [291]. We selected the two wavelengths as 276 nm and 480 nm. While doxorubicin has the same absorbance at these wavelengths, gemcitabine has negligible absorbance at 480 nm. Thus, gemcitabine can be determined at 276 nm by subtracting the absorbance of doxorubicin at 480 nm, and doxorubicin can be determined at 480 nm (Figure 4.11). The method was developed and validated by determining the linear dynamic range and reproducibility.

Size-distribution analysis

The dynamic light-scattering method (NanoZS 90 Zetasizer, Malvern Instruments) was used to study the polymersomes' size distribution. The polymersomes were dispersed in a 10 mM HEPES buffer (pH 7.4) at a concentration of 0.2 mg/mL in a DTS 0012 polystyrene, disposable sizing cuvette. The measurements were performed at a scattering angle of 90°. The samples were equilibrated for 60 seconds, and 10 readings were taken for a single sample at a constant temperature (25 °C). Each batch of polymersomes was studied for size distribution, and each experiment was repeated 5 times to check the repeatability of results and to calculate the standard deviation.

Atomic force microscopy

The polymersome samples in a 10 mM HEPES buffer (pH = 7.4) were placed onto a mica sheet and air dried. To perform AFM imaging, a Multimode™ atomic force microscope with a

Nanoscope III controller and J type piezo scanner (Veeco Metrology Group) was used. An antimony (n) doped Si-tip was used to obtain images in Tapping Mode under laboratory conditions. Images were taken before and after incubation with glutathione (5 mM) for an hour. The effect of the reducing agent on shape and morphology of polymersomes was studied.

Transmission electron microscopy

The polymersome samples were imaged using a JEOL JEM 2000 transmission electron microscope operating at 100 kV and at low magnifications with the beam spread (not converged) to reduce the amount of electron-beam interaction per unit area and, hence, beam damage to the sample if it were to occur. The polymersome samples in a 10 mM HEPES buffer (pH = 7.4) were dispersed to 1 mg/mL and dropped onto a 300-mesh, Formvar-coated copper grid previously coated with 0.01% poly-L-lysine and allowed to stand for 1 minute before wicking off with filter paper. Then, sample was allowed to air dry for 2 minutes, negatively stained with 1% phosphotungstic acid for 90 seconds, and subsequently wicked with filter paper and then allowed to dry before being beamed.

Ultrasound scattering experiment

We studied the echogenic properties of several contrast agents in our earlier publications [68, 169, 175] utilizing an in-vitro acoustic setup that included a large sample volume (100 mL). Here, we adopted a modified version of that setup with a smaller sample volume (20 mL) to enable experiments at a higher concentration of polymersomes (Figure 4.1). The present setup utilized the same confocal arrangement described in our previous publications to have a better signal-to-noise ratio. The setup employed two single-element focused immersion transducers (Olympus NDT, Waltham, MA). A 3.5-MHz and a 5-MHz transducer were used as the transmitter and receiver, respectively. Details about the instrumentation used and data-acquisition procedure can be found in our previous publication [175], and are omitted here for brevity. A 90° angle made of polycarbonate blocks was used for the confocal alignment of the

transducers. The drilled holes on each wall of the angle allowed for the insertion of traducers. The angle could be fixed to a base plate that was also made of polycarbonate. An acoustically transparent film (Saran™ wrap) was wrapped around the frame to provide an enclosure for the samples. It forms two acoustically transparent windows. Care was taken to keep the film taut and well stretched to keep film reflections from corrupting the data in our region of interest. When both the frame (wrapped with the film) and the angle fitted with transducers were affixed to the base plate, the confocal regions of the focused transducer aligned halfway between the acoustically transparent windows. The entire arrangement was placed in a large container with water to keep the sample chamber and the transducers submerged. The water level was adjusted to ensure that it did not spill into the sample chamber.

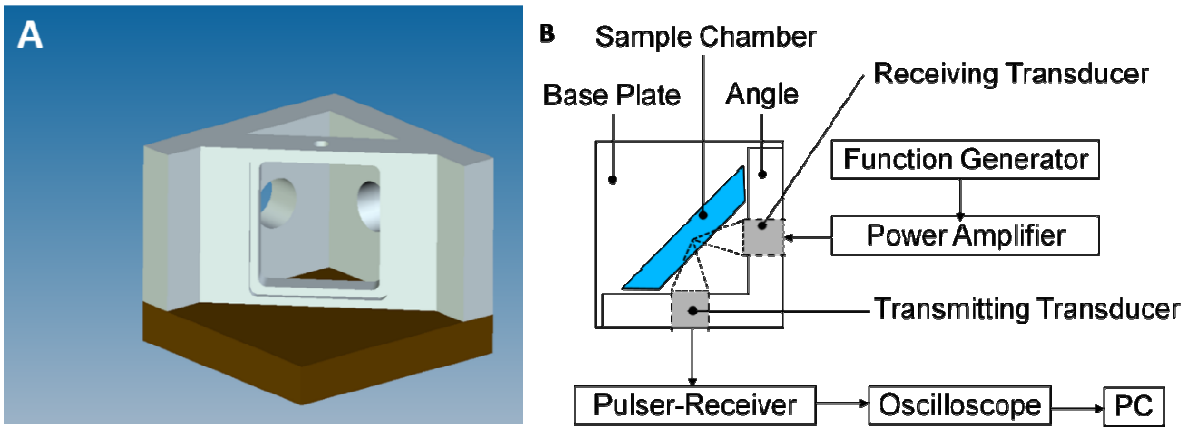

Figure 4.1. (**A**) A three-dimensional rendition of the setup used for the acoustic experiments. (**B**) A schematic representation of the setup for in-vitro scattering measurements.

Ultrasound Imaging

A Terason t3200 diagnostic ultrasound (MediCorp LLC) instrument was used to image the polymersome samples. A layer of Aquasonic 100 (Parker Laboratories) ultrasound gel was applied to a 15L4 linear ultrasound transducer (4-15 MHz; MediCorp, LLC). The gel was placed over parafilm that covered 96 well plates that each contained 200 µL of polymersomes (in 10 mM HEPES buffer, pH = 7.4). The ultrasound scan properties were fixed at 0.7 mechanical

index (MI) and 0.6 thermal index (omni Mean activated, level-C image map, level-C persistence, high frequency, level-three TeraVision, level-51 2D gain, level-60 dynamic range, 3-cm scan depth, and 22-Hz frame rate). The Terason diagnostic-imaging instrument measured the reflected ultrasound (not the attenuations) when constructing the images. The images were recorded for polymersomes (0.01 mg/mL) and saved. Images were further analyzed using ImageJ software (version 1.47v, NIH, USA) to calculate the mean and maximum grey scale.

Triggered-release studies

Redox-triggered release

We used the cobalt quenching method where external, unencapsulated calcein fluorescence is quenched by millimolar concentration of cobalt chloride [112]. The release was monitored using a spectrofluorimeter (Spectramax M5, Molecular Devices) by exciting at 495 nm and recording the emission at 515 nm using a 96-well plate. In each well, 20 µL of the polymersome solution (0.02 mg/mL) was incubated in 10 mM of HEPES buffer (pH 7.4). The release was monitored for 60 minutes, and measurements were taken at 30-second intervals. Each sample was taken in triplicate, and each study was repeated 3 times to check the repeatability of the results. Release was calculated using the following formula:

$$Percent\ Release = \frac{Intial\ Fluorescence - Final\ Fluorescence}{Intial\ Fluorescence} \times 100$$

Ultrasound-triggered release

For the release experiments, a Sonitron 1000® (Richmar) ultrasound instrument was employed. Calcein-encapsulated polymersomes (0.02 mg/mL) were incubated in a 48-well plate with HEPES buffer (10 mM, pH 7.4). The ultrasound-probe tip was immersed into the solution, and ultrasound was applied at different times after incubation for different time intervals. The ultrasound parameters were varied to obtain maximum release from the polymersomes (frequency 1 MHz, 100% duty cycles, 2 W/cm^2, 5 minutes of application time). The release was

monitored on a Spectramax (Molecular Devices) spectrofluorimeter (λ_{ex} = 495 nm, λ_{em} = 515 nm). The percentage release was calculated using the formula mentioned in the previous section. Although the setup used to carry out this study allows reflection of the ultrasound waves from the air-water interface, which gives rise to the standing wave pattern, we note that the setup is adequate to demonstrate the proof of concept. As mentioned in our previous publications, we noticed negligible (less than 1%) energy transfer to adjacent wells during stimulation, indicating almost no inter-well interferences [120, 121]. All experiments were performed three times and in triplicate each time to ensure reproducibility of results and to calculate standard deviations.

Simultaneous application of redox and ultrasound triggers

Three different designs were used for these experiments.

(1) Ultrasound (frequency 1 MHz, 100% duty cycles, 2 W/cm^2, 5 minutes of application time) was applied, followed by a redox trigger (5-mM GSH).

(2) The redox trigger was immediately followed by ultrasound.

(3) The redox trigger was followed by ultrasound after 60 minutes of incubation.

Folate-targeting studies:

For folate-targeted polymersome uptake studies, PANC-1 (pancreatic ductal carcinoma) and MCF-7 (breast cancer) cells were cultured in clear (without added Phenol red) RPMI media supplemented with 10% fetal bovine serum and 1% antibiotics (penicillin and streptomycin). Both cell lines were purchased from ATCC. The culture flasks were incubated at 37 °C in a humidified atmosphere that contained 5% CO_2. When 90% confluent, the cells were suspended using a trypsin-versene reagent. The suspended cells were then cultured onto sterile, 6-well culture plates until 90% confluent.

Once confluent, the media was removed, and cells were gently washed with HBSS (HyClone®, Thermo Scientific, UT) 5-6 times to completely remove any leftover media. Subsequently, the polymersomes (0.025 mg/mL) were suspended in HBSS and were incubated with the cells for different time intervals. HOESCHT 33342 dye (Enzo Life Sciences, 1 in 1000 dilution) was added to stain the cells' nuclei. After specific time intervals, the polymersome samples were removed from the wells, and the cells were, again, washed with HBSS to remove any polymersomes on the cell surface. Cells were then observed under a fluorescence microscope at different times for uptake. All images were obtained with an Olympus IX81® motorized inverted microscope, viewed using 20X objectives, and captured using CellSens Standard software (version 1.6).

Cell-viability studies (monolayer culture)

The cytotoxicity of targeted and non-targeted polymersomes was determined by AlamarBlue® assay, measuring the fluorescence of resorufin (red) formed by the reduction of resazurin (blue) in the cytosol of viable cells (metabolically active) [193]. Briefly, PANC-1 and MCF-7 cells were transferred to flat, clear-bottomed, 96-well tissue-culture plates (Corning) at a density of 2 $x10^4$ per well 24 hours prior to the assay (or 70-80% confluency). The culture medium in each well was carefully removed and replaced with gemcitabine + doxorubicin encapsulated folate-conjugated polymersomes, gemcitabine + doxorubicin encapsulated non-targeted polymersomes, and a free gemcitabine + doxorubicin solution mixed with media. After incubation at 37 °C for 48 hours, the cells were washed 3 times with sterile HBSS and incubated in a fresh culture medium. At this point, 20 μL of AlamarBlue® were added to each well, and the fluorescence readings (λ_{ex} = 560 nm, λ_{em} = 590 nm) were taken after 3 hours of incubation at 37 °C. Average readings were then compared to the control and plotted.

Spheroid- 3D cell culture studies

The MCF-7 cell spheroids were grown by modifying a published protocol [292]. Briefly, 3% w/v of agar solution were prepared by boiling until it became translucent, to which an equal volume of RPMI media (37°C) was added. To a 48-well plate, 200 μL of the above mixture were added to each well. Once it solidified, 1×10^5 cells were added to each well and centrifuged at 1000 g for 10 minutes. The plates were then slowly moved into a humidified incubator without disturbing them and were grown for 3 days. Spheroid growth was monitored for the entire study duration, and then, tests were conducted accordingly.

Cell-viability studies (spheroid 3D culture)

The spheroids were allowed to grow for 9 days after preparation. On the 10^{th} and 11^{th} days, gemcitabine + doxorubicin loaded polymersomes (targeted and non-targeted), and the free-drug combination were dispersed in media and incubated with the spheroids for 48 hours. Control spheroids were incubated with polymersomes without any encapsulated drugs. After treatment for 48 hours, the spheroid growth was monitored for 21 days by taking microscopic images.

Results and Discussion

Polymer synthesis, polymersome preparation, and structural characterization: The hydrophilic fraction (f) of an amphiphilic-block copolymer determines its ability to form bilayer vesicles. The formation of polymersomes is favored when the ratio of hydrophilic mass to the total mass of the polymer is similar to that of the naturally occurring phospholipids, with an f value of 35% ± 10% [275]. In order to optimize vesicle formation, we synthesized 5 polymers with varying f values from 25% to 68%. We kept the PEG molecular weight constant at 1900, and varied the molecular weights for the PLA (Polylactic acid) portion from 900 to 5800. Thus, we synthesized polymers with an average PLA molecular weight of 900, 1700, 1950, 3600, and 5800 by ring-opening polymerization [293]. To incorporate the disulfide bond, m-PEG (MW

1900) was first reacted with succinic anhydride, followed by conjugation of cystamine. The resulting m-PEG derivative with free amine at one terminal was used for all polymer syntheses (Scheme 4.1). Polymers were purified, and their average molecular weights were confirmed by ^{1}H NMR spectroscopy and gel-permeation chromatography (Appendix C).

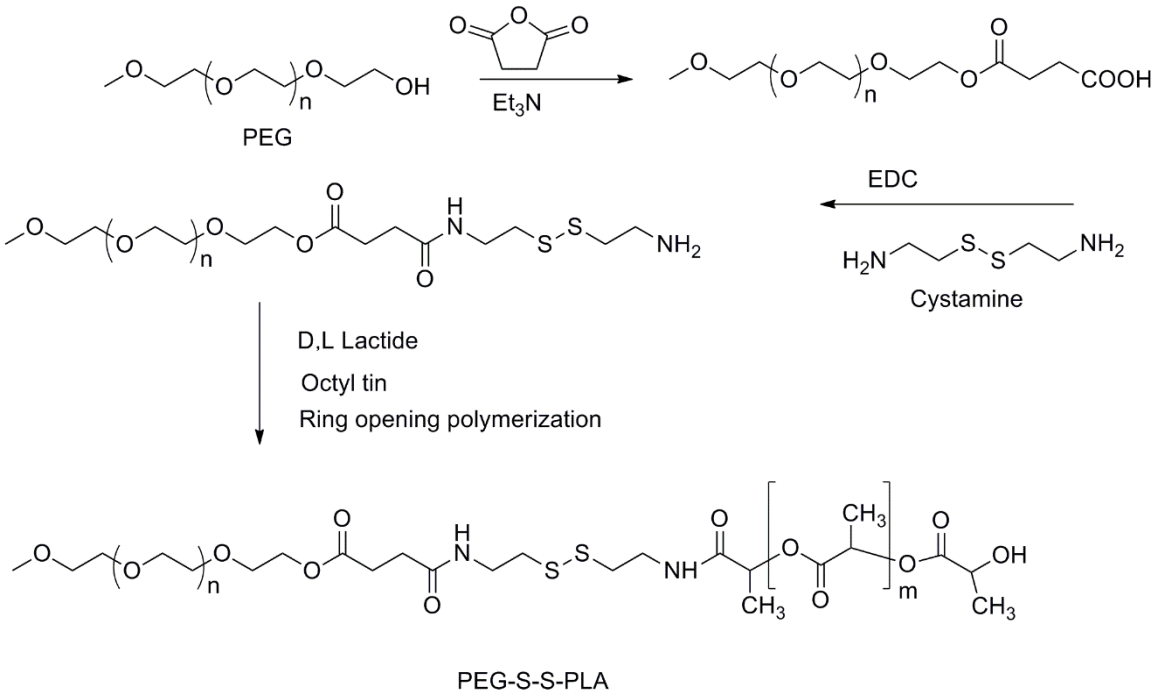

Scheme 4.1. Synthesis of the diblock disulfide-linked copolymer PEG-S-S-PLA employing the ring-opening polymerization.

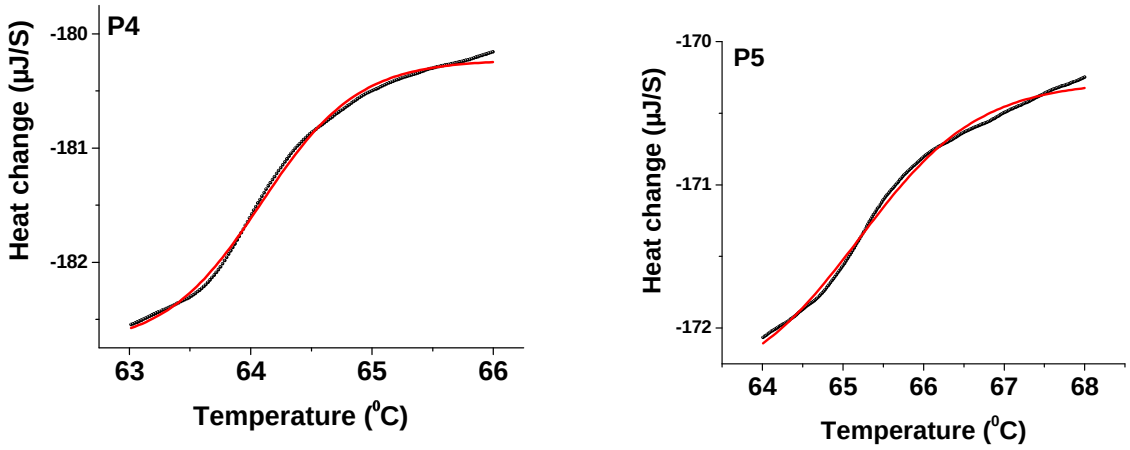

Figure 4.2. Differential scanning calorimetric thermograms of polymers (**A**) **PEG_{1900}-S-S-PLA_{5800}** and (**B**) **PEG_{1900}-S-S-PLA_{3600}** (black: observed data points; red: fitted curve).

Although several protocols have been reported for preparing polymersomes, the thin-film rehydration and solvent-exchange methods are most common [274]. If the copolymers have a low Tg (glass transition temperature below 25 °C), polymersomes can be prepared by directly putting them into water. In contrast, if the hydrophobic block has a high Tg (above 25 °C), the copolymers do not form polymersomes with such a treatment. In this situation, a suitable organic solvent needs to be used (solvent-exchange method) to lower the Tg of the hydrophobic polymer block. This solvent provides enough chain mobility for the polymers to form the bilayered vesicles [273].

To determine the optimal method to form the polymersomes, we analyzed the thermal properties of the synthesized polymers by using differential scanning calorimetry (DSC). We subjected the polymers in a 10 mM phosphate buffer (pH 7.0) to gradual (1 °C per minute) heating in DSC from 0 °C to 80 °C. We noticed that all the polymers had a transition temperature well above 60 °C (representative thermograms for **PEG_{1900}-S-S-PLA_{3600}** and **PEG_{1900}-S-S-PLA_{5800}** are shown in Figure 4.2). We observed that polymers **PEG_{1900}-S-S-PLA_{3600}** and **PEG_{1900}-S-S-PLA_{5800}** had glass transition temperatures of 64.1 °C and 65.2 °C, respectively (Figure 4.2). These results suggested that the solvent-exchange method would be most suitable for preparing the polymersomes. Glass transition temperatures well above the body temperature also ensured stability for the polymersomes in circulation with minimal passive leakage and, hence, reduced systemic toxicity.

Having determined the optimal method for preparing polymersomes, we dissolved the polymers in THF and slowly added this solution to an aqueous buffer. Subsequently, N_2 gas was slowly passed over the mixture to evaporate THF. The resultant samples were lyophilized and observed under transmission electron microscopy (Figure 4.3).

Due to the presence of the hydrophilic PEG and the hydrophobic PLA domains, PEG-PLA block copolymers spontaneously aggregated into different structures in an aqueous buffer [294]. We also observed that the hydrophilic fraction (f) of the synthesized amphiphilic-block copolymers (Table 4.1) determined their ability to form different structures, e.g., micelles, bicelles, worms, and vesicles (Figure 4.3). When the f value was highest (68% for PEG_{1900}-S-S-PLA_{900}; Table 1), micelles were formed with a size around 50-100 nm (Figure 4.3, Panel **A**). PEG_{1900}-S-S-PLA_{1700} (f = 53%) and PEG_{1900}-S-S-PLA_{1950} (f = 49%) polymers only showed bicelles and long, worm-like structures with a few ill-formed vesicles (Figure 4.3, Panels **B** and **C**). Well-structured vesicles were only formed from PEG_{1900}-S-S-PLA_{3600} (f = 35%) and PEG_{1900}-S-S-PLA_{5800} (f = 25%) polymers (Figure 4.3, Panels **D** and **E**). These results were also corroborated by atomic force microscopy (Figure 4.6, before treatment). We also noticed that the bilayer thickness was about 20-30 nm for the **P4** and **P5** polymersomes (Figure 4.3, Panels **D** and **E**), which is much larger than liposomes (with a bilayer thickness around 3-5 nm) [294].

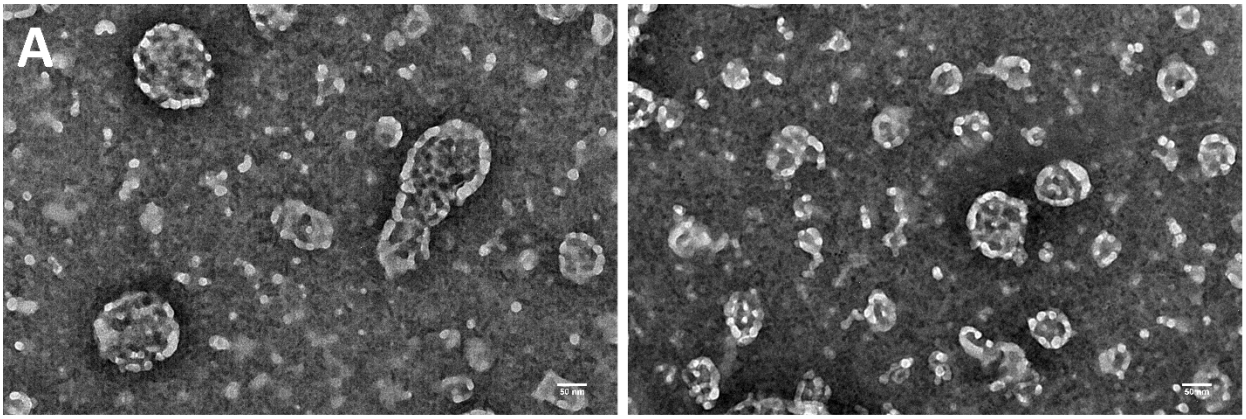

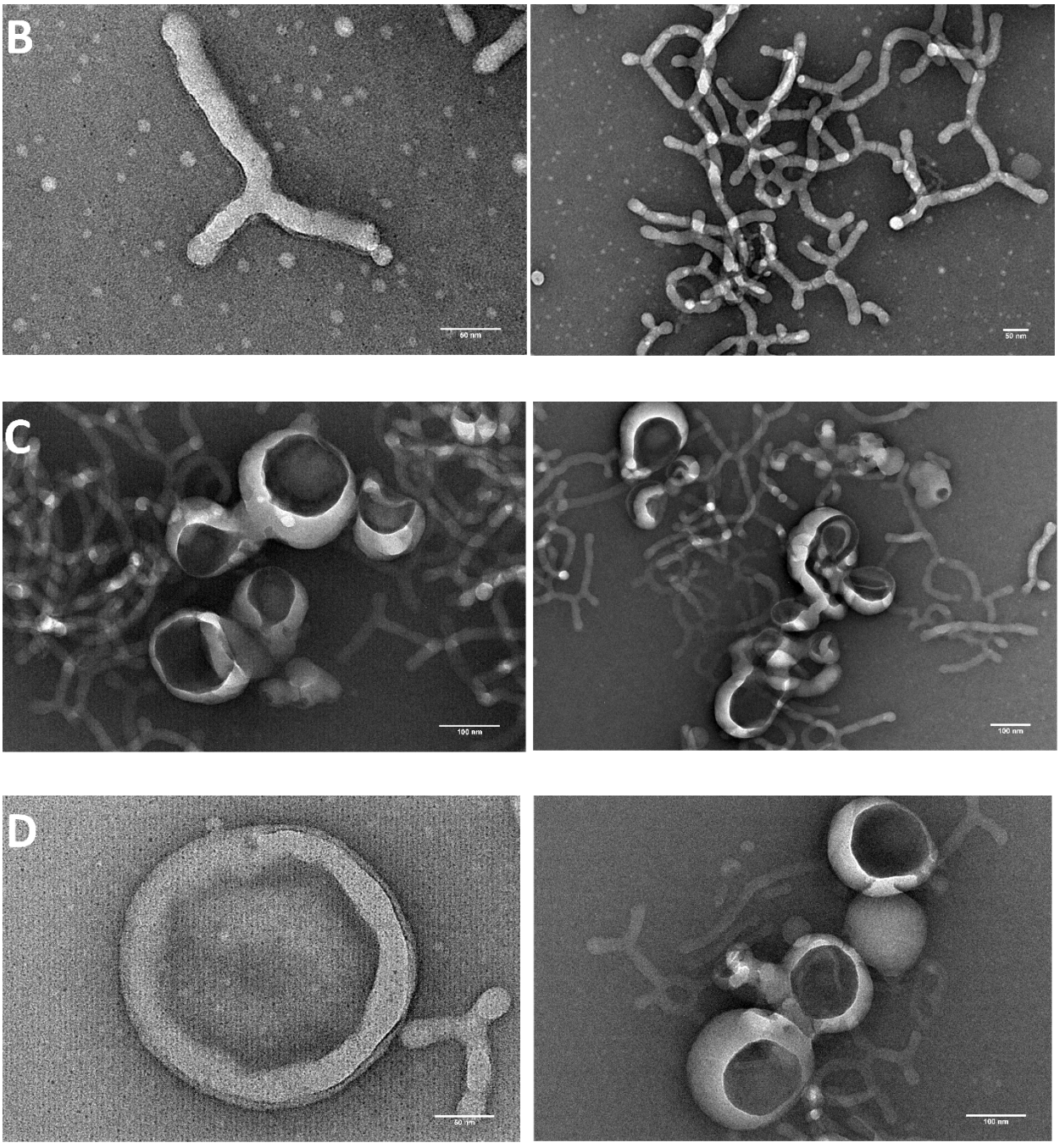
B
50 nm
50 nm
C
100 nm
100 nm
D
50 nm
100 nm

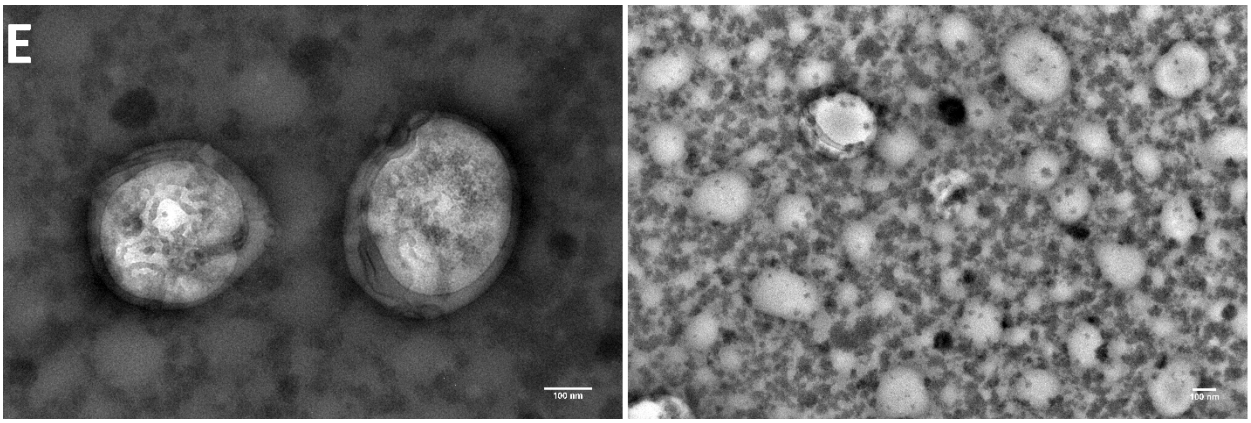

Figure 4.3. Transmission electron microscopic images of negatively stained polymersomes: (A) PEG_{1900}-S-S-PLA_{900}, (B) PEG_{1900}-S-S-PLA_{1700}, (C) PEG_{1900}-S-S-PLA_{1950}, (D) **P4**, and (E) **P5**.

Table 4.1: Diblock, amphiphilic, redox-sensitive copolymers and their observed morphology.

Polymer	**% Hydrophilic Fraction (f)**	**Observed Morphology**	**Polymersome Name**
PEG_{1900}-S-S-PLA_{900}	68	Micelles, small spheres	-
PEG_{1900}-S-S-PLA_{1700}	53	Mostly bicelles, worms	-
PEG_{1900}-S-S-PLA_{1950}	49	Mostly bicelles, a few vesicles	-
PEG_{1900}-S-S-PLA_{3600}	35	bilayered vesicles, a few bicelles	**P4**
PEG_{1900}-S-S-PLA_{5800}	25	Bilayered vesicles (polymersomes)	**P5**

Because only the PEG_{1900}-S-S-PLA_{3600} and PEG_{1900}-S-S-PLA_{5800} polymers formed vesicles (polymersomes **P4** and **P5**, respectively, Table 4.1), all further studies were performed with these two formulations. We determined the average size distributions, zeta potentials, and electrophoretic mobility values of these polymersomes using a dynamic light-scattering instrument (Table 4.2). We observed that the average hydrodynamic diameter of the **P5** polymersome (209 ± 34 nm) was higher compared to **P4** (157 ± 68 nm). This difference in size

is likely due to the higher molecular weight of the PEG_{1900}-S-S-PLA_{5800} polymer compared to PEG_{1900}-S-S-PLA_{3600}. Dynamic light-scattering experiments also showed that the size distribution was quite disperse, ranging from 25 nm to 700 nm (Figure 4.4). These sizes for the polymersomes are large and may not be ideal for passive tumor targeting that employs the enhanced permeability and retention effect [295]. However, the vesicles can be extruded to smaller sizes, if needed, for future applications.

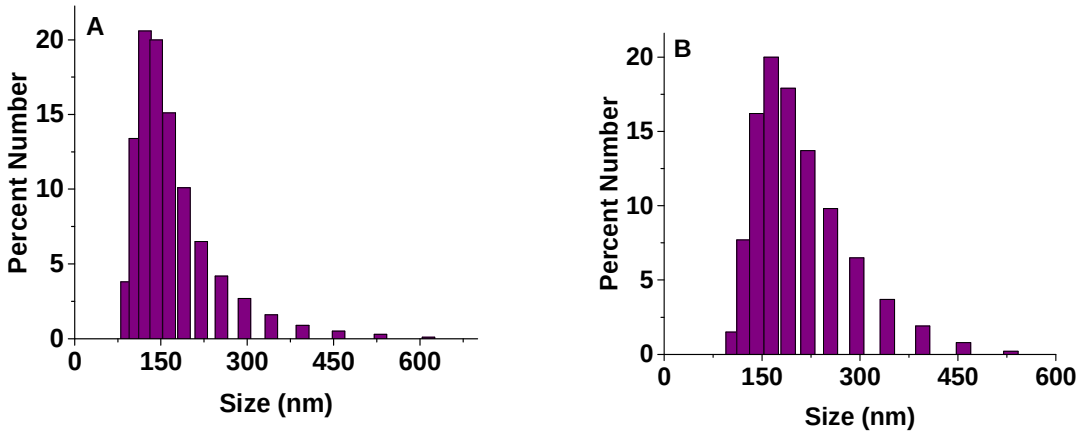

Figure 4.4. Representative size distribution for the number of structures formed by different polymers with the dynamic light-scattering method using a Zetasizer instrument: (A) P4 and (B) P5.

Table 4.2. Physical characterization of the **P4** and **P5** polymersomes (n = 5).

Polymersomes	Zeta Potential (mV)	Mobility (μm cm/Vs)	Size (nm)	PDI
P4	-3.2 ±0.5	-0.25 ± 0.03	157 ± 68	0.58 ± 0.07
P5	-2.4 ±0.6	-0.23 ± 0.04	209 ± 34	0.64 ± 0.03

Structural studies in the presence of reducing agents: Prior to any release studies with polymersomes, we tested the copolymers' sensitivity toward reducing agents. In this endeavor, the PEG_{1900}-S-S-PLA_{3600} and PEG_{1900}-S-S-PLA_{5800} $_{co}$polymers were dissolved in THF and

exposed to the reducing agent glutathione (GSH, 5 mM). Because cytosolic-concentration glutathione (GSH) ranges from 5 mM to 15 mM [186], we incubated the copolymers with 5 mM of GSH for an hour and then determined any degradation by gel permeation chromatography (Figure 4.5). The retention times (R_t) of both copolymers (PEG_{1900}-S-S-PLA_{3600} and PEG_{1900}-S-S-PLA_{5800}) showed a shift toward lower average molecular weight (increased R_t) components, indicating cleavage of the disulfide bond that connects the PEG and PLA parts.

We also studied the effect of glutathione (5 mM) on the morphology and size of the **P4** and **P5** polymersomes by employing atomic force microscopy. We observed that, before treatment, the polymersomes were spherical (Figure 4.6, before treatment). After 1 hour of incubation with 5 mM GSH, the spherical structures of the polymersomes were completely destroyed (Figure 4.6, after treatment).

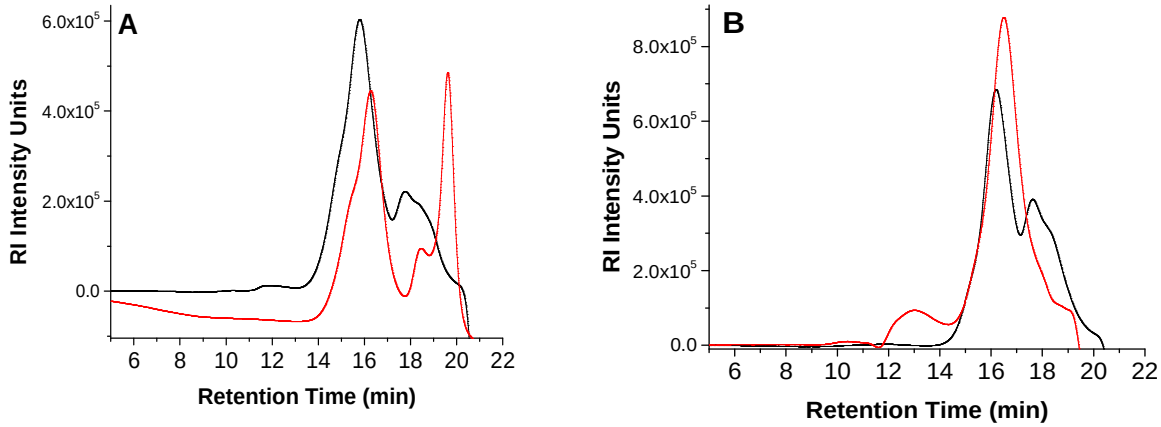

Figure 4.5. Gel permeation chromatography of the (**A**) PEG_{1900}-S-S-PLA_{3600} and (**B**) PEG_{1900}-S-S-PLA_{5800} polymers before (black trace) and after (red trace) incubation with 5 mM of GSH for 60 minutes.

Demonstration of the polymersomes' echogenicity: We have previously established that echogenic liposomes can be prepared in the presence of at least 100 mM of mannitol as a cryoprotectant [175], and the ideal concentration is 320 mM. In this study, we used 320 mM of mannitol to prepare the echogenic polymersomes. The defects in the encapsulating layer created during the freeze-thaw and lyophilization process (mannitol is a weak cryoprotectant and

cannot provide adequate protection for the bilayer) allow entrapment of air during the reconstitution of the lyophilized powder in a buffer solution [112, 172]. This method allows the entrapment of air inside vesicles, enabling them to reflect ultrasound. Although the exact location of air has not been determined conclusively, there are reports of air being trapped in the hydrophobic part of shell or inside the aqueous interior [230].

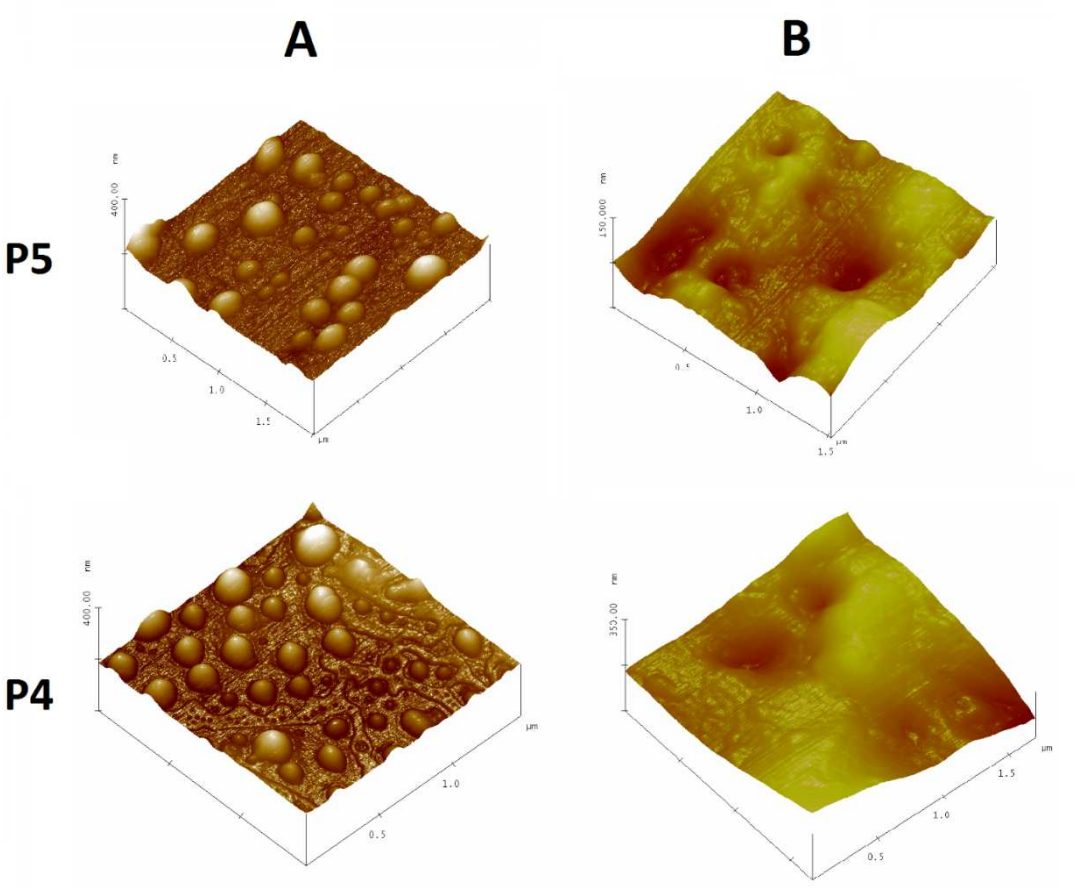

Figure 4.6. Atomic force microscopic images of **P5** polymersomes and **P4** polymersomes before (A) and after incubation (B) with 5 mM of glutathione for 1 hour.

To demonstrate echogenicity of the polymersomes, we studied their acoustic properties using an *in-vitro* acoustic setup (shown in Figure 4.1) and diagnostic ultrasound imaging. The excitation pulse consisted of a 32-cycle sinusoidal wave with a frequency of 3.5 MHz and with an acoustic pressure amplitude of 250 kPa. A polymersome concentration of 10 µg/mL was used for all *in-vitro* acoustic experiments without any problem of signal attenuation due to the setup

design. Figure 4.7 shows the scattered response from the **P4** and **P5** polymersome samples. Note that, for the **P5** batch, both second-harmonic and subharmonic components were detected in the scattered acoustic spectra. Hence, all three components, i.e., fundamental, subharmonic, and second-harmonic, are shown for comparison. Unlike the nonlinear response from microbubble-based contrast agents [296], the detection of nonlinear responses from the **P5** polymersomes was inconsistent. For the **P4** polymersomes, the nonlinear components were consistently absent in all experiments and, hence, are not shown here. The lack of a nonlinear response can either be due to the lower pressure amplitude (250 kPa) used here or due to the inherent acoustic properties of these polymersomes. Further studies are presently being conducted to verify these hypotheses.

We observed that the **P5** polymersomes show around 20 dB, 10 dB, and 4 dB enhancements over the control (i.e., without any polymersomes) for the fundamental, subharmonic, and second-harmonic components (Figure 4.7). However, the enhancement was much weaker for the **P4** polymersomes; it was around 8 dB for the fundamental component. This finding indicated that modifying the copolymers' PLA block enables us to tune their acoustic properties. Because the bilayers are made of ampliphilic copolymers, we expected these polymersomes to be mechanically stable. To test this hypothesis, we performed time-dependent scattering measurements with both batches (Figure 4.7C). The scattered response was stable for both batches with around 5 dB of decay over 10 minutes.

Echogenicity was also confirmed by imaging with a Terason t3200 ultrasonic medical imaging system using a 4-15 MHz transducer. Reconstituted polymersomes reflected the ultrasound, indicating the presence of entrapped air (Figure 4.8), whereas the control samples (polymersomes before freeze drying) were devoid of such reflections. The mean and maximum grey-scale values were obtained by analyzing images with ImageJ software, and the comparison is shown in Figures 4.8E and 8F. The echogenic **P4** and **P5** polymersomes (Figure 4.8, Panels C

and D) showed higher grey-scale values compared to their non-echogenic counterparts (controls; Figure 4.8, Panels A and B). Moreover, the response from **P5** polymersomes was higher than the **P4** polymersomes (Figure 4.8, panels C and D), further corroborating our results with the acoustic scattering experiments (Figure 4.7). We also noticed that adding 5 mM of GSH to the polymersome samples reduced the ultrasound reflectivity (Appendix C).

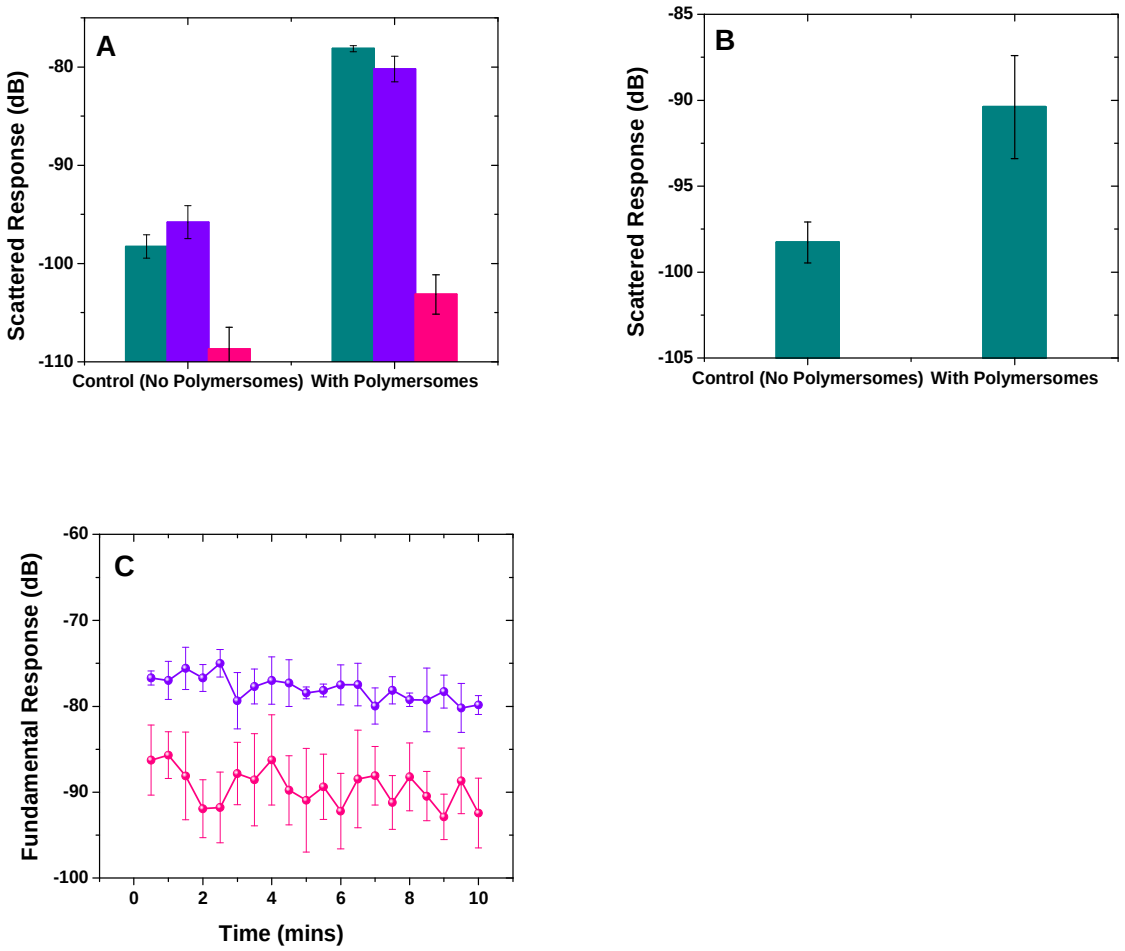

Figure 4.7. Ultrasound scattered responses from echogenic polymersomes (A) P5 and (B) P4 (dark cyan: fundamental, violet: subharmonic, and pink: second-harmonic responses). (C) Time-dependent scattering responses from polymersomes P5 (violet) and P4 (pink) (n = 3).

Demonstration of redox-triggered release from the polymersomes: After confirming the echogenicity, we checked the redox-triggered release from these polymersomes. In this

endeavor, we encapsulated 10 μM of calcein dye in the **P4** and **P5** polymersomes, and we monitored the release by using the cobalt (II) quenching method. We studied the release profiles with 3 different reducing agents: glutathione (GSH), cysteine (CYS), and dithiothreitol (DTT) at concentrations ranging from 50 μM (extracellular concentration of thiol) to 5 mM (cytosolic concentration of thiol) [197]. Glutathione and cysteine are the primary reducing agents that maintain the redox equilibrium between the intracellular (slightly reducing) and extracellular environments within tissues (slightly oxidizing) [185]. We observed that the reducing agents rapidly released contents from the polymersomes within 10 minutes of incubation.

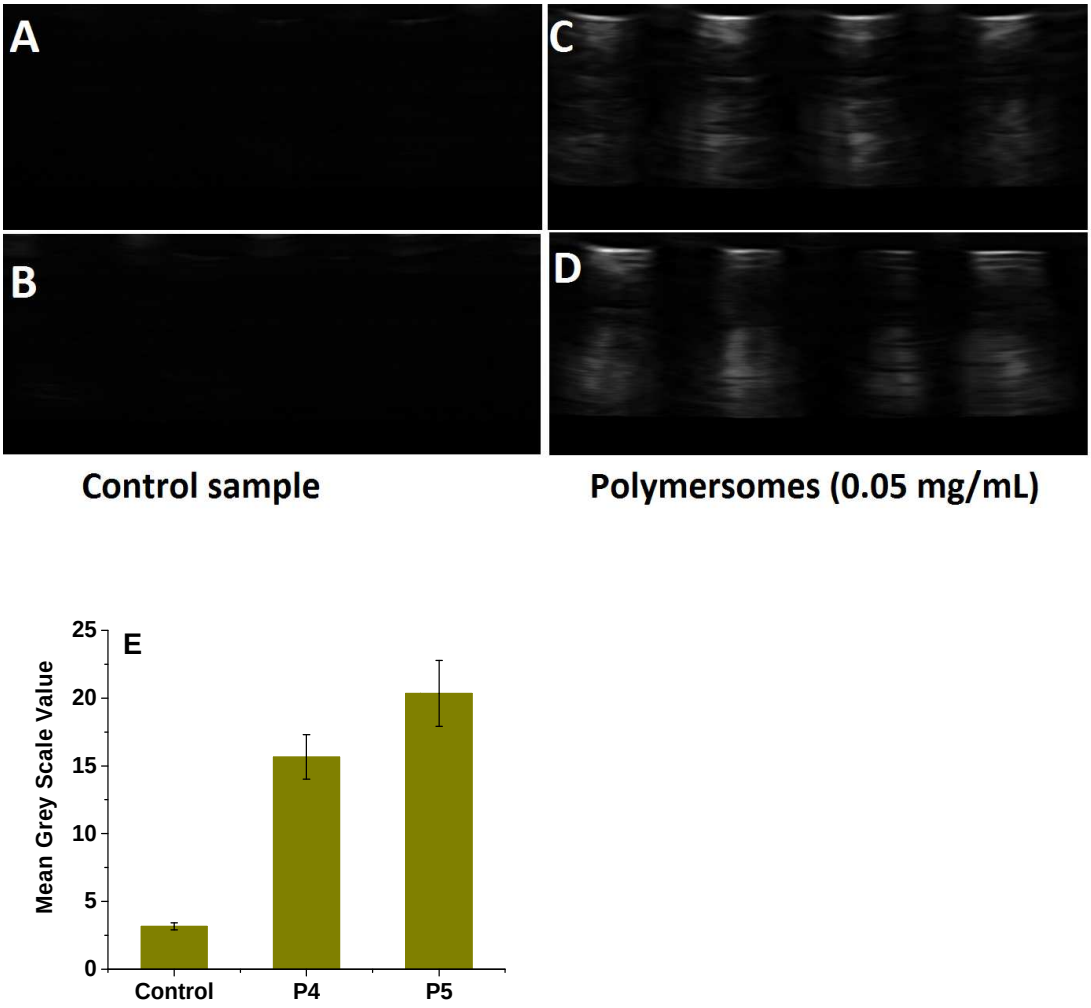

Figure 4.8. Diagnostic-frequency ultrasound imaging and mean grey-scale values for the polymersomes: (A) P5 polymersome before free drying (control), (B) P4 polymersome before

freeze drying (control), (C) P5 polymersomes after freeze drying, (D) P4 polymersomes after freeze drying, (E) mean grey-scale values, and (F) maximum grey-scale value (n = 3).

Figures 4.9 and 4.10 show the results for the release experiments with increasing concentrations of different reducing agents. When incubated in 5 mM of GSH and DTT, both the **P4** and **P5** polymersomes showed a very rapid burst release. We observed around 80% of content release from both polymersomes when incubated with 5 mM of GSH, whereas less than 5% release was observed when incubated with 50 µM of GSH.

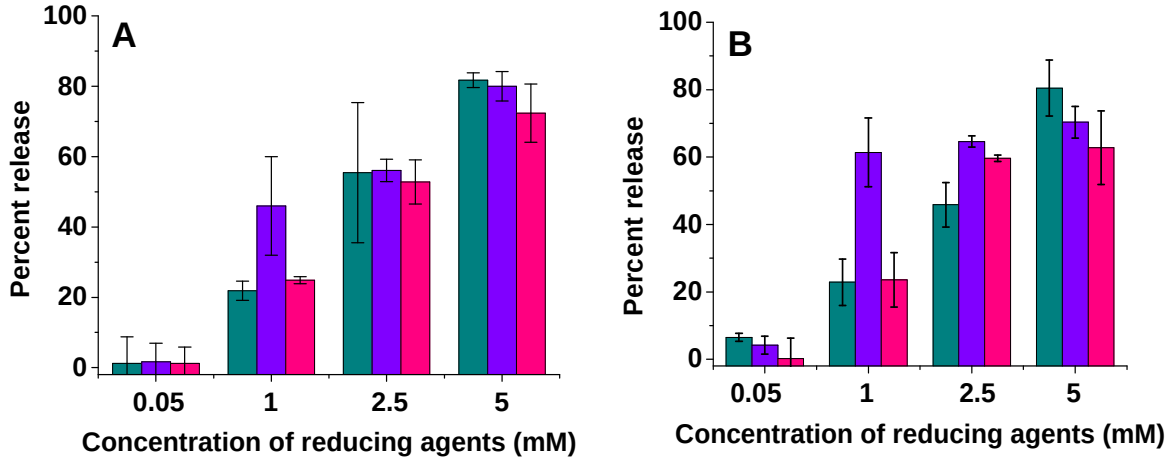

Figure 4.9. Redox-triggered release as a function of the reducing agents' concentration (dark cyan: glutathione, violet: dithiothreiotol, and pink: cysteine) from (**A**) polymersome **P5** and (**B**) polymersome **P4** (n = 3).

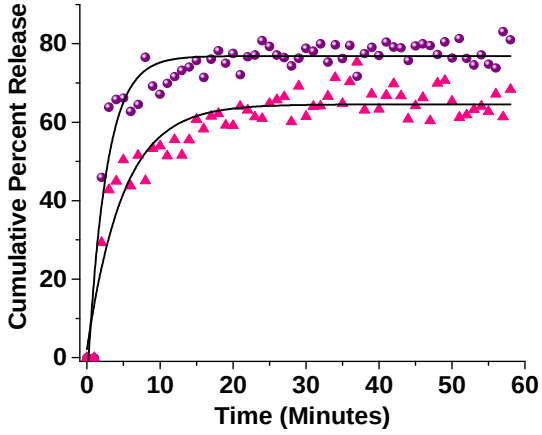

Figure 4.10. Representative release profiles of calcein from polymersomes **P4** (pink triangles) and **P5** (violet spheres) when incubated with 5 mM of cysteine for an hour. The fitted curves, according to a single exponential-rate equation, are shown as black traces.

DTT has a very low redox potential (E_o = −0.332 V at pH 7.0), and it rapidly reduces the disulfide bonds compared to glutathione (E_o = +0.062 V) and cysteine (E_o = +0.025 V) [199]. The release profiles of the polymersomes treated with 5 mM of cysteine can be fitted with a single exponential-rate equation (Figure 4.10, black trace) with rate constants of $(39 \pm 3) \times 10^{-2}$ s^{-1} for **P5** polymersomes and $(20 \pm 2) \times 10^{-2}$ s^{-1} for **P4** polymersomes. These results indicate that the polymersomes would be stable while circulating in the blood and extracellular spaces, releasing less than 5% of their contents. After endocytosis, they will rapidly release the encapsulated contents inside the cell cytosol.

Effect of ultrasound on the redox-triggered release from the polymersomes: Following the demonstration of reductive destabilization for the **P4** and **P5** polymersomes, we proceeded to determine their sensitivity to diagnostic-frequency ultrasound. For this purpose, we exposed the polymersomes to a 1 MHz ultrasound (continuous wave) for different time intervals, and monitored the release of the encapsulated calcein. We noted, *a priori*, that unlike liposomes, polymersomes do not exhibit high domain exchanges [297], and this may pose potential challenges for ultrasound-triggered release. We observed that both the **P4** and **P5** polymersomes failed to release the encapsulated dye in the presence of the applied ultrasound. Increasing the ultrasound's intensity (0.1 to 2 W/cm^2), duty cycles (10% to 100%), and duration (1 minute to 15 minutes) of application did not have any observable effects either. We attributed these negative results to the mechanical and thermodynamic stability of the polymersomes' bilayer. By employing transmission electron microscopy, we observed the bilayers to be 20-30 nm thick (Figure 4.3, Panels D and E), attesting to the mechanical stability of the polymersomes.

Subsequently, we studied the effects of simultaneously applying a reducing agent and ultrasound on the contents released from the polymersomes. Although we observed some enhancements (5-10%) in the release due to the application of ultrasound (with the reducing agents GSH and CYS), the results were inconsistent. This lack of consistency may be due to the wide size distribution of polymersomes with a polydispersity index of 0.6 (Table 4.2). Because the polymersomes have heterogeneous sizes, they are expected to respond to ultrasound differently; the larger-sized vesicles couple more efficiently with the ultrasound waves. In addition, the reducing agents alone release the encapsulated contents rather rapidly (Figures 4.9 and 4.10). Because the reducing agents destroy the polymersome structures (Figure 4.6), the entrapped air is likely to escape, making polymersomes less responsive to the applied ultrasound.

Simultaneous encapsulation of gemcitabine and doxorubicin in the polymersomes: Following these studies, we proceeded to simultaneously encapsulate the anticancer drugs, gemcitabine and doxorubicin, into the **P4** and **P5** polymersomes. This combination is reported to be more effective compared to the individual drugs [298]. Currently, more than 80 clinical trials are in progress (www.clinicaltrials.gov; accessed on February 28, 2014) to test the efficacy of liposomal doxorubicin (Doxil) in combination with injections of gemcitabine for the treatment of various cancers [258, 267, 299].

Prior to encapsulating doxorubicin and gemcitabine into the polymersomes, we developed a UV-spectrophotometric, dual-wavelength method to determine their solution concentrations. Although liquid chromatographic methods are frequently-used for simultaneous determination of two or more drugs, they are expensive and time consuming [300, 301]. Specifically, we selected two wavelengths so that doxorubicin has equal absorbance at both the wavelengths and that, at one of the wavelengths, gemcitabine absorbance is negligible. By comparing the absorption spectra for the two drugs (Figure 4.11), we selected 480 nm and 276

nm as the wavelengths of choice. At 480 nm, doxorubicin can be determined reliably because gemcitabine absorbance is negligible at this wavelength. Because doxorubicin absorbs equally at 276 nm and 480 nm, gemcitabine can be determined at 276 nm by subtracting the absorbance of doxorubicin at 480 nm from the total absorbance at 276 nm (Figure 4.11). Following this strategy, we established a standard calibration curve for both drugs (Appendix C).

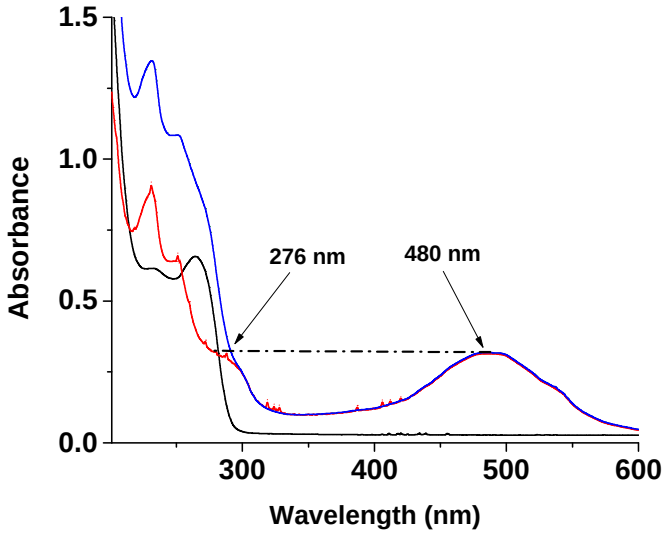

Figure 4.11. Dual-wavelength UV spectrophotometric method for simultaneous determination of gemcitabine and doxorubicin. The absorption spectra for gemcitabine (black trace), doxorubicin (red trace), and the combination (blue trace) are shown.

We compared the efficiencies for the passive- and active-loading methods to encapsulate gemcitabine and doxorubicin into the polymersomes. For passive entrapment, the drugs were dissolved in a 10 mM HEPES buffer (pH = 7.4), and the solutions of the polymers in THF were added slowly. For active loading, we used the pH gradient method. We prepared the polymersomes in a citrate buffer (pH 4.0), and the external pH was neutralized by adding solid sodium bicarbonate. The polymersomes were then incubated with the drug combination. The unencapsulated drugs were separated from the polymersomes, and encapsulation efficiency was established by measuring the absorbance before and after gel filtration.

The encapsulation efficiencies with the passive entrapment method were 43 ± 8% for gemcitabine and only 13 ± 4% for doxorubicin with both the **P4** and **P5** polymersomes. The pH gradient method produced a similar encapsulation efficiency for gemcitabine (43 ± 2%); however, the efficiency for doxorubicin entrapment was higher (27 ± 7%). We noticed that entrapment efficiencies were similar for both **P4** and **P5** as well as for targeted and non-targeted polymersomes (Table 4.3). We attributed the moderate drug entrapment to the rigidity of the polymersome bilayers which minimizes the molecules' entry into the aqueous core. We also noted that the higher molecular weight and larger size of doxorubicin (MW: 543) led to a lower encapsulation efficiency compared to gemcitabine (MW: 263.) Heating the polymersomes above their glass transition temperature (65 °C) did not improve the encapsulation.

Table 4.3. Encapsulation efficiencies of gemcitabine and doxorubicin into the polymersomes using the pH gradient method (n = 3).

Polymersomes	**Gemcitabine**		**Doxorubicin**	
	Conc. (μg/mL)	**Percent Entrapment**	**Conc. (μg/mL)**	**Percent Entrapment**
P5	31.6 ± 6.1	41.7 ± 4.5	20.8 ± 7.4	27.2 ± 7.5
P5 Folate	39.6 ± 9.8	46.1 ± 9.1	20.8 ± 5.8	27.4 ± 5.5
P4	34.7 ± 7.5	45.7 ± 6.0	20.7 ± 7.9	27.2 ± 7.0
P4 Folate	29.9 ± 4.3	39.4 ± 2.2	16.9 ± 5.7	22.2 ± 5.7

Demonstration of release using monolayer cell culture: Having optimized the encapsulation of the drugs, we proceeded to evaluate the active targeting of these polymersomes to cancer cells. For this endeavor, 1 mol% folate conjugated lipid (DSPE-PEG-Folate, commercially available from NANOCS, NY) with PEG_{3400} (for **P4** polymersomes) and PEG_{5000} (for **P5** polymersomes) was added to the polymers during polymersome preparation. We

selected the folate receptor overexpressing pancreatic ductal carcinoma (PANC-1) and breast cancer (MCF-7) cells for the uptake studies. After incubating the polymersomes for different times, we imaged the cells using a fluorescence microscope (Figure 4.12 for the PANC-1 cells; the corresponding images for the MCF-7 cells are included in the Appendix C). We noticed that polymersomes incorporating 1 mol% of the folate lipid were taken up by cells more effectively compared to the polymersomes without the folate lipid or the free drugs. The MCF-7 cells showed faster and higher uptake of the folate-targeted polymersomes compared to PANC-1 cells. Analyses of the mean red fluorescence intensities for all images indicated that there was no significant uptake difference for the initial 30 minutes (Figure 4.13). However, as the incubation period increased to 60 minutes, we observed enhanced cellular uptake for the folate-targeted polymersomes compared to the non-targeted counterparts and free drugs (Figures 4.12 and 4.13).

After demonstrating successful uptake for folate-targeted polymersomes, we assessed their ability to kill these folate-receptor overexpressing cancer cells. We exposed the MCF-7 and PANC-1 cells to different treatments for various time intervals, and we analyzed cell viability by employing the AlamarBlue® assay [302]. Both the **P4** and **P5** polymersomes showed significantly higher killing of MCF-7 cells compared to the free gemcitabine + doxorubicin combination (Figure 4.14A). Even non-targeted **P5** polymersomes showed significant toxicity enhancement toward MCF-7 cells compared to the free drugs together. We also tested these polymersomes with the PANC-1 cell line, and we noticed that, although there was significant killing (around 60%) with folate-targeted polymersomes, it was not significantly better than non-targeted polymersomes and free drugs. These observations supported our results with uptake experiments where a significant uptake enhancement for folate-targeted polymersomes was observed in MCF-7 cells compared to the PANC-1 cells.

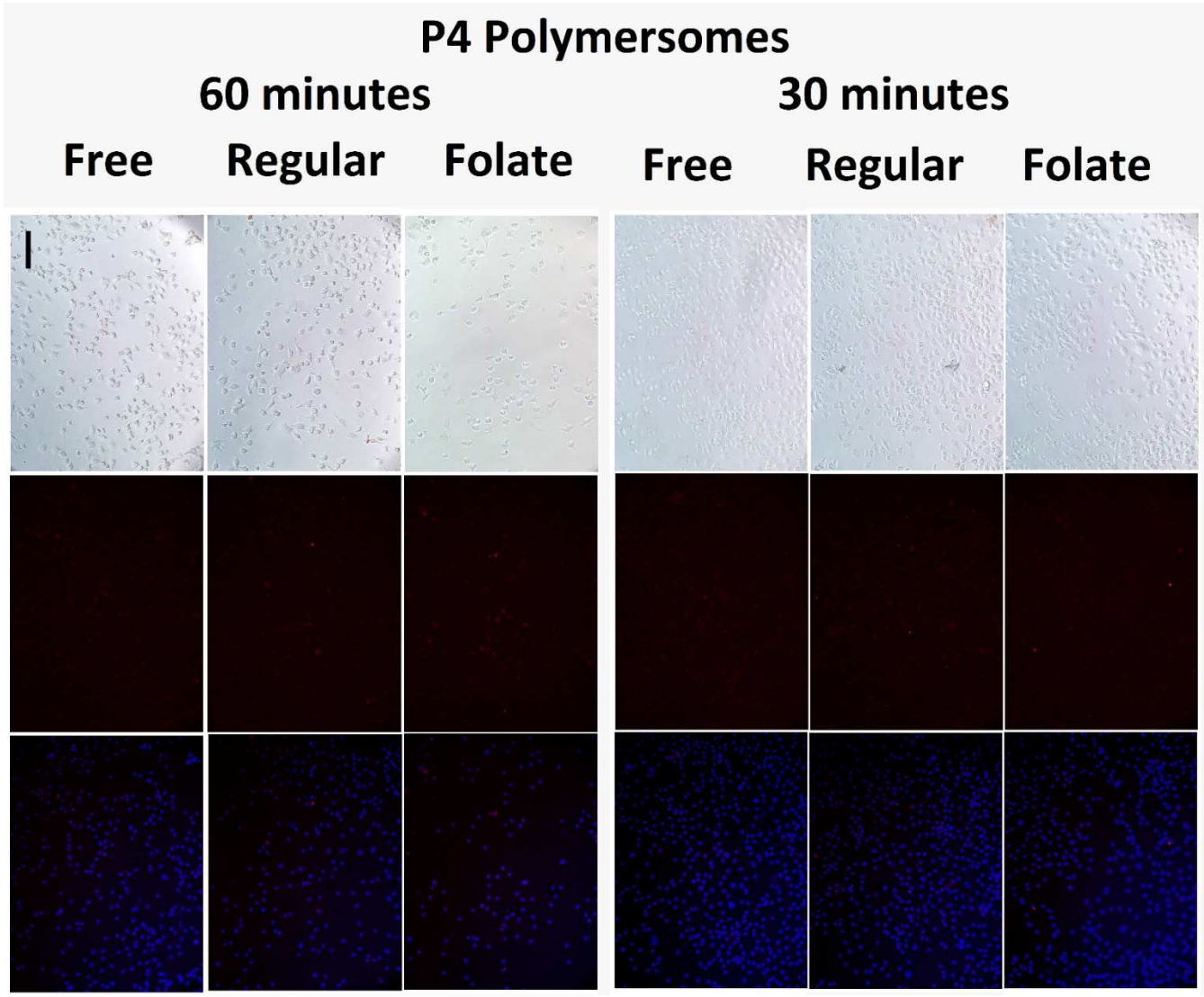
P4 Polymersomes
60 minutes
30 minutes
Free
Regular
Folate
Free
Regular
Folate

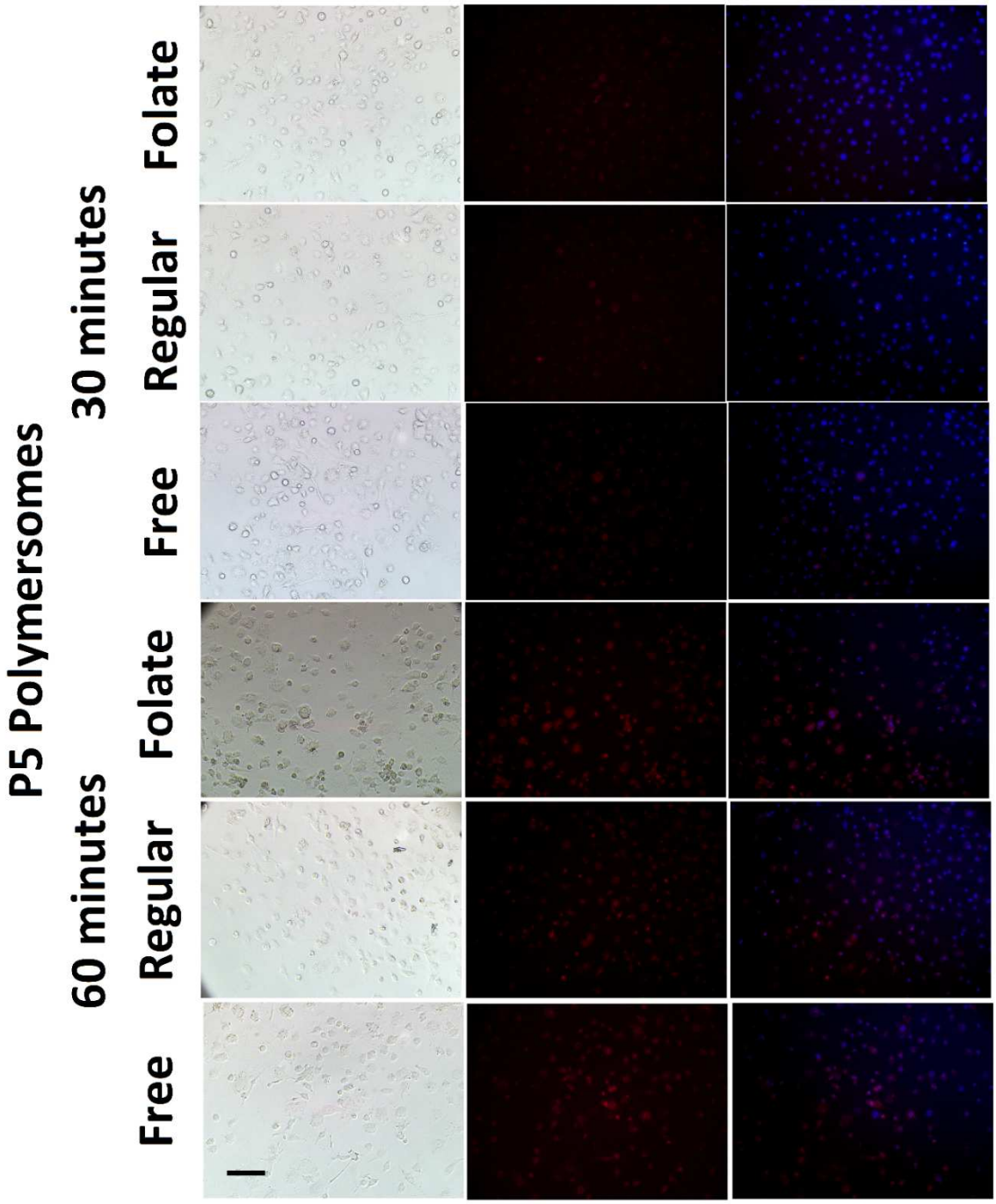

Figure 4.12. Fluorescence microscopic images of folate-targeted **P4** and **P5** polymersomes' uptake by PANC-1 cells as a function time. (Scale bar: 100 μm).

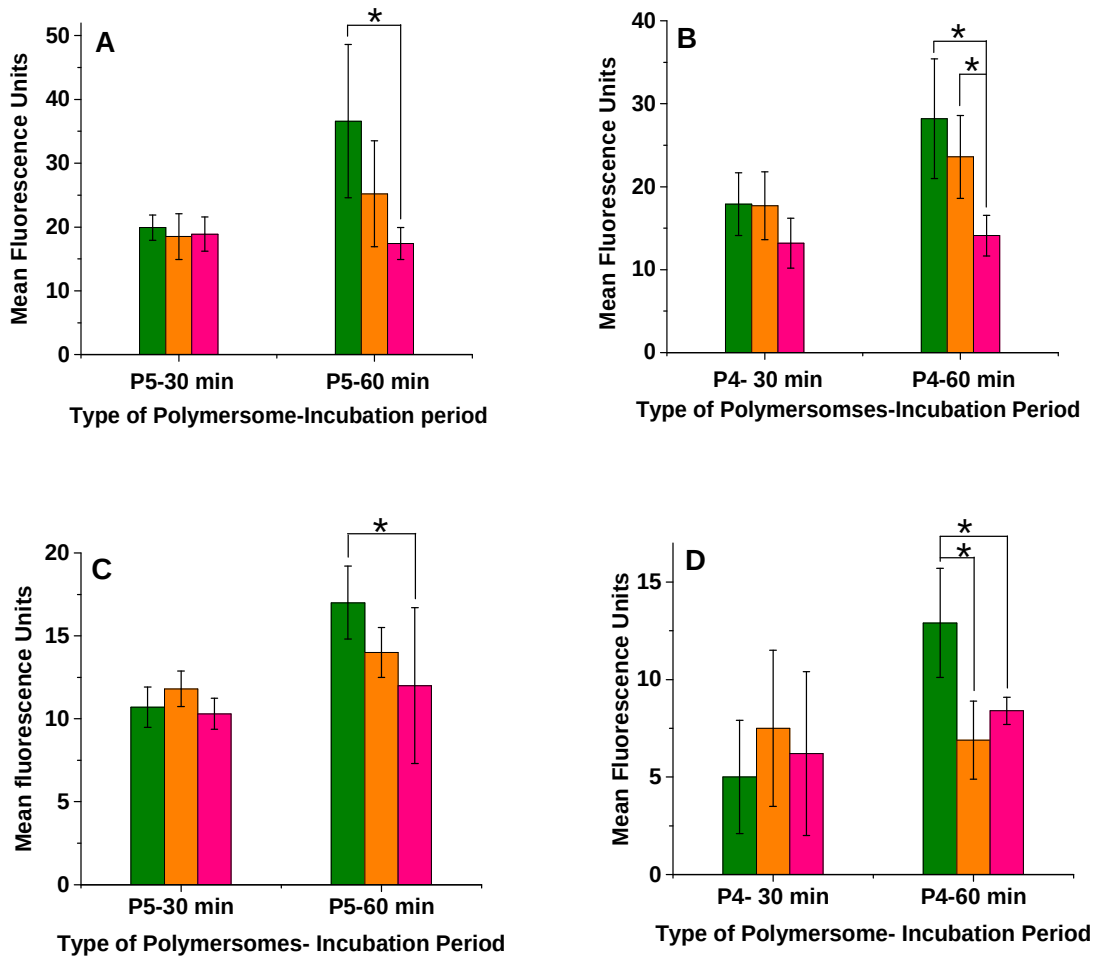

Figure 4.13. Mean fluorescence analysis for the uptake of polymersomes by MCF-7 (**A** and **B**) and PANC-1 (**C** and **D**) cells. Green: folate-targeted polymersomes; orange: non-targeted, regular polymersomes; and pink: free gemcitabine and doxorubicin. (*P < 0.05, n = 4).

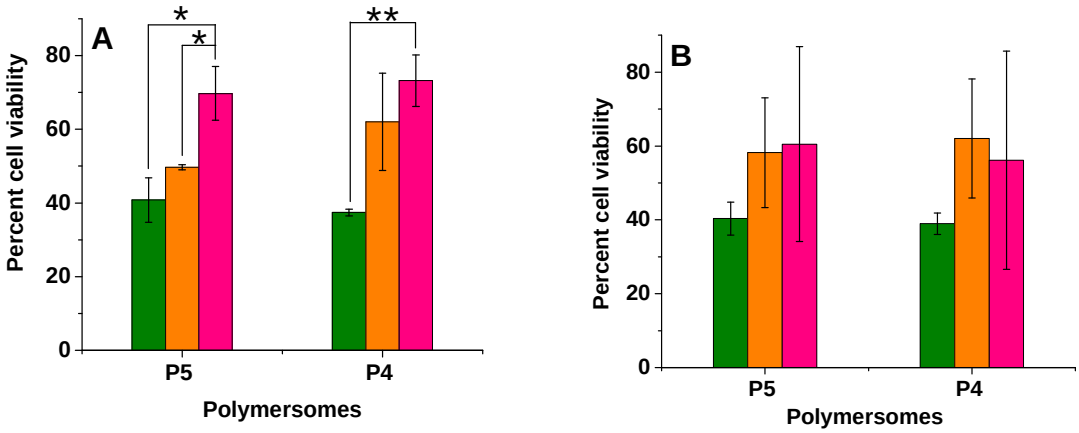

Figure 4.14. Cell viability with folate-overexpressing MCF-7 cells (**A**) and PANC-1 cells (**B**) after 48-hours incubation. Green: folate-targeted polymersomes, orange: non-targeted polymersomes, and pink: free gemcitabine and doxorubicin. (*P < 0.05, **P < 0.01, n = 5).

Demonstration of release using three-dimensional, spheroid cell culture: Although studies with a monolayer cell culture are fast, cost effective, and demonstrate a proof of concept, they also have limitations. For example, a monolayer cell culture bears little resemblance to the complex, three-dimensional growth of tumors *in vivo*. Multicellular tumor spheroids (3D cell culture) are models of intermediate complexity between the monolayer culture and tumors *in vivo* [303]. Among the various reported procedures to prepare the 3D spheroids, the liquid overlay method is widely used and convenient [292]. Following this protocol, we embedded the MCF-7 cells onto agar and added the growth media. Subsequently, the spheroids were prepared in 24-well plates by centrifuging to aggregate the cells at the center (Figure 4.15A). The plates were placed in an incubator, undisturbed, and we measured the spheroid area after 3 days. When observed under a light microscope, the growing cell spheroids showed three distinct regions, similar to in vivo tumors (Figure 4.15B). The center of the spheroid was necrotic; the cells died due to the limited availability of oxygen and nutrition (region 1). This center was surrounded by a region of inactive, but live cells (region 2). The actively proliferating cells were at the periphery of the spheroids (region 3), which had direct access to the media (region 4). This morphology of 3D spheroids makes them a better tool for conducting *in-vitro* cellular experiments. Spheroids varied in size from 1 mm to 2 mm with distinct areas as explained earlier.

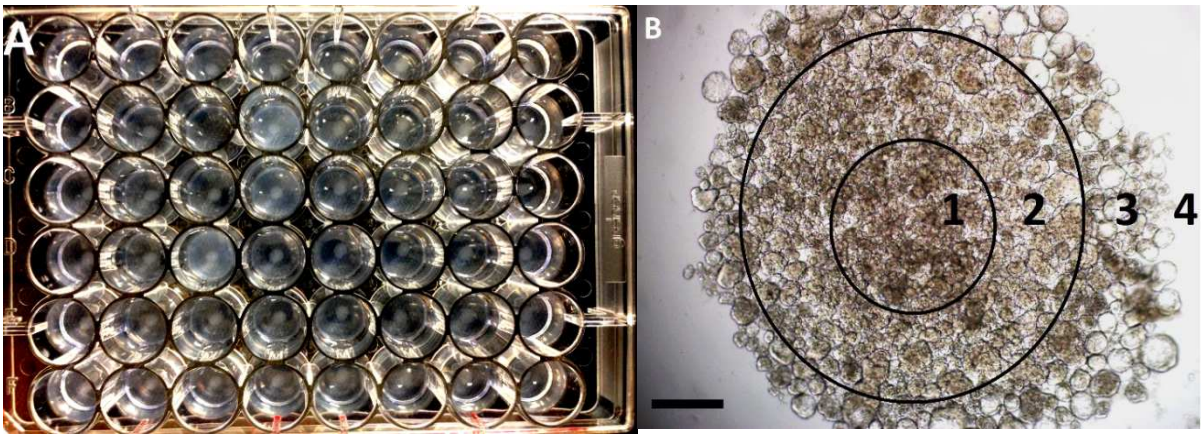

Figure 4.15. Spheroid culture of MCF-7 cells: (A) 24-well plate coated with agar; cell aggregation was facilitated by centrifugation. (B) A cell spheroid showing three distinct regions which mimic the in vivo conditions. Region **1**: central necrotic area (hypoxic) which gets a lesser amount of nutrition and oxygen; Region **2**: inactive/resting cells which grow slowly; Region **3**: active/proliferating cells which grow rapidly; and Region **4**: nutrition/media. (Scale bar at the bottom: 400 μ).

On 10th and 11th day after preparation, we exposed the MCF-7-cell spheroids to different treatments for 48 hours (Figure 4.16A). Areas of spheroids were monitored for each treatment group, normalized and plotted as a function of time (Figures 4.16B and 4.16C). We observed that folate-targeted **P5** polymersomes were most effective among all the treatments, eliciting a significant reduction in size for the spheroids (Figure 4.16B) compared to the non-targeted polymersomes and the free drugs. While the control spheroids grew by 185% of their initial size, average growth was restricted to only 73% in the presence of the folate-targeted **P5** polymersomes. We also noticed that non-targeted polymersomes did not show any improvement over the free-drug treatment. This implies that the folate targeting improved the uptake of polymersomes not only in the monolayer, but also in the three-dimensional spheroid cell culture. To our surprise, the folate-targeted **P4** polymersomes did not show any additional advantage over non-targeted polymersomes and the free-drug combination (Appendix C). We do not have an explanation for this observation.

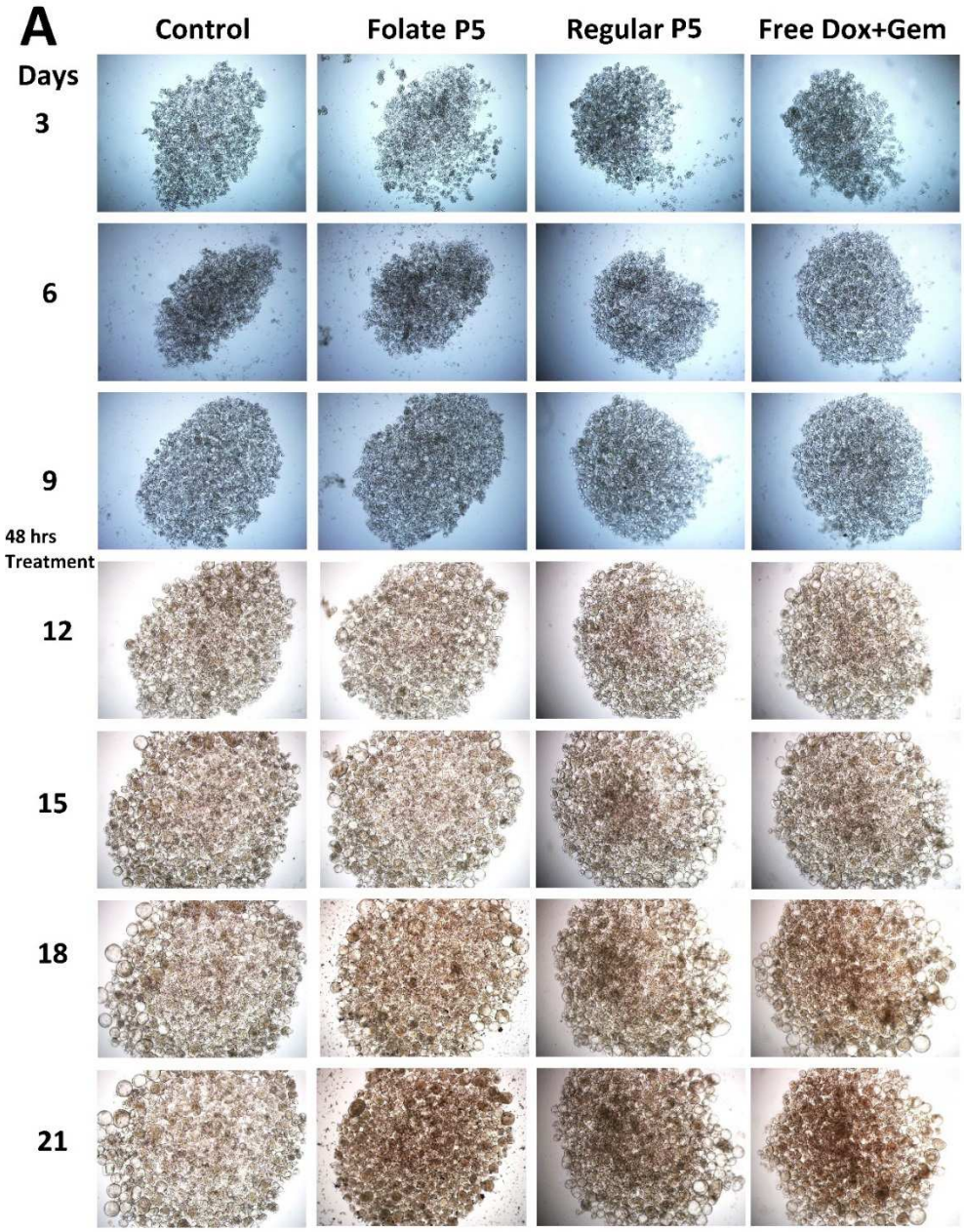
A
Control
Folate P5
Regular P5
Free Dox+Gem
Days
3
6
9
48 hrs
Treatment
12
15
18
21

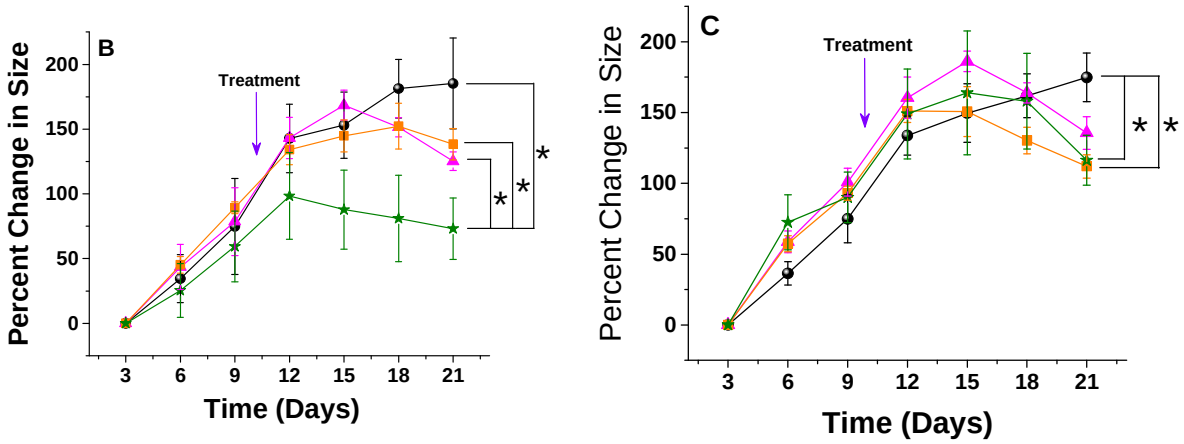

Figure 4.16. (**A**) Images of MCF-7 cellular spheroids treated with **P5** polymersomes. Spheroids were exposed to three different treatments for 48 hours on the 10th and 11th days. (**B**) Growth curves for the spheroids treated with **P5** polymersomes. (**C**) Growth curves for spheroids treated with **P4** polymersomes. Green stars: folate-targeted polymersomes, orange rectangles: non-targeted polymersomes, pink triangles: free gemcitabine and doxorubicin, and black spheres: control samples. (*P < 0.05, n = 5).

Conclusion

We have successfully prepared echogenic, redox-sensitive, targeted polymersomes. Ultrasound-scattering and imaging experiments confirmed the echogenicity of the vesicles. These polymersomes showed excellent release profiles when incubated with cytosolic concentrations of reducing agents, releasing more than 80% of the contents within 20 minutes. However, in serum levels of reducing agents, minimal release was observed. When a folate lipid was incorporated in the bilayer, the polymersomes showed an enhanced uptake with folate-receptor overexpressing breast- and pancreatic-cancer cells. A combination of the two anticancer drugs, gemcitabine and doxorubicin, was successfully encapsulated in the polymersomes. These targeted, dual-drug encapsulating polymersomes significantly decreased the viability of breast- and pancreatic-cancer cells in the monolayer as well as in spheroid cultures. Our results are expected to encourage further research about the use of ultrasound-

reflective polymersomes as multimodal drug carriers with targeting and triggered release properties.

GENERAL CONCLUSION AND FUTURE STUDIES

We have successfully addressed the problem of slow contents release with echogenic nanoparticles. We have demonstrated that echogenic nanoparticles can be successfully coupled to an internal trigger to rapidly release encapsulated contents. Combining two triggers offered better control over the release profiles of drugs from the nanoparticles. As these nanoparticles also carry air bubbles along with drug, they can be imaged using diagnostic frequency ultrasound, and have the potential to be tracked while in blood circulation. Folate targeting showed improved uptake of these particles by cancer cells leading to enhanced cytotoxicity. We have successfully demonstrated that proper combination of triggering and targeting strategies can be advantageous over existing nano formulations.

The nanoparticulate systems developed need further improvements to make them suitable for *in vivo* applications. For example, the liposomes need the PEG layer to render them long circulating characteristic. This step is not necessary for the polymersomes developed, as they contain PEG as the hydrophilic polymer block. PEGylation is reported to improve retention of echogenicity [304], thus it would be important to study its effect on ultrasound imaging as well triggered release. PEGylation would have different effects on different parameters of nanoparticles. After PEGlylation of MMP-9 responsive liposomes (Chapter 1), MMP-9 could find it difficult to access the **LP-4** peptide, and hydrolyze it to release the contents. Percent of peptide and PEGylated lipids in the bilayer could be very crucial to optimize the formulation. In case of PEGylated polymer coated ARLINs (Chapter 2), PEG groups can interfere with the linker reacting with POPE-G. This can potentially affect the polymerization and thus release and stability of ARLINs. For the polymersomes (Chapter 4), we have studied effect of changing the PLA molecular weight on structure and morphology. In future, it would be interesting to study the effect of molecular weights of the PEG part on size and morphology of the vesicles. The “f” value can be fine-tuned further to improve the encapsulation efficiency of polymersomes.

Lipid bilayer composition is very important for the stability of liposomes. In this dissertation, we have used POPC as the major lipid for the liposomes. Due to the low glass transition temperature, POPC may not be the optimal lipid for *in vivo* studies. Addition of cholesterol (up to 5%) is reported to improve stability of liposomes. It would be interesting to study the effect of cholesterol on stability these systems. Making the lipid bilayer stronger would definitely minimize passive release of contents from the liposomes. However, it should also be noted that as bilayer becomes stronger, it is more difficult for triggers to disturb the bilayer sufficiently to release the contents. Clearly, these two parameters needs to be carefully optimized such that we do not compromise either safety or efficiency of these nanoparticles.

After optimizing the composition and PEGylation of nanoparticles, next step for validation would be *in vivo* testing. Xenograft nude mouse models can be used to test efficacy of these particles to reduce/inhibit growth of tumors. We can inject either of the folate receptor over-expressing MCF-7, HeLa, or PANC-1 cells subcutaneously to obtain xenograft tumor. Anticancer drug (such as doxorubicin or/and gemcitabine) loaded nanoparticles can be injected to tumor bearing mice, and the size of tumor can be monitored to demonstrate the effectiveness. Diagnostic ultrasound imaging of mice will give us idea about the retention of echogenicity inside the *in vivo* system. It would be interesting to track echogenic nanoparticle, and observe their accumulation at tumor site employing diagnostic frequency ultrasound imaging.

REFERENCES

[1] Couvreur P. Nanoparticles in drug delivery: past, present and future. Adv Drug Deliv Rev. 2013;65:21-3.
[2] De Jong WH, Borm PJ. Drug delivery and nanoparticles:applications and hazards. Int J Nanomedicine. 2008;3:133-49.
[3] Kepczynski M, Nawalany K, Kumorek M, Kobierska A, Jachimska B, Nowakowska M. Which physical and structural factors of liposome carriers control their drug-loading efficiency? Chem Phys Lipids. 2008;155:7-15.
[4] Bangham AD, Standish MM, Watkins JC. Diffusion of univalent ions across the lamellae of swollen phospholipids. J Mol Biol. 1965;13:238-52.
[5] Gregoriadis G, Ryman BE. Liposomes as carriers of enzymes or drugs: a new approach to the treatment of storage diseases. Biochem J. 1971;124:58P.
[6] Gregoriadis G. Drug entrapment in liposomes. FEBS Lett. 1973;36:292-6.
[7] Gregoriadis G, Wills EJ, Swain CP, Tavill AS. Drug-carrier potential of liposomes in cancer chemotherapy. Lancet. 1974;1:1313-6.
[8] Kimelberg HK, Tracy TF, Jr., Biddlecome SM, Bourke RS. The effect of entrapment in liposomes on the in vivo distribution of [3H]methotrexate in a primate. Cancer Res. 1976;36:2949-57.
[9] Poste G, Papahadjopoulos D. Lipid vesicles as carriers for introducing materials into cultured cells: influence of vesicle lipid composition on mechanism(s) of vesicle incorporation into cells. Proc Natl Acad Sci U S A. 1976;73:1603-7.
[10] Olson F, Hunt C, Szoka F, Vail W, Papahadjopoulos D. Preparation of liposomes of defined size distribution by extrusion through polycarbonate membranes. Biochimica et Biophysica Acta (BBA)-Biomembranes. 1979;557:9-23.
[11] Szoka F, Jr., Papahadjopoulos D. Procedure for preparation of liposomes with large internal aqueous space and high capture by reverse-phase evaporation. Proc Natl Acad Sci U S A. 1978;75:4194-8.
[12] Huang C. Studies on phosphatidylcholine vesicles. Formation and physical characteristics. Biochemistry. 1969;8:344-52.
[13] Colley CM, Ryman BE. Liposomes as carriers in vivo for methotrexate. Biochem Soc Trans. 1975;3:157-9.
[14] Forssen EA, Tokes ZA. In vitro and in vivo studies with adriamycin liposomes. Biochem Biophys Res Commun. 1979;91:1295-301.
[15] Forssen EA, Tokes ZA. Use of anionic liposomes for the reduction of chronic doxorubicin-induced cardiotoxicity. Proc Natl Acad Sci U S A. 1981;78:1873-7.
[16] Forssen EA, Tokes ZA. Improved therapeutic benefits of doxorubicin by entrapment in anionic liposomes. Cancer Res. 1983;43:546-50.
[17] Gabizon A, Peretz T, Sulkes A, Amselem S, Ben-Yosef R, Ben-Baruch N, et al. Systemic administration of doxorubicin-containing liposomes in cancer patients: a phase I study. Eur J Cancer Clin Oncol. 1989;25:1795-803.
[18] Storm G, Roerdink FH, Steerenberg PA, de Jong WH, Crommelin DJ. Influence of lipid composition on the antitumor activity exerted by doxorubicin-containing liposomes in a rat solid tumor model. Cancer Res. 1987;47:3366-72.
[19] Maurer N, Wong KF, Hope MJ, Cullis PR. Anomalous solubility behavior of the antibiotic ciprofloxacin encapsulated in liposomes: a 1H-NMR study. Biochim Biophys Acta. 1998;1374:9-20.
[20] Zhigaltsev IV, Winters G, Srinivasulu M, Crawford J, Wong M, Amankwa L, et al. Development of a weak-base docetaxel derivative that can be loaded into lipid nanoparticles. J Control Release. 2010;144:332-40.

[21] Abuchowski A, McCoy JR, Palczuk NC, van Es T, Davis FF. Effect of covalent attachment of polyethylene glycol on immunogenicity and circulating life of bovine liver catalase. J Biol Chem. 1977;252:3582-6.
[22] Gabizon A, Catane R, Uziely B, Kaufman B, Safra T, Cohen R, et al. Prolonged circulation time and enhanced accumulation in malignant exudates of doxorubicin encapsulated in polyethylene-glycol coated liposomes. Cancer Res. 1994;54:987-92.
[23] James ND, Coker RJ, Tomlinson D, Harris JR, Gompels M, Pinching AJ, et al. Liposomal doxorubicin (Doxil): an effective new treatment for Kaposi's sarcoma in AIDS. Clin Oncol (R Coll Radiol). 1994;6:294-6.
[24] Barenholz Y. Doxil(R)--the first FDA-approved nano-drug: lessons learned. J Control Release. 2012;160:117-34.
[25] Bareford LM, Swaan PW. Endocytic mechanisms for targeted drug delivery. Adv Drug Deliv Rev. 2007;59:748-58.
[26] Suzuki R, Takizawa T, Kuwata Y, Mutoh M, Ishiguro N, Utoguchi N, et al. Effective anti-tumor activity of oxaliplatin encapsulated in transferrin-PEG-liposome. Int J Pharm. 2008;346:143-50.
[27] Nellis DF, Giardina SL, Janini GM, Shenoy SR, Marks JD, Tsai R, et al. Preclinical manufacture of anti-HER2 liposome-inserting, scFv-PEG-lipid conjugate. 2. Conjugate micelle identity, purity, stability, and potency analysis. Biotechnol Prog. 2005;21:221-32.
[28] Byrne JD, Betancourt T, Brannon-Peppas L. Active targeting schemes for nanoparticle systems in cancer therapeutics. Adv Drug Deliv Rev. 2008;60:1615-26.
[29] Folkman J. Fighting cancer by attacking its blood supply. Sci Am. 1996;275:150-4.
[30] Backer MV, Gaynutdinov TI, Patel V, Bandyopadhyaya AK, Thirumamagal BT, Tjarks W, et al. Vascular endothelial growth factor selectively targets boronated dendrimers to tumor vasculature. Mol Cancer Ther. 2005;4:1423-9.
[31] Nasongkla N, Shuai X, Ai H, Weinberg BD, Pink J, Boothman DA, et al. cRGD-functionalized polymer micelles for targeted doxorubicin delivery. Angew Chem Int Ed Engl. 2004;43:6323-7.
[32] Gosk S, Moos T, Gottstein C, Bendas G. VCAM-1 directed immunoliposomes selectively target tumor vasculature in vivo. Biochim Biophys Acta. 2008;1778:854-63.
[33] Hatakeyama H, Akita H, Ishida E, Hashimoto K, Kobayashi H, Aoki T, et al. Tumor targeting of doxorubicin by anti-MT1-MMP antibody-modified PEG liposomes. Int J Pharm. 2007;342:194-200.
[34] Kirpotin DB, Drummond DC, Shao Y, Shalaby MR, Hong K, Nielsen UB, et al. Antibody targeting of long-circulating lipidic nanoparticles does not increase tumor localization but does increase internalization in animal models. Cancer Res. 2006;66:6732-40.
[35] Bellocq NC, Pun SH, Jensen GS, Davis ME. Transferrin-containing, cyclodextrin polymer-based particles for tumor-targeted gene delivery. Bioconjug Chem. 2003;14:1122-32.
[36] Ratnam M, Hao H, Zheng X, Wang H, Qi H, Lee R, et al. Receptor induction and targeted drug delivery: a new antileukaemia strategy. Expert Opin Biol Ther. 2003;3:563-74.
[37] Low PS, Antony AC. Folate receptor-targeted drugs for cancer and inflammatory diseases. Adv Drug Deliv Rev. 2004;56:1055-8.
[38] Shmeeda H, Mak L, Tzemach D, Astrahan P, Tarshish M, Gabizon A. Intracellular uptake and intracavitary targeting of folate-conjugated liposomes in a mouse lymphoma model with up-regulated folate receptors. Mol Cancer Ther. 2006;5:818-24.
[39] Turek JJ, Leamon CP, Low PS. Endocytosis of folate-protein conjugates: ultrastructural localization in KB cells. J Cell Sci. 1993;106 (Pt 1):423-30.
[40] Morris RT, Joyrich RN, Naumann RW, Shah NP, Maurer AH, Strauss HW, et al. Phase II study of treatment of advanced ovarian cancer with folate-receptor-targeted therapeutic (vintafolide) and companion SPECT-based imaging agent (99mTc-etarfolatide). Ann Oncol. 2014;25:852-8.

[41] Graybill WS, Coleman RL. Vintafolide: a novel targeted agent for epithelial ovarian cancer. Future Oncol. 2014;10:541-8.
[42] Bibi S, Lattmann E, Mohammed AR, Perrie Y. Trigger release liposome systems: local and remote controlled delivery? J Microencapsul. 2012;29:262-76.
[43] Li L, ten Hagen TL, Schipper D, Wijnberg TM, van Rhoon GC, Eggermont AM, et al. Triggered content release from optimized stealth thermosensitive liposomes using mild hyperthermia. J Control Release. 2010;143:274-9.
[44] Anderson VC, Thompson DH. Triggered release of hydrophilic agents from plasmalogen liposomes using visible light or acid. Biochim Biophys Acta. 1992;1109:33-42.
[45] Huang SL, MacDonald RC. Acoustically active liposomes for drug encapsulation and ultrasound-triggered release. Biochim Biophys Acta. 2004;1665:134-41.
[46] Amstad E, Kohlbrecher J, Muller E, Schweizer T, Textor M, Reimhult E. Triggered release from liposomes through magnetic actuation of iron oxide nanoparticle containing membranes. Nano Lett. 2011;11:1664-70.
[47] Sarkar NR, Rosendahl T, Krueger AB, Banerjee AL, Benton K, Mallik S, et al. "Uncorking" of liposomes by matrix metalloproteinase-9. Chem Commun (Camb). 2005:999-1001.
[48] Venugopalan P, Jain S, Sankar S, Singh P, Rawat A, Vyas SP. pH-sensitive liposomes: mechanism of triggered release to drug and gene delivery prospects. Pharmazie. 2002;57:659-71.
[49] Ong W, Yang Y, Cruciano AC, McCarley RL. Redox-triggered contents release from liposomes. J Am Chem Soc. 2008;130:14739-44.
[50] Bird R, Freemont TJ, Saunders BR. Hollow polymer particles that are pH-responsive and redox sensitive: two simple steps to triggered particle swelling, gelation and disassembly. Chem Commun (Camb). 2011;47:1443-5.
[51] Allen TM, Cullis PR. Liposomal drug delivery systems: from concept to clinical applications. Adv Drug Deliv Rev. 2013;65:36-48.
[52] Weinstein JN, Magin RL, Yatvin MB, Zaharko DS. Liposomes and local hyperthermia: selective delivery of methotrexate to heated tumors. Science. 1979;204:188-91.
[53] Needham D, Anyarambhatla G, Kong G, Dewhirst MW. A new temperature-sensitive liposome for use with mild hyperthermia: characterization and testing in a human tumor xenograft model. Cancer Res. 2000;60:1197-201.
[54] Lim SK, Shin DH, Choi MH, Kim JS. Enhanced antitumor efficacy of gemcitabine-loaded temperature-sensitive liposome by hyperthermia in tumor-bearing mice. Drug Dev Ind Pharm. 2014;40:470-6.
[55] Kakinuma K, Tanaka R, Takahashi H, Sekihara Y, Watanabe M, Kuroki M. Drug delivery to the brain using thermosensitive liposome and local hyperthermia. Int J Hyperthermia. 1996;12:157-65.
[56] Vujaskovic Z, Kim DW, Jones E, Lan L, McCall L, Dewhirst MW, et al. A phase I/II study of neoadjuvant liposomal doxorubicin, paclitaxel, and hyperthermia in locally advanced breast cancer. Int J Hyperthermia. 2010;26:514-21.
[57] Francis RJ, Sharma SK, Springer C, Green AJ, Hope-Stone LD, Sena L, et al. A phase I trial of antibody directed enzyme prodrug therapy (ADEPT) in patients with advanced colorectal carcinoma or other CEA producing tumours. Br J Cancer. 2002;87:600-7.
[58] May JP, Li SD. Hyperthermia-induced drug targeting. Expert Opin Drug Deliv. 2013;10:511-27.
[59] Phillips DJ, Gibson MI. Redox-Sensitive Materials for Drug Delivery: Targeting the Correct Intracellular Environment, Tuning Release Rates, and Appropriate Predictive Systems. Antioxid Redox Signal. 2014.
[60] Cho H, Bae J, Garripelli VK, Anderson JM, Jun HW, Jo S. Redox-sensitive polymeric nanoparticles for drug delivery. Chem Commun (Camb). 2012.

[61] Paliwal SR, Paliwal R, Vyas SP. A review of mechanistic insight and application of pH-sensitive liposomes in drug delivery. Drug Deliv. 2014.
[62] Yoshida T, Lai TC, Kwon GS, Sako K. pH- and ion-sensitive polymers for drug delivery. Expert Opin Drug Deliv. 2013;10:1497-513.
[63] Mitragotri S. Healing sound: the use of ultrasound in drug delivery and other therapeutic applications. Nat Rev Drug Discov. 2005;4:255-60.
[64] Kee PH, Kim H, Huang S, Laing ST, Moody MR, Vela D, et al. Nitric Oxide Pretreatment Enhances Atheroma Component Highlighting in Vivo with Intercellular Adhesion Molecule-1-Targeted Echogenic Liposomes. Ultrasound Med Biol. 2014.
[65] Demos SM, Alkan-Onyuksel H, Kane BJ, Ramani K, Nagaraj A, Greene R, et al. In vivo targeting of acoustically reflective liposomes for intravascular and transvascular ultrasonic enhancement. J Am Coll Cardiol. 1999;33:867-75.
[66] Jung SH, Na K, Lee SA, Cho SH, Seong H, Shin BC. Gd(III)-DOTA-modified sonosensitive liposomes for ultrasound-triggered release and MR imaging. Nanoscale Res Lett. 2012;7:462.
[67] Omata D, Negishi Y, Hagiwara S, Yamamura S, Endo-Takahashi Y, Suzuki R, et al. Enhanced gene delivery using Bubble liposomes and ultrasound for folate-PEG liposomes. J Drug Target. 2012;20:355-63.
[68] Nahire R, Haldar MK, Paul S, Mergoum A, Ambre AH, Katti KS, et al. Polymer-coated echogenic lipid nanoparticles with dual release triggers. Biomacromolecules. 2013;14:841-53.
[69] Kopechek JA, Abruzzo TM, Wang B, Chrzanowski SM, Smith DAB, Kee PH, et al. Ultrasound-Mediated Release of Hydrophilic and Lipophilic Agents From Echogenic Liposomes. Journal of Ultrasound in Medicine. 2008;27:1597-606.
[70] Lian T, Ho RJY. Trends and developments in liposome drug delivery systems. Journal of Pharmaceutical Sciences. 2001;90:667-80.
[71] Moghimi SM, Szebeni J. Stealth liposomes and long circulating nanoparticles: critical issues in pharmacokinetics, opsonization and protein-binding properties. Progress in Lipid Research. 2003;42:463-78.
[72] Torchilin VP. Recent advances with liposomes as pharmaceutical carriers. Nature Reviews Drug Discovery. 2005;4:145-60.
[73] Zhang L, Gu FX, Chan JM, Wang AZ, Langer RS, Farokhzad OC. Nanoparticles in medicine: Therapeutic applications and developments. Clinical Pharmacology & Therapeutics. 2008;83:761-9.
[74] Ding N, Lu Y, Lee RJ, Yang C, Huang L, Liu J, et al. Folate receptor-targeted fluorescent paramagnetic bimodal liposomes for tumor imaging. Int J Nanomedicine. 2011;6:2513-20.
[75] Soares DC, Cardoso VN, de Barros AL, de Souza CM, Cassali GD, de Oliveira MC, et al. Antitumoral activity and toxicity of PEG-coated and PEG-folate-coated pH-sensitive liposomes containing (1)(5)(9)Gd-DTPA-BMA in Ehrlich tumor bearing mice. Eur J Pharm Sci. 2012;45:58-64.
[76] Andresen TL, Thompson DH, Kaasgaard T. Enzyme-triggered nanomedicine: drug release strategies in cancer therapy. Mol Membr Biol. 2010;27:353-63.
[77] Tagami T, Ernsting MJ, Li SD. Efficient tumor regression by a single and low dose treatment with a novel and enhanced formulation of thermosensitive liposomal doxorubicin. J Control Release. 2011;152:303-9.
[78] Torres E, Mainini F, Napolitano R, Fedeli F, Cavalli R, Aime S, et al. Improved paramagnetic liposomes for MRI visualization of pH triggered release. J Control Release. 2011;154:196-202.
[79] Paasonen L, Laaksonen T, Johans C, Yliperttula M, Kontturi K, Urtti A. Gold nanoparticles enable selective light-induced contents release from liposomes. J Control Release. 2007;122:86-93.
[80] Zhigaltsev IV, Maurer N, Wong KF, Cullis PR. Triggered release of doxorubicin following mixing of cationic and anionic liposomes. Biochim Biophys Acta. 2002;1565:129-35.

[81] Aili D, Mager M, Roche D, Stevens MM. Hybrid nanoparticle-liposome detection of phospholipase activity. Nano Lett. 2011;11:1401-5.
[82] Banerjee J, Hanson AJ, Gadam B, Elegbede AI, Tobwala S, Ganguly B, et al. Release of liposomal contents by cell-secreted matrix metalloproteinase-9. Bioconjug Chem. 2009;20:1332-9.
[83] Elegbede AI, Banerjee J, Hanson AJ, Tobwala S, Ganguli B, Wang R, et al. Mechanistic studies of the triggered release of liposomal contents by matrix metalloproteinase-9. J Am Chem Soc. 2008;130:10633-42.
[84] van Beijnum JR, Petersen K, Griffioen AW. Tumor endothelium is characterized by a matrix remodeling signature. Front Biosci (Schol Ed). 2009;1:216-25.
[85] Nagase H, Woessner JF, Jr. Matrix metalloproteinases. J Biol Chem. 1999;274:21491-4.
[86] Bauvois B. New facets of matrix metalloproteinases MMP-2 and MMP-9 as cell surface transducers: outside-in signaling and relationship to tumor progression. Biochim Biophys Acta. 2012;1825:29-36.
[87] Fisher JF, Mobashery S. Mechanism-based profiling of MMPs. Methods Mol Biol. 2010;622:471-87.
[88] Jin R, Yang G, Li G. Molecular insights and therapeutic targets for blood-brain barrier disruption in ischemic stroke: critical role of matrix metalloproteinases and tissue-type plasminogen activator. Neurobiol Dis. 2010;38:376-85.
[89] Busti C, Falcinelli E, Momi S, Gresele P. Matrix metalloproteinases and peripheral arterial disease. Intern Emerg Med. 2010;5:13-25.
[90] Konstantino Y, Nguyen TT, Wolk R, Aiello RJ, Terra SG, Fryburg DA. Potential implications of matrix metalloproteinase-9 in assessment and treatment of coronary artery disease. Biomarkers. 2009;14:118-29.
[91] Roy R, Yang J, Moses MA. Matrix metalloproteinases as novel biomarkers and potential therapeutic targets in human cancer. J Clin Oncol. 2009;27:5287-97.
[92] Hu J, Van den Steen PE, Sang QX, Opdenakker G. Matrix metalloproteinase inhibitors as therapy for inflammatory and vascular diseases. Nat Rev Drug Discov. 2007;6:480-98.
[93] Shaw GJ, Meunier JM, Huang SL, Lindsell CJ, McPherson DD, Holland CK. Ultrasound-enhanced thrombolysis with tPA-loaded echogenic liposomes. Thromb Res. 2009;124:306-10.
[94] Schroeder A, Honen R, Turjeman K, Gabizon A, Kost J, Barenholz Y. Ultrasound triggered release of cisplatin from liposomes in murine tumors. J Control Release. 2009;137:63-8.
[95] Evjen TJ, Nilssen EA, Rognvaldsson S, Brandl M, Fossheim SL. Distearoylphosphatidylethanolamine-based liposomes for ultrasound-mediated drug delivery. Eur J Pharm Biopharm. 2010;75:327-33.
[96] Hoskins P. Diagnostic ultrasound : physics and equipment. London ; San Francisco: Greenwich Medical Media : Distributed ... in the USA by Jamco Distribution; 2003.
[97] Leighton TG. The acoustic bubble. First printing pbk. ed. San Diego ; London: Academic Press; 1997.
[98] Lin HY, Thomas JL. PEG-Lipids and oligo(ethylene glycol) surfactants enhance the ultrasonic permeabilizability of liposomes. Langmuir : the ACS journal of surfaces and colloids. 2003;19:1098-105.
[99] Lin HY, Thomas JL. Factors affecting responsivity of unilamellar liposomes to 20 kHz ultrasound. Langmuir : the ACS journal of surfaces and colloids. 2004;20:6100-6.
[100] Schroeder A, Avnir Y, Weisman S, Najajreh Y, Gabizon A, Talmon Y, et al. Controlling liposomal drug release with low frequency ultrasound: Mechanism and feasibility. Langmuir : the ACS journal of surfaces and colloids. 2007;23:4019-25.
[101] Schroeder A, Kost J, Barenholz Y. Ultrasound, liposomes, and drug delivery: principles for using ultrasound to control the release of drugs from liposomes. Chem Phys Lipids. 2009;162:1-16.

[102] Cohen-Levi D, Kost J, Barenholz Y. Ultrasound for targeted delivery of cytotoxic drugs from liposomes. MSc Thesis Ben Gurion University, Beer Sheva,Israel. 2000:115.
[103] Kono K, Nakashima S, Kokuryo D, Aoki I, Shimomoto H, Aoshima S, et al. Multi-functional liposomes having temperature-triggered release and magnetic resonance imaging for tumor-specific chemotherapy. Biomaterials. 2011;32:1387-95.
[104] Britton GL, Kim H, Kee PH, Aronowski J, Holland CK, McPherson DD, et al. In vivo therapeutic gas delivery for neuroprotection with echogenic liposomes. Circulation. 2010;122:1578-87.
[105] Kopechek JA, Haworth KJ, Raymond JL, Douglas Mast T, Perrin SR, Klegerman ME, et al. Acoustic characterization of echogenic liposomes: frequency-dependent attenuation and backscatter. J Acoust Soc Am. 2011;130:3472-81.
[106] Huang SL, Hamilton AJ, Nagaraj A, Tiukinhoy SD, Klegerman ME, McPherson DD, et al. Improving ultrasound reflectivity and stability of echogenic liposomal dispersions for use as targeted ultrasound contrast agents. Journal of Pharmaceutical Sciences. 2001;90:1917-26.
[107] Huang SL, McPherson DD, Macdonald RC. A method to co-encapsulate gas and drugs in liposomes for ultrasound-controlled drug delivery. Ultrasound in medicine & biology. 2008;34:1272-80.
[108] Paul S, Russakow D, Nahire R, Nandy T, Ambre AH, Katti K, et al. In vitro measurement of attenuation and nonlinear scattering from echogenic liposomes. Ultrasonics. 2012.
[109] Huang SL. Liposomes in ultrasonic drug and gene delivery. Advanced Drug Delivery Reviews. 2008;60:1167-76.
[110] Huang SL, MacDonald RC. Acoustically active liposomes for drug encapsulation and ultrasound-triggered release. Biochimica Et Biophysica Acta-Biomembranes. 2004;1665:134-41.
[111] Smith DAB, Vaidya SS, Kopechek JA, Huang SL, Klegerman ME, Mcpherson DD, et al. Ultrasound-Triggered Release of Recombinant Tissue-Type Plasminogen Activator from Echogenic Liposomes. Ultrasound in Medicine and Biology. 2010;36:145-57.
[112] Kopechek JA, Abruzzo TM, Wang B, Chrzanowski SM, Smith DA, Kee PH, et al. Ultrasound-mediated release of hydrophilic and lipophilic agents from echogenic liposomes. J Ultrasound Med. 2008;27:1597-606.
[113] Banerjee J, Hanson AJ, Muhonen WW, Shabb JB, Mallik S. Microwave-assisted synthesis of triple-helical, collagen-mimetic lipopeptides. Nat Protoc. 2010;5:39-50.
[114] Shi WT, Forsberg F. Ultrasonic characterization of the nonlinear properties of contrast microbubbles. Ultrasound in Medicine and Biology. 2000;26:93-104.
[115] Sarkar K, Shi WT, Chatterjee D, Forsberg F. Characterization of ultrasound contrast microbubbles using in vitro experiments and viscous and viscoelastic interface models for encapsulation. Journal of the Acoustical Society of America. 2005;118:539-50.
[116] Omata D, Negishi Y, Yamamura S, Hagiwara S, Endo-Takahashi Y, Suzuki R, et al. Involvement of Ca(2)(+) and ATP in enhanced gene delivery by bubble liposomes and ultrasound exposure. Mol Pharm. 2012;9:1017-23.
[117] Omata D, Negishi Y, Hagiwara S, Yamamura S, Endo-Takahashi Y, Suzuki R, et al. Bubble liposomes and ultrasound promoted endosomal escape of TAT-PEG liposomes as gene delivery carriers. Mol Pharm. 2011;8:2416-23.
[118] Negishi Y, Omata D, Iijima H, Takabayashi Y, Suzuki K, Endo Y, et al. Enhanced laminin-derived peptide AG73-mediated liposomal gene transfer by bubble liposomes and ultrasound. Mol Pharm. 2010;7:217-26.
[119] Negishi Y, Endo Y, Fukuyama T, Suzuki R, Takizawa T, Omata D, et al. Delivery of siRNA into the cytoplasm by liposomal bubbles and ultrasound. J Control Release. 2008;132:124-30.
[120] Hensel K, Mienkina MP, Schmitz G. Analysis of ultrasound fields in cell culture wells for in vitro ultrasound therapy experiments. Ultrasound Med Biol. 2011;37:2105-15.
[121] Kopechek JA, Kim H, McPherson DD, Holland CK. Calibration of the 1-MHz Sonitron ultrasound system. Ultrasound Med Biol. 2010;36:1762-6.

[122] Birkedal-Hansen H, Moore WG, Bodden MK, Windsor LJ, Birkedal-Hansen B, DeCarlo A, et al. Matrix metalloproteinases: a review. Crit Rev Oral Biol Med. 1993;4:197-250.
[123] Motooka D, Kawahara K, Nakamura S, Doi M, Nishi Y, Nishiuchi Y, et al. The triple helical structure and stability of collagen model peptide with 4(S)-hydroxyprolyl-Pro-Gly units. Biopolymers. 2012;98:111-21.
[124] Raabe HM, Molsen H, Mlinaric SM, Acil Y, Sinnecker GH, Notbohm H, et al. Biochemical alterations in collagen IV induced by in vitro glycation. Biochem J. 1996;319 (Pt 3):699-704.
[125] Basel MT, Shrestha TB, Troyer DL, Bossmann SH. Protease-sensitive, polymer-caged liposomes: a method for making highly targeted liposomes using triggered release. ACS Nano. 2011;5:2162-75.
[126] Lauer-Fields JL, Sritharan T, Stack MS, Nagase H, Fields GB. Selective hydrolysis of triple-helical substrates by matrix metalloproteinase-2 and -9. J Biol Chem. 2003;278:18140-5.
[127] de la Rica R, Aili D, Stevens MM. Enzyme-responsive nanoparticles for drug release and diagnostics. Adv Drug Deliv Rev. 2012;64:967-78.
[128] Chen C, Han D, Cai C, Tang X. An overview of liposome lyophilization and its future potential. J Control Release. 2010;142:299-311.
[129] Glavas-Dodov M, Fredro-Kumbaradzi E, Goracinova K, Simonoska M, Calis S, Trajkovic-Jolevska S, et al. The effects of lyophilization on the stability of liposomes containing 5-FU. Int J Pharm. 2005;291:79-86.
[130] Crowe JH, Crowe LM, Carpenter JF, Aurell Wistrom C. Stabilization of dry phospholipid bilayers and proteins by sugars. Biochem J. 1987;242:1-10.
[131] AlkanOnyuksel H, Demos SM, Lanza GM, Vonesh MJ, Klegerman ME, Kane BJ, et al. Development of inherently echogenic liposomes as an ultrasonic contrast agent. Journal of Pharmaceutical Sciences. 1996;85:486-90.
[132] Huang SL, Hamilton AJ, Pozharski E, Nagaraj A, Klegerman ME, McPherson DD, et al. Physical correlates of the ultrasonic reflectivity of lipid dispersions suitable as diagnostic contrast agents. Ultrasound in Medicine and Biology. 2002;28:339-48.
[133] Kopechek JA, Haworth KJ, Raymond JL, Douglas Mast T, Perrin SR, Klegerman ME, et al. Acoustic characterization of echogenic liposomes: Frequency-dependent attenuation and backscatter. The Journal of the Acoustical Society of America. 2011;130:3472.
[134] Suzuki R, Takizawa T, Negishi Y, Utoguchi N, Sawamura K, Tanaka K, et al. Tumor specific ultrasound enhanced gene transfer in vivo with novel liposomal bubbles. J Control Release. 2008;125:137-44.
[135] Pitt WG, Husseini GA, Maruyama K. Letter to the Editor :On Bubbles and Liposomes, Response by the authors, Letter to the Editor 2. Journal of Controlled Release. 2008;125:174-7.
[136] Huang SL, Tiukinhoy S, Wang L, MacDonald R, Nagaraj A, McPherson D. Acoustically-active liposomes of novel cationic-anionic composition in conjunction with ultrasound for gene delivery into vascular smooth muscle cells. Molecular Therapy. 2003;7:S167-S.
[137] Kopechek JA, Haworth KJ, Raymond JL, Mast TD, Perrin SR, Klegerman ME, et al. Acoustic characterization of echogenic liposomes: Frequency-dependent attenuation and backscatter. Journal of the Acoustical Society of America. 2011;130:3472-81.
[138] Sarkar K, Katiyar A, Jain P. Growth and dissolution of an encapsulated contrast microbubble Ultrasound in Medicine and Biology. 2009;35:1385-96.
[139] Katiyar A, Sarkar K, Jain P. Effects of Encapsulation Elasticity on the stability of an Encapsulated Microbubble. Journal of Colloid and Interface Science. 2009;336:519-25.
[140] Katiyar A, Sarkar K. Stability analysis of an encapsulated microbubble against gas diffusion. Journal of Colloid and Interface Science. 2010;343:42-7.
[141] Chatterjee D, Sarkar K. A Newtonian rheological model for the interface of microbubble contrast agents. Ultrasound in Medicine and Biology. 2003;29:1749-57.
[142] Paul S, Katiyar A, Sarkar K, Chatterjee D, Shi WT, Forsberg F. Material characterization of the encapsulation of an ultrasound contrast microbubble and its subharmonic response: Strain-

softening interfacial elasticity model. Journal of the Acoustical Society of America. 2010;127:3846-57.
[143] Chatterjee D, Jain P, Sarkar K. Ultrasound-mediated destruction of contrast microbubbles used for medical imaging and drug delivery. Physics of Fluids. 2005;17:100603.
[144] Minond D, Lauer-Fields JL, Cudic M, Overall CM, Pei D, Brew K, et al. The roles of substrate thermal stability and P2 and P1' subsite identity on matrix metalloproteinase triple-helical peptidase activity and collagen specificity. J Biol Chem. 2006;281:38302-13.
[145] Baker KG, Robertson VJ, Duck FA. A review of therapeutic ultrasound: biophysical effects. Phys Ther. 2001;81:1351-8.
[146] Roomi MW, Monterrey JC, Kalinovsky T, Rath M, Niedzwiecki A. Patterns of MMP-2 and MMP-9 expression in human cancer cell lines. Oncol Rep. 2009;21:1323-33.
[147] Chen F, Ohashi N, Li W, Eckman C, Nguyen JH. Disruptions of occludin and claudin-5 in brain endothelial cells in vitro and in brains of mice with acute liver failure. Hepatology. 2009;50:1914-23.
[148] Edwards DR, Handsley MM, Pennington CJ. The ADAM metalloproteinases. Mol Aspects Med. 2008;29:258-89.
[149] Bhattacharjee H, Balabathula P, Wood GC. Targeted nanoparticulate drug-delivery systems for treatment of solid tumors: a review. Ther Deliv. 2010;1:713-34.
[150] Barenholz YC. Doxil(R) - The first FDA-approved nano-drug: Lessons learned. J Control Release. 2012;160:117-34.
[151] Gordon KB, Tajuddin A, Guitart J, Kuzel TM, Eramo LR, VonRoenn J. Hand-foot syndrome associated with liposome-encapsulated doxorubicin therapy. Cancer. 1995;75:2169-73.
[152] Sarkar N, Banerjee J, Hanson AJ, Elegbede AI, Rosendahl T, Krueger AB, et al. Matrix metalloproteinase-assisted triggered release of liposomal contents. Bioconjug Chem. 2008;19:57-64.
[153] Hu FQ, Zhang YY, You J, Yuan H, Du YZ. pH triggered doxorubicin delivery of PEGylated glycolipid conjugate micelles for tumor targeting therapy. Mol Pharm. 2012;9:2469-78.
[154] Turner DC, Moshkelani D, Shemesh CS, Luc D, Zhang H. Near-infrared image-guided delivery and controlled release using optimized thermosensitive liposomes. Pharm Res. 2012;29:2092-103.
[155] Leung SJ, Kachur XM, Bobnick MC, Romanowski M. Wavelength-Selective Light-Induced Release from Plasmon Resonant Liposomes. Adv Funct Mater. 2011;21:1113-21.
[156] Smith DA, Vaidya SS, Kopechek JA, Huang SL, Klegerman ME, McPherson DD, et al. Ultrasound-triggered release of recombinant tissue-type plasminogen activator from echogenic liposomes. Ultrasound Med Biol. 2010;36:145-57.
[157] Melancon MP, Zhou M, Li C. Cancer theranostics with near-infrared light-activatable multimodal nanoparticles. Acc Chem Res. 2011;44:947-56.
[158] Sciallero C, Paradossi G, Trucco A. A preliminary in vitro assessment of polymer-shelled microbubbles in contrast-enhanced ultrasound imaging. Ultrasonics. 2012;52:456-64.
[159] Mohan P, Rapoport N. Doxorubicin as a molecular nanotheranostic agent: effect of doxorubicin encapsulation in micelles or nanoemulsions on the ultrasound-mediated intracellular delivery and nuclear trafficking. Mol Pharm. 2010;7:1959-73.
[160] Tang SY, Sivakumar M, Ng AM, Shridharan P. Anti-inflammatory and analgesic activity of novel oral aspirin-loaded nanoemulsion and nano multiple emulsion formulations generated using ultrasound cavitation. Int J Pharm. 2012;430:299-306.
[161] Thirumalai S, Mobed-Miremadi M, Sridhar-Keralapura M. Effect of therapeutic ultrasound on acoustically sensitive microcapsules. Conf Proc IEEE Eng Med Biol Soc. 2011;2011:7207-10.

[162] Min HS, Kang E, Koo H, Lee J, Kim K, Park RW, et al. Gas-generating polymeric microspheres for long-term and continuous in vivo ultrasound imaging. Biomaterials. 2012;33:936-44.
[163] Wrenn S, Dicker S, Small E, Mleczko M. Controlling cavitation for controlled release. Ultrasonics Symposium (IUS), 2009 IEEE International2009. p. 104-7.
[164] Negishi Y, Matsuo K, Endo-Takahashi Y, Suzuki K, Matsuki Y, Takagi N, et al. Delivery of an Angiogenic Gene into Ischemic Muscle by Novel Bubble Liposomes Followed by Ultrasound Exposure. Pharm Res. 2011;28:712-9.
[165] Pong M, Umchid S, Guarino AJ, Lewin PA, Litniewski J, Nowicki A, et al. In vitro ultrasound-mediated leakage from phospholipid vesicles. Ultrasonics. 2006;45:133-45.
[166] Husseini GA, Myrup GD, Pitt WG, Christensen DA, Rapoport NAY. Factors affecting acoustically triggered release of drugs from polymeric micelles. Journal of Controlled Release. 2000;69:43-52.
[167] Buchanan KD, Huang SL, Kim H, McPherson DD, MacDonald RC. Encapsulation of NF-kappaB decoy oligonucleotides within echogenic liposomes and ultrasound-triggered release. J Control Release. 2010;141:193-8.
[168] Herbst SM, Klegerman ME, Kim H, Qi J, Shelat H, Wassler M, et al. Delivery of stem cells to porcine arterial wall with echogenic liposomes conjugated to antibodies against CD34 and intercellular adhesion molecule-1. Mol Pharm. 2010;7:3-11.
[169] Nahire R, Paul S, Scott MD, Singh RK, Muhonen WW, Shabb J, et al. Ultrasound enhanced matrix metalloproteinase-9 triggered release of contents from echogenic liposomes. Mol Pharm. 2012;9:2554-64.
[170] Kheirolomoom A, Dayton PA, Lum AFH, Little E, Paoli EE, Zheng HR, et al. Acoustically-active microbubbles conjugated to liposomes: Characterization of a proposed drug delivery vehicle. Journal of Controlled Release. 2007;118:275-84.
[171] Huang SL, Hamilton AJ, Nagaraj A, Tiukinhoy SD, Klegerman ME, McPherson DD, et al. Improving ultrasound reflectivity and stability of echogenic liposomal dispersions for use as targeted ultrasound contrast agents. J Pharm Sci. 2001;90:1917-26.
[172] Alkan-Onyuksel H, Demos SM, Lanza GM, Vonesh MJ, Klegerman ME, Kane BJ, et al. Development of inherently echogenic liposomes as an ultrasonic contrast agent. J Pharm Sci. 1996;85:486-90.
[173] Waseda K, Ako J, Yamasaki M, Koizumi T, Ormiston J, Worthley SG, et al. Short- and mid-term intravascular ultrasound analysis of the new zotarolimus-eluting stent with durable polymer - results from the RESOLUTE trial. Circ J. 2010;74:2097-102.
[174] Laing ST, Moody M, Smulevitz B, Kim H, Kee P, Huang S, et al. Ultrasound-enhanced thrombolytic effect of tissue plasminogen activator-loaded echogenic liposomes in an in vivo rabbit aorta thrombus model--brief report. Arterioscler Thromb Vasc Biol. 2011;31:1357-9.
[175] Paul S, Russakow D, Nahire R, Nandy T, Ambre AH, Katti K, et al. In vitro measurement of attenuation and nonlinear scattering from echogenic liposomes. Ultrasonics. 2012;52:962-9.
[176] Kr zel A, Lesniak W, Jezowska-Bojczuk M, Mlynarz P, Brasun J, Kozlowski H, et al. Coordination of heavy metals by dithiothreitol, a commonly used thiol group protectant. J Inorg Biochem. 2001;84:77-88.
[177] Hub HH, Hupfer B, Koch H, Ringsdorf H. Polymerizable phospholipid analogues--new stable biomembrane and cell models. Angew Chem Int Ed Engl. 1980;19:938-40.
[178] Raderer M, Scheithauer W. Clinical trials of agents that reverse multidrug resistance. A literature review. Cancer. 1993;72:3553-63.
[179] Perry RR, Mazetta JA, Levin M, Barranco SC. Glutathione levels and variability in breast tumors and normal tissue. Cancer. 1993;72:783-7.
[180] Berger SJ, Gosky D, Zborowska E, Willson JK, Berger NA. Sensitive enzymatic cycling assay for glutathione: measurements of glutathione content and its modulation by buthionine sulfoximine in vivo and in vitro in human colon cancer. Cancer Res. 1994;54:4077-83.

[181] Cook JA, Pass HI, Iype SN, Friedman N, DeGraff W, Russo A, et al. Cellular glutathione and thiol measurements from surgically resected human lung tumor and normal lung tissue. Cancer Res. 1991;51:4287-94.
[182] Joncourt F, Oberli-Schrammli AE, Stadler M, Buser K, Franscini L, Fey MF, et al. Patterns of drug resistance parameters in adult leukemia. Leuk Lymphoma. 1995;17:101-9.
[183] Mulder TP, Manni JJ, Roelofs HM, Peters WH, Wiersma A. Glutathione S-transferases and glutathione in human head and neck cancer. Carcinogenesis. 1995;16:619-24.
[184] Cotgreave IA, Gerdes RG. Recent trends in glutathione biochemistry--glutathione-protein interactions: a molecular link between oxidative stress and cell proliferation? Biochem Biophys Res Commun. 1998;242:1-9.
[185] Saito G, Swanson JA, Lee KD. Drug delivery strategy utilizing conjugation via reversible disulfide linkages: role and site of cellular reducing activities. Adv Drug Deliv Rev. 2003;55:199-215.
[186] West KR, Otto S. Reversible covalent chemistry in drug delivery. Curr Drug Discov Technol. 2005;2:123-60.
[187] Goldenbogen B, Brodersen N, Gramatica A, Loew M, Liebscher J, Herrmann A, et al. Reduction-sensitive liposomes from a multifunctional lipid conjugate and natural phospholipids: reduction and release kinetics and cellular uptake. Langmuir. 2011;27:10820-9.
[188] Graf N, Lippard SJ. Redox activation of metal-based prodrugs as a strategy for drug delivery. Adv Drug Deliv Rev. 2012;64:993-1004.
[189] Wen H, Dong C, Dong H, Shen A, Xia W, Cai X, et al. Engineered redox-responsive PEG detachment mechanism in PEGylated nano-graphene oxide for intracellular drug delivery. Small. 2012;8:760-9.
[190] Zhang S, Zhao Y. Controlled release from cleavable polymerized liposomes upon redox and pH stimulation. Bioconjug Chem. 2011;22:523-8.
[191] Niu G, Cogburn B, Hughes J. Preparation and characterization of doxorubicin liposomes. Methods Mol Biol. 2010;624:211-9.
[192] Hensel K, Mienkina MP, Schmitz G. Analysis of ultrasound fields in cell culture wells for in vitro ultrasound therapy experiments. Ultrasound in medicine & biology. 2011;37:2105-15.
[193] Albrecht T, Patel N, Cosgrove DO, Jayaram V, Blomley MJ, Eckersley R. Enhancement of power Doppler signals from breast lesions with the ultrasound contrast agent EchoGen emulsion: subjective and quantitative assessment. Acad Radiol. 1998;5 Suppl 1:S195-8; discussion S9.
[194] Hitchcock KE, Caudell DN, Sutton JT, Klegerman ME, Vela D, Pyne-Geithman GJ, et al. Ultrasound-enhanced delivery of targeted echogenic liposomes in a novel ex vivo mouse aorta model. J Control Release. 2010;144:288-95.
[195] Li X, Zhao Y. Protection/Deprotection of surface activity and its applications in the controlled release of liposomal contents. Langmuir. 2012;28:4152-9.
[196] Karathanasis E, Bhavane R, Annapragada AV. Triggered release of inhaled insulin from the agglomerated vesicles: pharmacodynamic studies in rats. J Control Release. 2006;113:117-27.
[197] Cleland WW. Dithiothreitol, a New Protective Reagent for Sh Groups. Biochemistry. 1964;3:480-2.
[198] Tanaka N, Kolthoff IM, Stricks W. Oxidation of Ferrous-Cysteinate Complex by Cystine. Oxidation Potential of the Cystine-Cysteine System. J Am Chem Soc. 1955;77:2004-6.
[199] Green DE. The reduction potentials of cysteine, glutathione and glycylcysteine. Biochem J. 1933;27:678-89.
[200] Antony AC. Folate receptors. Annu Rev Nutr. 1996;16:501-21.
[201] Kamen BA, Capdevila A. Receptor-mediated folate accumulation is regulated by the cellular folate content. Proc Natl Acad Sci U S A. 1986;83:5983-7.

[202] Leamon CP, Low PS. Delivery of macromolecules into living cells: a method that exploits folate receptor endocytosis. Proc Natl Acad Sci U S A. 1991;88:5572-6.
[203] Li X, Tian X, Zhang J, Zhao X, Chen X, Jiang Y, et al. In vitro and in vivo evaluation of folate receptor-targeting amphiphilic copolymer-modified liposomes loaded with docetaxel. Int J Nanomedicine. 2011;6:1167-84.
[204] Li H, Piao L, Yu B, Yung BC, Zhang W, Wang PG, et al. Delivery of calf thymus DNA to tumor by folate receptor targeted cationic liposomes. Biomaterials. 2011;32:6614-20.
[205] Zhao XB, Muthusamy N, Byrd JC, Lee RJ. Cholesterol as a bilayer anchor for PEGylation and targeting ligand in folate-receptor-targeted liposomes. J Pharm Sci. 2007;96:2424-35.
[206] Gabizon A, Horowitz AT, Goren D, Tzemach D, Shmeeda H, Zalipsky S. In vivo fate of folate-targeted polyethylene-glycol liposomes in tumor-bearing mice. Clin Cancer Res. 2003;9:6551-9.
[207] Pan X, Lee RJ. Tumour-selective drug delivery via folate receptor-targeted liposomes. Expert Opin Drug Deliv. 2004;1:7-17.
[208] Pan J, Feng SS. Targeting and imaging cancer cells by folate-decorated, quantum dots (QDs)- loaded nanoparticles of biodegradable polymers. Biomaterials. 2009;30:1176-83.
[209] Lee ES, Na K, Bae YH. Doxorubicin loaded pH-sensitive polymeric micelles for reversal of resistant MCF-7 tumor. J Control Release. 2005;103:405-18.
[210] Lee ES, Na K, Bae YH. Polymeric micelle for tumor pH and folate-mediated targeting. J Control Release. 2003;91:103-13.
[211] Muthu MS, Kulkarni SA, Raju A, Feng SS. Theranostic liposomes of TPGS coating for targeted co-delivery of docetaxel and quantum dots. Biomaterials. 2012;33:3494-501.
[212] Paolino D, Licciardi M, Celia C, Giammona G, Fresta M, Cavallaro G. Folate-targeted supramolecular vesicular aggregates as a new frontier for effective anticancer treatment in in vivo model. Eur J Pharm Biopharm. 2012;82:94-102.
[213] Kaye SB, Richardson VJ. Potential of liposomes as drug-carriers in cancer chemotherapy: a review. Cancer Chemother Pharmacol. 1979;3:81-5.
[214] Yang F, Jin C, Jiang Y, Li J, Di Y, Ni Q, et al. Liposome based delivery systems in pancreatic cancer treatment: from bench to bedside. Cancer Treat Rev. 2011;37:633-42.
[215] Yu X, Zhang Y, Chen C, Yao Q, Li M. Targeted drug delivery in pancreatic cancer. Biochim Biophys Acta. 2010;1805:97-104.
[216] Torchilin VP. Recent advances with liposomes as pharmaceutical carriers. Nat Rev Drug Discov. 2005;4:145-60.
[217] Felber AE, Dufresne MH, Leroux JC. pH-sensitive vesicles, polymeric micelles, and nanospheres prepared with polycarboxylates. Adv Drug Deliv Rev. 2012;64:979-92.
[218] Leite EA, Souza CM, Carvalho-Junior AD, Coelho LG, Lana AM, Cassali GD, et al. Encapsulation of cisplatin in long-circulating and pH-sensitive liposomes improves its antitumor effect and reduces acute toxicity. Int J Nanomedicine. 2012;7:5259-69.
[219] Kim HK, Van den Bossche J, Hyun SH, Thompson DH. Acid-triggered release via dePEGylation of fusogenic liposomes mediated by heterobifunctional phenyl-substituted vinyl ethers with tunable pH-sensitivity. Bioconjug Chem. 2012;23:2071-7.
[220] Yao L, Daniels J, Wijesinghe D, Andreev OA, Reshetnyak YK. pHLIP(R)-mediated delivery of PEGylated liposomes to cancer cells. J Control Release. 2013;167:228-37.
[221] Wehunt MP, Winschel CA, Khan AK, Guo TL, Abdrakhmanova GR, Sidorov V. Controlled drug-release system based on pH-sensitive chloride-triggerable liposomes. J Liposome Res. 2013;23:37-46.
[222] Unnikrishnan S, Klibanov AL. Microbubbles as ultrasound contrast agents for molecular imaging: preparation and application. AJR Am J Roentgenol. 2012;199:292-9.
[223] Jing Y, Zhu Y, Yang X, Shen J, Li C. Ultrasound-triggered smart drug release from multifunctional core-shell capsules one-step fabricated by coaxial electrospray method. Langmuir. 2011;27:1175-80.

[224] Wu D, Wan M. A novel fluoride anion modified gelatin nanogel system for ultrasound-triggered drug release. J Pharm Pharm Sci. 2008;11:32-45.
[225] De Geest BG, Skirtach AG, Mamedov AA, Antipov AA, Kotov NA, De Smedt SC, et al. Ultrasound-triggered release from multilayered capsules. Small. 2007;3:804-8.
[226] Figueiredo M, Esenaliev R. PLGA Nanoparticles for Ultrasound-Mediated Gene Delivery to Solid Tumors. J Drug Deliv. 2012;2012:767839.
[227] Zhang H, Jiang H, Wang H, Zhao J, Chen B, Wang X. Ultrasound mediated drug-loaded nanoparticles crossing cell membranes as a new strategy to reverse cancer multidrug resistance. J Nanosci Nanotechnol. 2011;11:1834-40.
[228] Barati AH, Mokhtari-Dizaji M, Mozdarani H, Bathaie SZ, Hassan ZM. Treatment of murine tumors using dual-frequency ultrasound in an experimental in vivo model. Ultrasound Med Biol. 2009;35:756-63.
[229] Ahmadi F, McLoughlin IV, Chauhan S, ter-Haar G. Bio-effects and safety of low-intensity, low-frequency ultrasonic exposure. Prog Biophys Mol Biol. 2012;108:119-38.
[230] Paul S, Nahire R, Mallik S, Sarkar K. Encapsulated microbubbles and echogenic liposomes for contrast ultrasound imaging and targeted drug delivery. Computational Mechanics. 2013:1-23.
[231] Radhakrishnan K, Haworth KJ, Huang SL, Klegerman ME, McPherson DD, Holland CK. Stability of echogenic liposomes as a blood pool ultrasound contrast agent in a physiologic flow phantom. Ultrasound Med Biol. 2012;38:1970-81.
[232] Smith DA, Porter TM, Martinez J, Huang S, MacDonald RC, McPherson DD, et al. Destruction thresholds of echogenic liposomes with clinical diagnostic ultrasound. Ultrasound Med Biol. 2007;33:797-809.
[233] Chen KJ, Liang HF, Chen HL, Wang Y, Cheng PY, Liu HL, et al. A thermoresponsive bubble-generating liposomal system for triggering localized extracellular drug delivery. ACS Nano. 2013;7:438-46.
[234] Kopechek JA, Haworth KJ, Radhakrishnan K, Huang SL, Klegerman ME, McPherson DD, et al. The impact of bubbles on measurement of drug release from echogenic liposomes. Ultrason Sonochem. 2013;20:1121-30.
[235] Davis PJ, Fleming BD, Coolbear KP, Keough KM. Gel to liquid-crystalline transition temperatures of water dispersions of two pairs of positional isomers of unsaturated mixed-acid phosphatidylcholines. Biochemistry. 1981;20:3633-6.
[236] Chen RF, Knutson JR. Mechanism of fluorescence concentration quenching of carboxyfluorescein in liposomes: energy transfer to nonfluorescent dimers. Anal Biochem. 1988;172:61-77.
[237] Shimshick EJ, McConnell HM. Lateral phase separation in phospholipid membranes. Biochemistry. 1973;12:2351-60.
[238] Chung MF, Chen KJ, Liang HF, Liao ZX, Chia WT, Xia Y, et al. A liposomal system capable of generating CO2 bubbles to induce transient cavitation, lysosomal rupturing, and cell necrosis. Angew Chem Int Ed Engl. 2012;51:10089-93.
[239] Liong M, Lu J, Kovochich M, Xia T, Ruehm SG, Nel AE, et al. Multifunctional Inorganic Nanoparticles for Imaging, Targeting, and Drug Delivery. ACS Nano. 2008;2:889-96.
[240] Stathis A, Moore MJ. Advanced pancreatic carcinoma: current treatment and future challenges. Nat Rev Clin Oncol. 2010;7:163-72.
[241] Klein AP. Identifying people at a high risk of developing pancreatic cancer. Nat Rev Cancer. 2013;13:66-74.
[242] Kratz F, Azab S, Zeisig R, Fichtner I, Warnecke A. Evaluation of combination therapy schedules of doxorubicin and an acid-sensitive albumin-binding prodrug of doxorubicin in the MIA PaCa-2 pancreatic xenograft model. Int J Pharm. 2013;441:499-506.

[243] Syrigos KN, Michalaki B, Alevyzaki F, Machairas A, Mandrekas D, Kindilidis K, et al. A phase-II study of liposomal doxorubicin and docetaxel in patients with advanced pancreatic cancer. Anticancer Res. 2002;22:3583-8.
[244] Halford S, Yip D, Karapetis CS, Strickland AH, Steger A, Khawaja HT, et al. A phase II study evaluating the tolerability and efficacy of CAELYX (liposomal doxorubicin, Doxil) in the treatment of unresectable pancreatic carcinoma. Ann Oncol. 2001;12:1399-402.
[245] Lentacker I, Geers B, Demeester J, De Smedt SC, Sanders NN. Design and evaluation of doxorubicin-containing microbubbles for ultrasound-triggered doxorubicin delivery: cytotoxicity and mechanisms involved. Mol Ther. 2010;18:101-8.
[246] Mehier-Humbert S, Bettinger T, Yan F, Guy RH. Plasma membrane poration induced by ultrasound exposure: implication for drug delivery. J Control Release. 2005;104:213-22.
[247] Takada M, Hirata K, Ajiki T, Suzuki Y, Kuroda Y. Expression of receptor for advanced glycation end products (RAGE) and MMP-9 in human pancreatic cancer cells. Hepatogastroenterology. 2004;51:928-30.
[248] Ellenrieder V, Alber B, Lacher U, Hendler SF, Menke A, Boeck W, et al. Role of MT-MMPs and MMP-2 in pancreatic cancer progression. Int J Cancer. 2000;85:14-20.
[249] Frenkel V. Ultrasound mediated delivery of drugs and genes to solid tumors. Adv Drug Deliv Rev. 2008;60:1193-208.
[250] Toschi L, Finocchiaro G, Bartolini S, Gioia V, Cappuzzo F. Role of gemcitabine in cancer therapy. Future Oncol. 2005;1:7-17.
[251] Dasanu CA. Gemcitabine: vascular toxicity and prothrombotic potential. Expert Opin Drug Saf. 2008;7:703-16.
[252] Moog R, Burger AM, Brandl M, Schuler J, Schubert R, Unger C, et al. Change in pharmacokinetic and pharmacodynamic behavior of gemcitabine in human tumor xenografts upon entrapment in vesicular phospholipid gels. Cancer Chemother Pharmacol. 2002;49:356-66.
[253] Farrell JJ, Elsaleh H, Garcia M, Lai R, Ammar A, Regine WF, et al. Human equilibrative nucleoside transporter 1 levels predict response to gemcitabine in patients with pancreatic cancer. Gastroenterology. 2009;136:187-95.
[254] Lee GY, Qian WP, Wang L, Wang YA, Staley CA, Satpathy M, et al. Theranostic nanoparticles with controlled release of gemcitabine for targeted therapy and MRI of pancreatic cancer. ACS Nano. 2013;7:2078-89.
[255] Dalla Pozza E, Lerda C, Costanzo C, Donadelli M, Dando I, Zoratti E, et al. Targeting gemcitabine containing liposomes to CD44 expressing pancreatic adenocarcinoma cells causes an increase in the antitumoral activity. Biochim Biophys Acta. 2013;1828:1396-404.
[256] Zhu S, Wonganan P, Lansakara PD, O'Mary HL, Li Y, Cui Z. The effect of the acid-sensitivity of 4-(N)-stearoyl gemcitabine-loaded micelles on drug resistance caused by RRM1 overexpression. Biomaterials. 2013;34:2327-39.
[257] Kotopoulis S, Dimcevski G, Gilja OH, Hoem D, Postema M. Treatment of human pancreatic cancer using combined ultrasound, microbubbles, and gemcitabine: a clinical case study. Med Phys. 2013;40:072902.
[258] Julka PK, Chacko RT, Nag S, Parshad R, Nair A, Koppiker CB, et al. A phase 2 study of sequential neoadjuvant chemotherapy with gemcitabine and doxorubicin followed by gemcitabine and cisplatin in patients with large or locally advanced operable breast cancer: results from long-term follow-up. Breast Cancer. 2013;20:357-62.
[259] Crespo G, Sierra M, Losa R, Berros JP, Villanueva N, Fra J, et al. Pegylated liposomal doxorubicin and gemcitabine in a fixed dose rate infusion for the treatment of patients with poor prognosis of recurrent ovarian cancer: a phase Ib study. Int J Gynecol Cancer. 2011;21:478-85.
[260] Del Barco S, Colomer R, Calvo L, Tusquets I, Adrover E, Sanchez P, et al. Non-pegylated liposomal doxorubicin combined with gemcitabine as first-line treatment for metastatic or

locally advanced breast cancer. Final results of a phase I/II trial. Breast Cancer Res Treat. 2009;116:351-8.
[261] Roubaud G, Gross-Goupil M, Wallerand H, de Clermont H, Dilhuydy MS, Ravaud A. Combination of gemcitabine and doxorubicin in rapidly progressive metastatic renal cell carcinoma and/or sarcomatoid renal cell carcinoma. Oncology. 2011;80:214-8.
[262] Franchina T, Adamo B, Ricciardi GR, Caristi N, Agostino RM, Proto C, et al. Activity of pegylated liposomal doxorubicin in combination with gemcitabine in triple negative breast cancer with skin involvement: two case reports. Cancer Biol Ther. 2012;13:472-6.
[263] Rivera E, Valero V, Arun B, Royce M, Adinin R, Hoelzer K, et al. Phase II study of pegylated liposomal doxorubicin in combination with gemcitabine in patients with metastatic breast cancer. J Clin Oncol. 2003;21:3249-54.
[264] Fabi A, Ferretti G, Papaldo P, Salesi N, Ciccarese M, Lorusso V, et al. Pegylated liposomal doxorubicin in combination with gemcitabine: a phase II study in anthracycline-naive and anthracycline pretreated metastatic breast cancer patients. Cancer Chemother Pharmacol. 2006;57:615-23.
[265] Liu D, Chen Y, Feng X, Deng M, Xie G, Wang J, et al. Micellar nanoparticles loaded with gemcitabine and doxorubicin showed synergistic effect. Colloids Surf B Biointerfaces. 2013;113C:158-68.
[266] Rivera E, Valero V, Syrewicz L, Rahman Z, Esteva FJ, Theriault RL, et al. Phase I study of stealth liposomal doxorubicin in combination with gemcitabine in the treatment of patients with metastatic breast cancer. J Clin Oncol. 2001;19:1716-22.
[267] D'Agostino G, Ferrandina G, Ludovisi M, Testa A, Lorusso D, Gbaguidi N, et al. Phase II study of liposomal doxorubicin and gemcitabine in the salvage treatment of ovarian cancer. Br J Cancer. 2003;89:1180-4.
[268] Jacquin JP, Chargari C, Thorin J, Mille D, Melis A, Orfeuvre H, et al. Phase II trial of pegylated liposomal doxorubicin in combination with gemcitabine in metastatic breast cancer patients. Am J Clin Oncol. 2012;35:18-21.
[269] Lammers T, Subr V, Ulbrich K, Peschke P, Huber PE, Hennink WE, et al. Simultaneous delivery of doxorubicin and gemcitabine to tumors in vivo using prototypic polymeric drug carriers. Biomaterials. 2009;30:3466-75.
[270] Maeda H, Matsumura Y. EPR effect based drug design and clinical outlook for enhanced cancer chemotherapy. Adv Drug Deliv Rev. 2011;63:129-30.
[271] Discher DE, Ortiz V, Srinivas G, Klein ML, Kim Y, Christian D, et al. Emerging applications of polymersomes in delivery: from molecular dynamics to shrinkage of tumors. Progress in polymer science. 2007;32:838-57.
[272] Szebeni J, Baranyi L, Savay S, Bodo M, Morse DS, Basta M, et al. Liposome-induced pulmonary hypertension: properties and mechanism of a complement-mediated pseudoallergic reaction. Am J Physiol Heart Circ Physiol. 2000;279:H1319-28.
[273] Lee JS, Feijen J. Polymersomes for drug delivery: design, formation and characterization. J Control Release. 2012;161:473-83.
[274] Meng F, Zhong Z, Feijen J. Stimuli-responsive polymersomes for programmed drug delivery. Biomacromolecules. 2009;10:197-209.
[275] Jain JP, Ayen WY, Kumar N. Self assembling polymers as polymersomes for drug delivery. Curr Pharm Des. 2011;17:65-79.
[276] Choucair A, Soo PL, Eisenberg A. Active loading and tunable release of doxorubicin from block copolymer vesicles. Langmuir. 2005;21:9308-13.
[277] Ahmed F, Discher DE. Self-porating polymersomes of PEG-PLA and PEG-PCL: hydrolysis-triggered controlled release vesicles. J Control Release. 2004;96:37-53.
[278] Chiang WH, Huang WC, Chang CW, Shen MY, Shih ZF, Huang YF, et al. Functionalized polymersomes with outlayered polyelectrolyte gels for potential tumor-targeted delivery of multimodal therapies and MR imaging. J Control Release. 2013;168:280-8.

[279] Canton I, Battaglia G. Polymersomes-mediated delivery of fluorescent probes for targeted and long-term imaging in live cell microscopy. Methods Mol Biol. 2013;991:343-51.
[280] Petersen MA, Hillmyer MA, Kokkoli E. Bioresorbable polymersomes for targeted delivery of Cisplatin. Bioconjug Chem. 2013;24:533-43.
[281] Zhang Y, Zhang W, Johnston AH, Newman TA, Pyykko I, Zou J. Targeted delivery of Tet1 peptide functionalized polymersomes to the rat cochlear nerve. Int J Nanomedicine. 2012;7:1015-22.
[282] Zhou W, Meng F, Engbers GH, Feijen J. Biodegradable polymersomes for targeted ultrasound imaging. J Control Release. 2006;116:e62-4.
[283] !!! INVALID CITATION !!!
[284] Kim H, Kang YJ, Kang S, Kim KT. Monosaccharide-responsive release of insulin from polymersomes of polyboroxole block copolymers at neutral pH. J Am Chem Soc. 2012;134:4030-3.
[285] Cerritelli S, Velluto D, Hubbell JA. PEG-SS-PPS: reduction-sensitive disulfide block copolymer vesicles for intracellular drug delivery. Biomacromolecules. 2007;8:1966-72.
[286] Kamat NP, Robbins GP, Rawson JS, Therien MJ, Dmochowski IJ, Hammer DA. A Generalized System for Photo-Responsive Membrane Rupture in Polymersomes. Adv Funct Mater. 2010;20:2588-96.
[287] Amstad E, Kim SH, Weitz DA. Photo- and thermoresponsive polymersomes for triggered release. Angew Chem Int Ed Engl. 2012;51:12499-503.
[288] Oliveira H, Perez-Andres E, Thevenot J, Sandre O, Berra E, Lecommandoux S. Magnetic field triggered drug release from polymersomes for cancer therapeutics. J Control Release. 2013.
[289] Robert JL, Aubrecht KB. Ring-Opening Polymerization of Lactide To Form a Biodegradable Polymer. Journal of Chemical Education. 2008;85:258.
[290] Mayer LD, Tai LC, Bally MB, Mitilenes GN, Ginsberg RS, Cullis PR. Characterization of liposomal systems containing doxorubicin entrapped in response to pH gradients. Biochimica et Biophysica Acta (BBA)-Biomembranes. 1990;1025:143-51.
[291] Rahul R. Nahire SSJ, Varsha Meghnani, Nalini Shastri, K. V. Surendra Nath and J. Sathish. Zero Absorbance UV Spectrophotometric Assay Method for Simultaneous Determination of Amlodipine Besylate and Valsartan. Current Research in Biological and Pharmaceutical Sciences2013. p. 1-5.
[292] Ho WY, Yeap SK, Ho CL, Rahim RA, Alitheen NB. Development of multicellular tumor spheroid (MCTS) culture from breast cancer cell and a high throughput screening method using the MTT assay. PLoS One. 2012;7:e44640.
[293] Jeong B, Bae YH, Lee DS, Kim SW. Biodegradable block copolymers as injectable drug-delivery systems. Nature. 1997;388:860-2.
[294] Discher DE, Ahmed F. Polymersomes. Annu Rev Biomed Eng. 2006;8:323-41.
[295] Liu D, Mori A, Huang L. Role of liposome size and RES blockade in controlling biodistribution and tumor uptake of GM1-containing liposomes. Biochim Biophys Acta. 1992;1104:95-101.
[296] Jimenez-Fernandez J. Nonlinear response to ultrasound of encapsulated microbubbles. Ultrasonics. 2012;52:784-93.
[297] Spinler K, Tian A, Christian DA, Pantano DA, Baumgart T, Discher DE. Dynamic domains in polymersomes: mixtures of polyanionic and neutral diblocks respond more rapidly to changes in calcium than to pH. Langmuir. 2013;29:7499-508.
[298] Perez-Manga G, Lluch A, Alba E, Moreno-Nogueira JA, Palomero M, Garcia-Conde J, et al. Gemcitabine in combination with doxorubicin in advanced breast cancer: final results of a phase II pharmacokinetic trial. J Clin Oncol. 2000;18:2545-52.
[299] Lombardi G, Zustovich F, Farinati F, Cillo U, Vitale A, Zanus G, et al. Pegylated liposomal doxorubicin and gemcitabine in patients with advanced hepatocellular carcinoma: results of a phase 2 study. Cancer. 2011;117:125-33.

[300] Nahire RR, Joshi SS, Meghnani V, Shastri N, Nath KS, Sathish J. Stability indicating RP-HPLC method for simultaneous determination of amlodipine besylate and valsartan combination in bulk and commercial dosage forms. Asian Journal of Pharmacy and Life Science. 2012;2:280-90.
[301] Joshi S, Nahire R, Shastri N, Surendranath K, Satish J. Validated stability-indicating RP-HPLC UV method for simultaneous determination of metformin and repaglinide. Acta Chromatographica. 2012;24:419-32.
[302] Hamid R, Rotshteyn Y, Rabadi L, Parikh R, Bullock P. Comparison of alamar blue and MTT assays for high through-put screening. Toxicol In Vitro. 2004;18:703-10.
[303] Goodman TT, Ng CP, Pun SH. 3-D tissue culture systems for the evaluation and optimization of nanoparticle-based drug carriers. Bioconjug Chem. 2008;19:1951-9.
[304] Sax N, Kodama T. Optimization of acoustic liposomes for improved in vitro and in vivo stability. Pharm Res. 2013;30:218-24.

APPENDIX A

Quenching effect of ELIPs on carboxyfluorescein fluorescence

To study effect of echogenic liposomes on the fluorescence of carboxyfluorescein, two batches of liposomes were prepared, regular liposomes and echogenic liposomes without encapsulation of dye following same protocol as described in main manuscript. Reconstituted liposomal solutions (0.02 mg/ml) were then incubated in 0.5 μM carboxyfluorescein in 25 mM HEPES buffer pH 8 with added Ca^{+2} and Zn^{+2} for an hour and fluorescence was monitored with excitation at 480 nm and emission spectra were recorded at 525 nm at different time intervals (0 min, 30 min and 60 min).

Table A1. Fluorescence intensities of dye when incubated with regular (non-echogenic) and echogenic liposomes.

	Fluorescence Intensities (units)	
Incubation time (min)	**Regular Liposomes**	**Echogenic Liposomes**
0	13130	13633
30	13099	13228
60	13095	13221

APPENDIX B

Fluorescence correction for carboxyfluorescein

Fluorescence emission intensity of carboxyfluorescein decreases with decrease in pH. To compensate for this decrease, we obtained a calibration curve for carboxyfluorescein emission intensity by exciting at the isosbestic absorption (460 nm) and monitoring emission at the isosbestic point at 497 nm.

$I_tpH = rpH \cdot I_tmpH$ ..... Equation (1)

Where I_tpH is the corrected fluorescence intensity, rpH is the correction factor for the effect of pH and I_t,mpH is the measured fluorescence intensity at a particular pH and time (t) of interest. To calculate correction factor for the effect of pH (rpH), calibration curves were generated for the fluorescence intensity of free carboxyfluorescein at pH 7.4, 6 and 5. Concentrations of carboxyfluorescein were taken from desired range for all the release experiments (0.5 μM to 5 μM). Correction factor (rpH) = Slope at pH 7.4 / Slope at particular pH

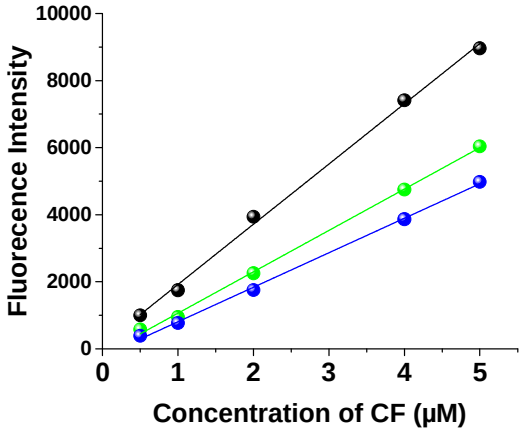

Figure B1. Calibration graphs for intensity of carboxyfluorescein (CF) as a function of pH. Black: pH 7.4; blue: pH 6.0 ; green: pH 5.0.

Corrections factors were found be 1.45 and 1.74 for pH 6, and 5 respectively. Corrected fluorescence emission intensity at particular pH was calculated each time by using equation 1.

pH triggered release profile of sodium bicarbonate encapsulating POPC liposomes

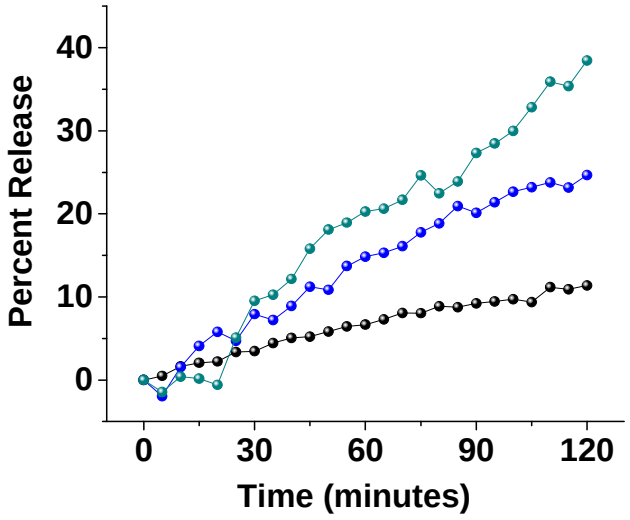

Figure B2. Release profiles of carboxyfluorescein from 400 mM sodium bicarbonate encapsulated liposomes, incubated in HEPES buffer pH 7.4 (black spheres), pH 6 (blue spheres), and pH 5 (dark cyan spheres). The lines are generated by connecting the observed data points.

pH triggered release from sodium bicarbonate encapsulating POPC liposomes

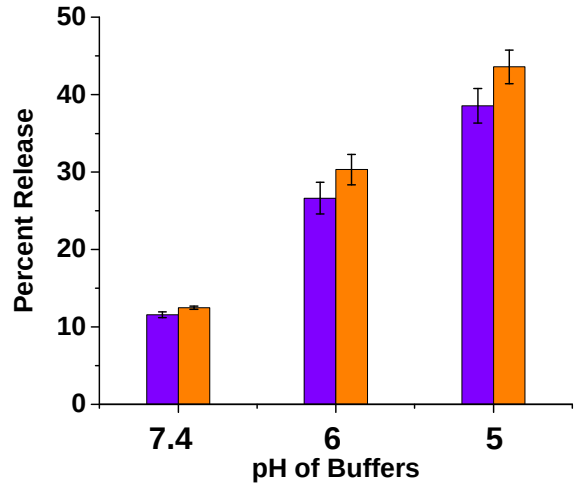

Figure B3. Release from pH tunable echogenic liposomes encapsulating 400 mM sodium bicarbonate after incubation in 25 mM HEPES buffer for 2 hours (violet) and 3 hours (orange) (n = 3).

Release from control POPC liposomes (without bicarbonate encapsulation) when incubated in different pH buffers for 2 hrs

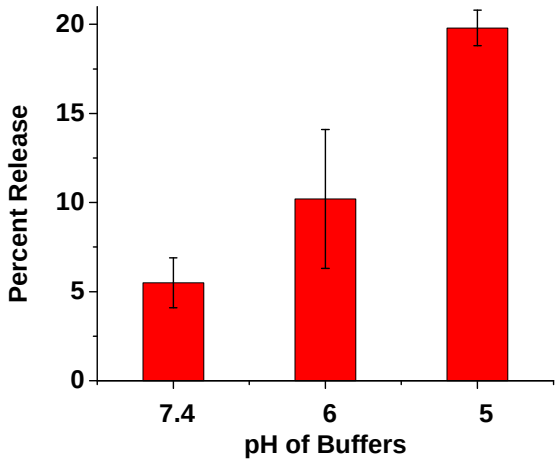

Figure B4. Release of carboxyfluorescein from POPC liposomes (without bicarbonate encapsulation) when incubated in different pH buffers for 2 hours (n = 3).

pH triggered release from ammonium bicarbonate encapsulating DSPC liposomes:

Table B1. Percent release of carboxyfluorescein from 400 mM ammonium bicarbonate and 400 mM sodium bicarbonate encapsulated DSPC liposomes after incubation for 2 hours (Avg ± SD; n = 3).

Type of Precursor (400 mM)	**pH 7.4**	**pH 6**	**pH 5**
Ammonium bicarbonate	< 1	< 5	5 ± 1
Sodium bicarbonate	< 1	< 5	< 5

Uptake studies with MCF-7 cells and POPC liposomes

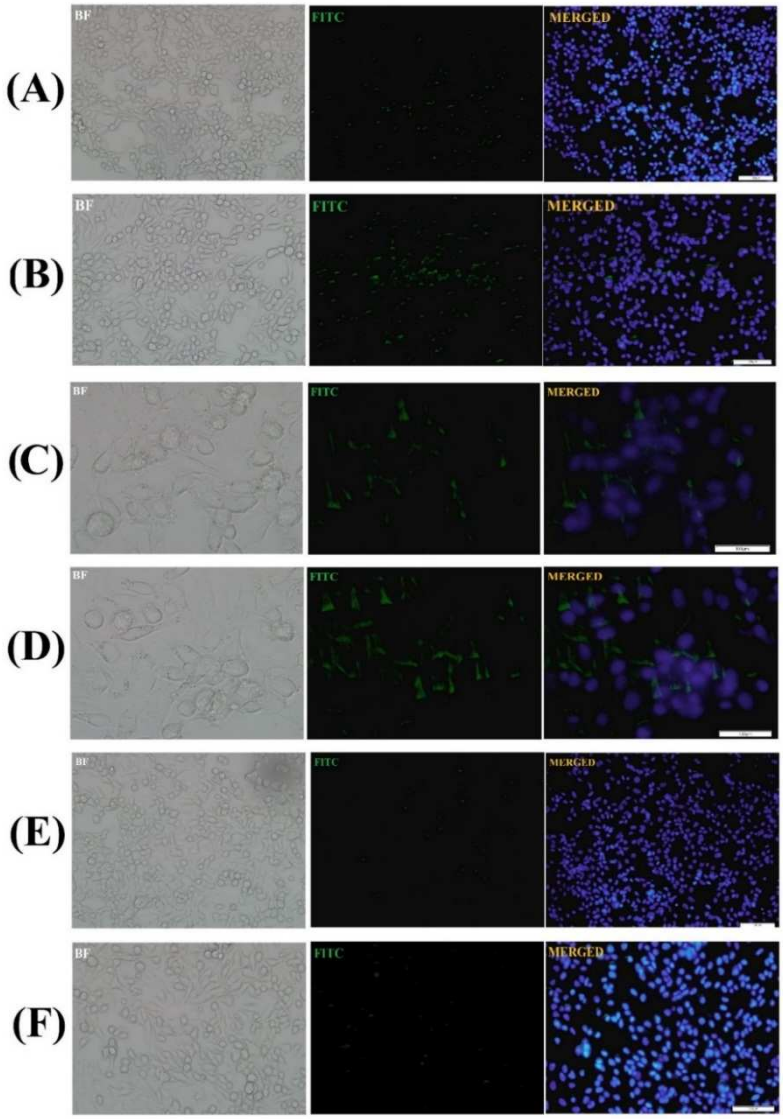

Figure B5. Fluorescence microscopic images for the uptake of pH tunable echogenic liposomes by folate receptor overexpressing MCF-7 cancer cells as a function of incubation time. (**A**) Incubation time: 10 minutes (magnification: 20X); (**B**) Incubation time: 20 minutes (magnification: 20X); (**C**) Incubation time: 10 minutes (magnification: 40X); (**D**) Incubation time: 20 minutes (magnification: 40X); (**E**) Non-targeted pH tunable echogenic liposomes; Incubation time: 10 minutes (magnification: 20X); (**F**) Non-targeted pH tunable echogenic liposomes; Incubation time: 20 minutes (magnification: 20X).

APPENDIX C

Synthesis and characterization of the polymers

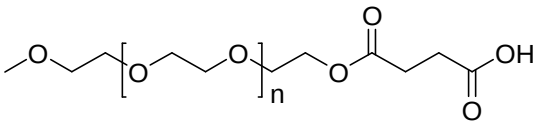

To a stirred solution of methoxy PEG (MW 1900, 5.7 g, 3 mmol) in dichloromethane (50 mL), succinic anhydride (450 mg, 4.5 mmol) was added followed by triethylamine (303 mg, 3 mmol). The reaction mixture was stirred overnight under nitrogen at room temperature. Upon completion of the reaction, majority of the solvent was evaporated off under reduced pressure, and the residual solution was added slowly to cold ether. The precipitate thus formed was centrifuged, washed with ether and dried under vacuum to afford a white powder (5.3 g, 88%).

^{1}H NMR ($CDCl_3$): 4.23 (s, 2H), 3.52-3.57 (m, 175 H), 3.35 (s, 3H), 2.61 (s, 4H).

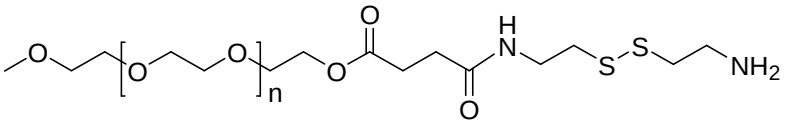

Acid terminated m-PEG (2 g, 1 mM) was dissolved in dichloromethane (40 mL). To this stirred solution, cystamine dihydrochloride (336 mg, 1.5 mmol) was added followed by triethylamine (401 mg, 4 mM). After 5 minutes, EDC (194 mg, 1.25 mmol) was added and the reaction mixture was stirred overnight under nitrogen and at room temperature. Subsequently, the reaction mixture was washed with brine, and dried over Na_2SO_{47}. Removal of solvent, precipitation in ether, and drying under vacuum afforded the desired product in 76% Yield (1.62 g).

^{1}H NMR ($CDCl_3$): 4.23 (m, 2H), 3.48-3.65 (m, 175 H), 3.3 (s, 3H), 3.05 (br S, 4H), 2.7 (m, 2H), 2.5- 2.6 (m, 4H), 2.4 (m, 2H).

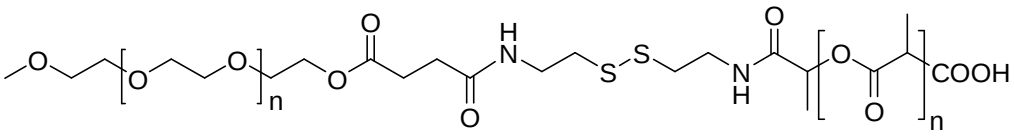

The PEG-cystamine conjugate was taken into toluene (40 mL) and was subjected to azeotropic distillation with the aid of Dean Stark apparatus for 5 hours. The solution was then cooled under nitrogen. Upon addition of required amount of D,L-lactide and catalytic quantity of octyl tin , the reaction mixture was further refluxed for six hours under nitrogen. Subsequently, the resulting reaction mixture was cooled, and slowly added to chilled ether causing precipitation. The sticky semi-solid precipitate was collected, washed, and reprecipitated in ether. Drying under vacuum afforded desired PEG-S-S-PLA conjugate in fair to good yield.

PLA= 5800 (PEG cystamine- 200 mg, D,L- lactide 700 mg, octyl tin 15 mg, Yield- 82%) ^{1}H NMR ($CDCl_3$): 5.07-5.19 (m, 72H), 4.16-4.20(m, 2H), 3.50-3.64(m, 174 H), 3.32 (s, 3H), 2.74-2.77 (m, 2H), 2.62-2.68 (m, 2H), 2.44-2.47 (m, 2H), 1.46-1.53 (m, 231 H)

PLA 3600 (PEG cystamine- 200 mg, D,L- lactide 450 mg, octyl tin 11 mg, Yield- 69 %) ^{1}H NMR ($CDCl_3$): 5.04-5.13 (m, 51H), 4.13-4.17(m, 2H), 3.51-3.67(m, 174 H), 3.32 (s, 3H), 2.74-2.77 (m, 2H), 2.62-2.68 (m, 3H), 2.44-2.47 (m, 4H), 1.46-1.53 (m, 152 H)

Size Distribution by dynamic light scattering

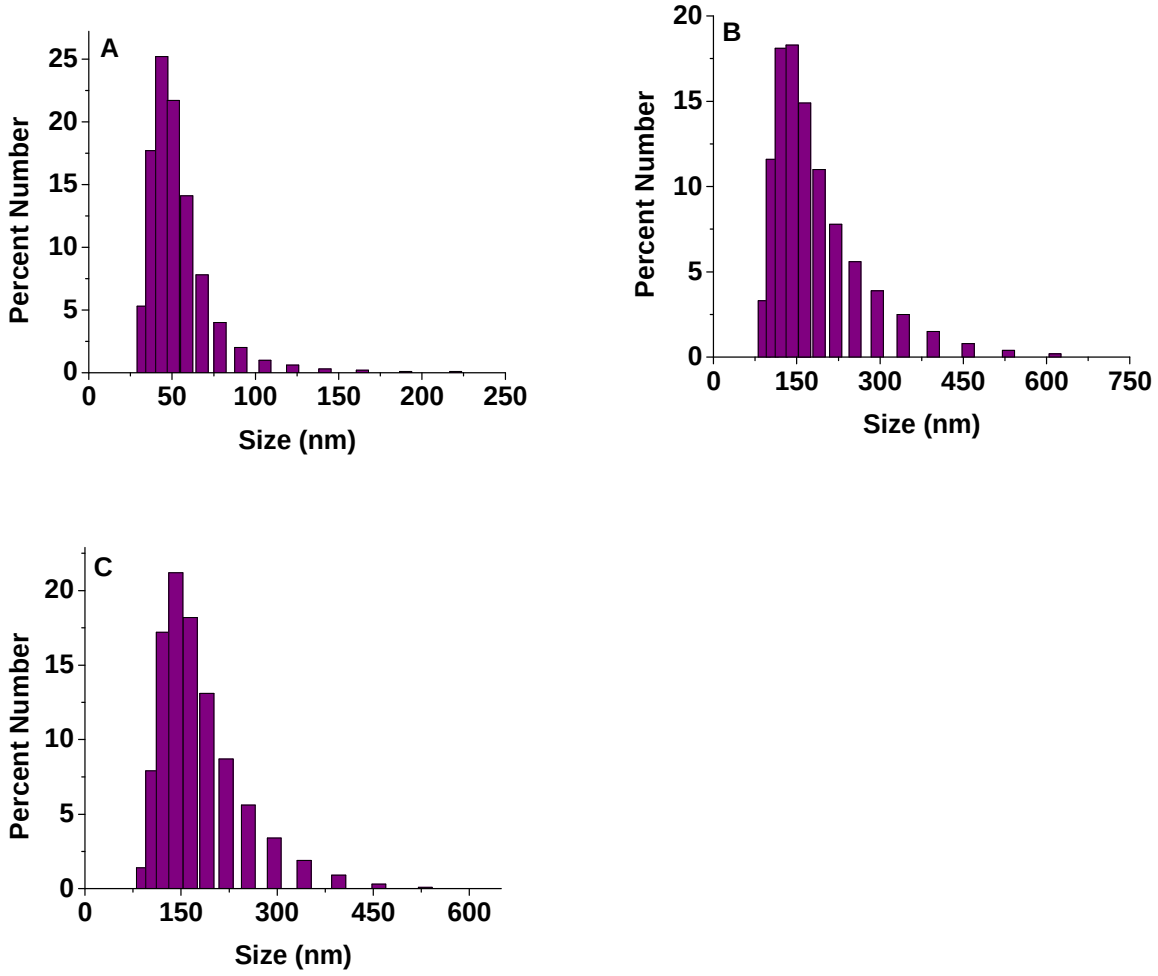

Figure C1. Representative size distribution by number of the structures formed by different polymers by dynamic light scattering method using Zetasizer instrument (A) PEG_{1900}-S-S-PLA_{900} (B) PEG_{1900}-S-S-PEG_{1700} (C) PEG_{1900}-S-S-PEG_{1950}.

Effect of 5 mM GSH on echogenicity of polymersomes

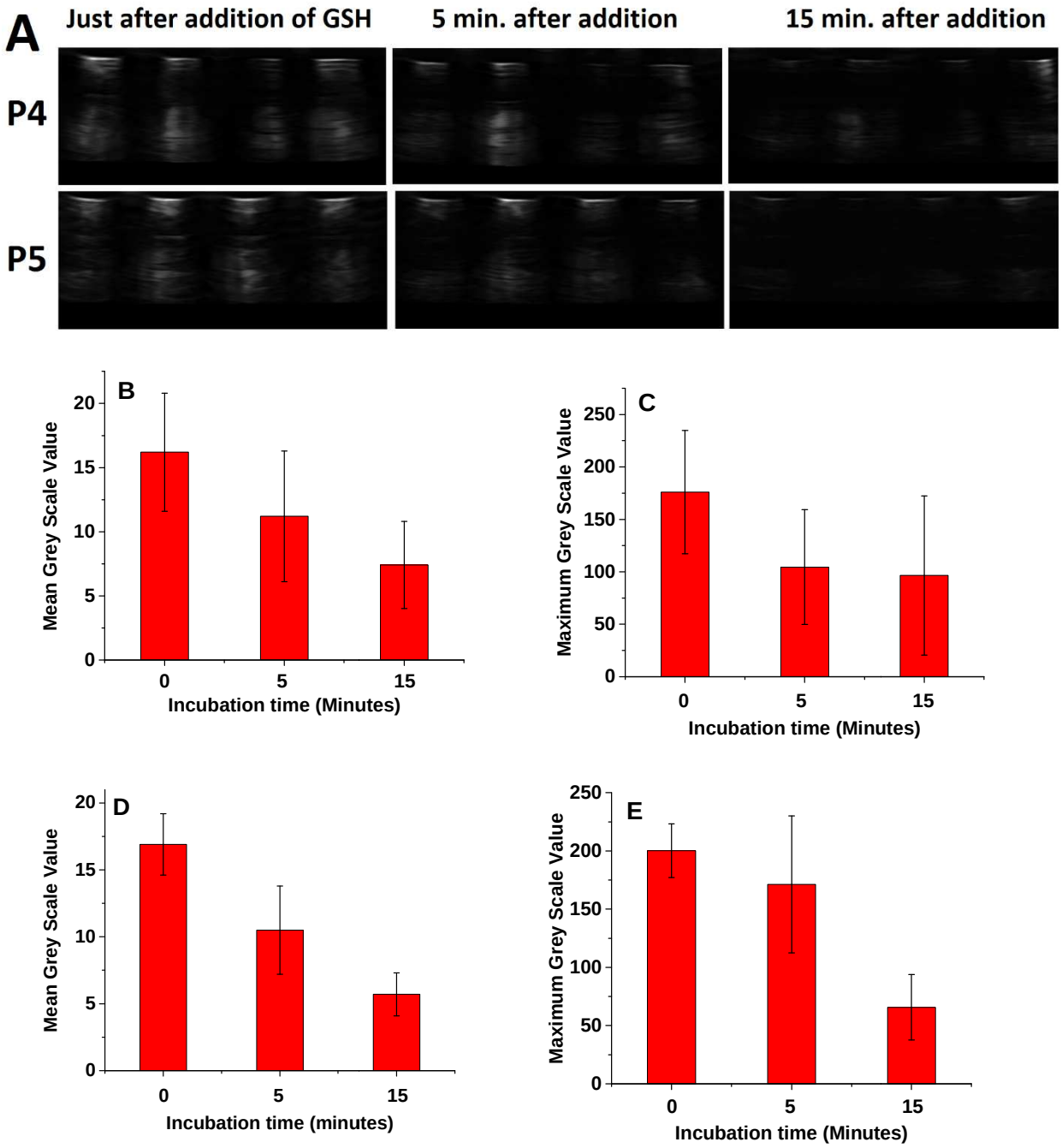

Figure C2. Effect of 5 mM GSH on echogenicity of polymersomes (A) Diagnotic ultrasound images of polymersomes exposed to 5 mM GSH (B) Mean grey scale values of P4 polymersomes incubated in 5 mM GSH as a function of time (C) Maximum grey scale values of P4 polymersomes incubated in 5 mM GSH as a function of time (D) Mean grey scale values of P5 polymersomes incubated in 5 mM GSH as a function of time (E) Maximum grey scale values of P5 polymersomes incubated in 5 mM GSH as a function of time.

Calibration curves for simultaneous determination of gemcitabine and doxorubicin

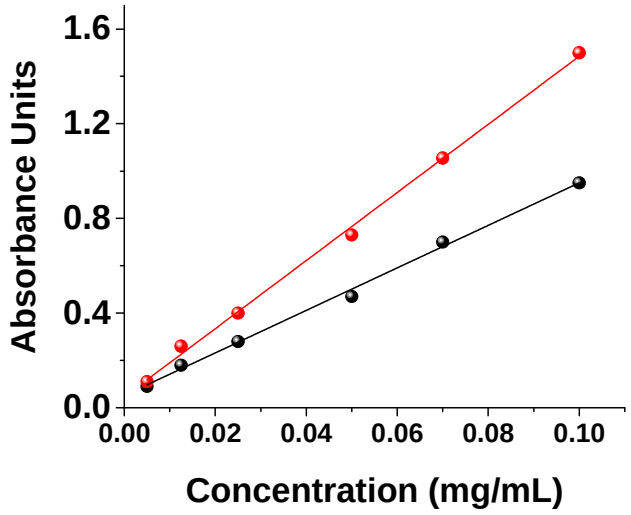

Figure C3. Calibration curve for simultaneous determination of doxorubicin at 480 nm (black) and gemcitabine (red) at 276 nm. Spheres indicate the observed data points whereas lines indicate fitted straight lines.

Linear equation:

Doxorubicin: $Y = (8.98 \pm 0.24)*X + (0.052 \pm 0.013,)$ $R^2 = 0.996$

Gemcitabine: $Y = (14.39 \pm 0.32)*X + (0.046 \pm 0.01)$, $R^2 = 0.997$

Cellular uptake studies with MCF-7 cells

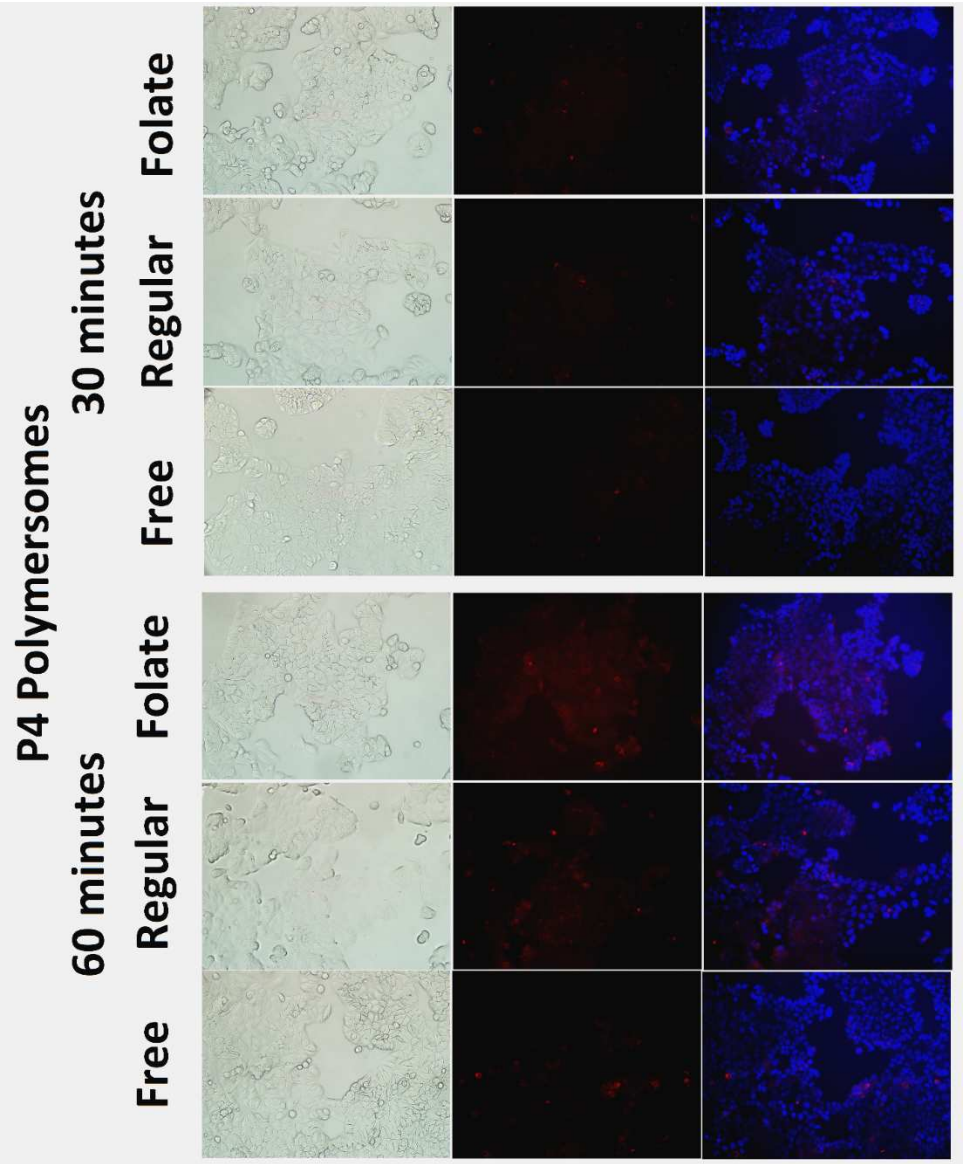

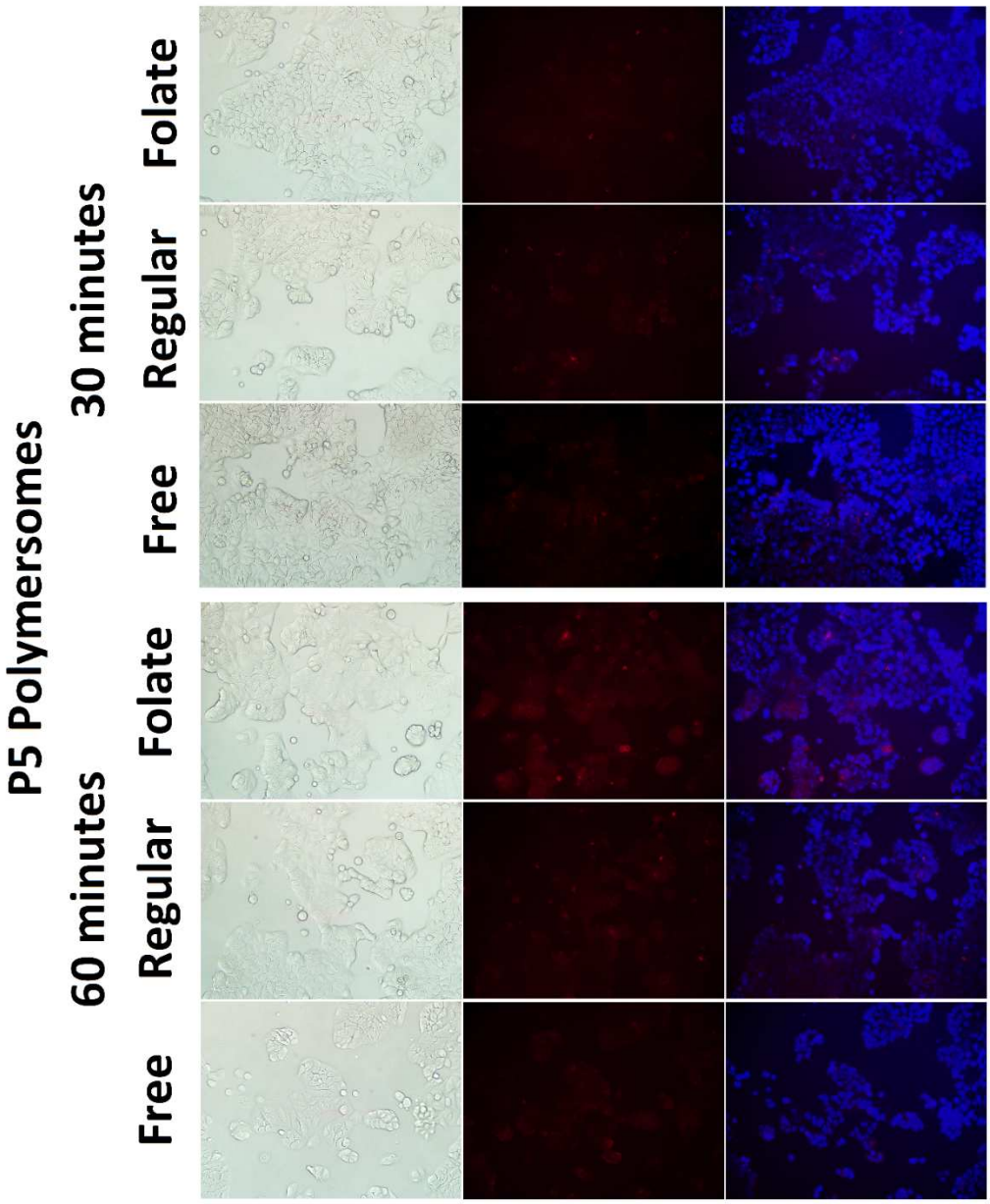

Figure C4. P4 and P5 polymersomes uptake studies with MCF-7 cells as a function time and folate targeting.

Cell viability of MCF-7 spheroids

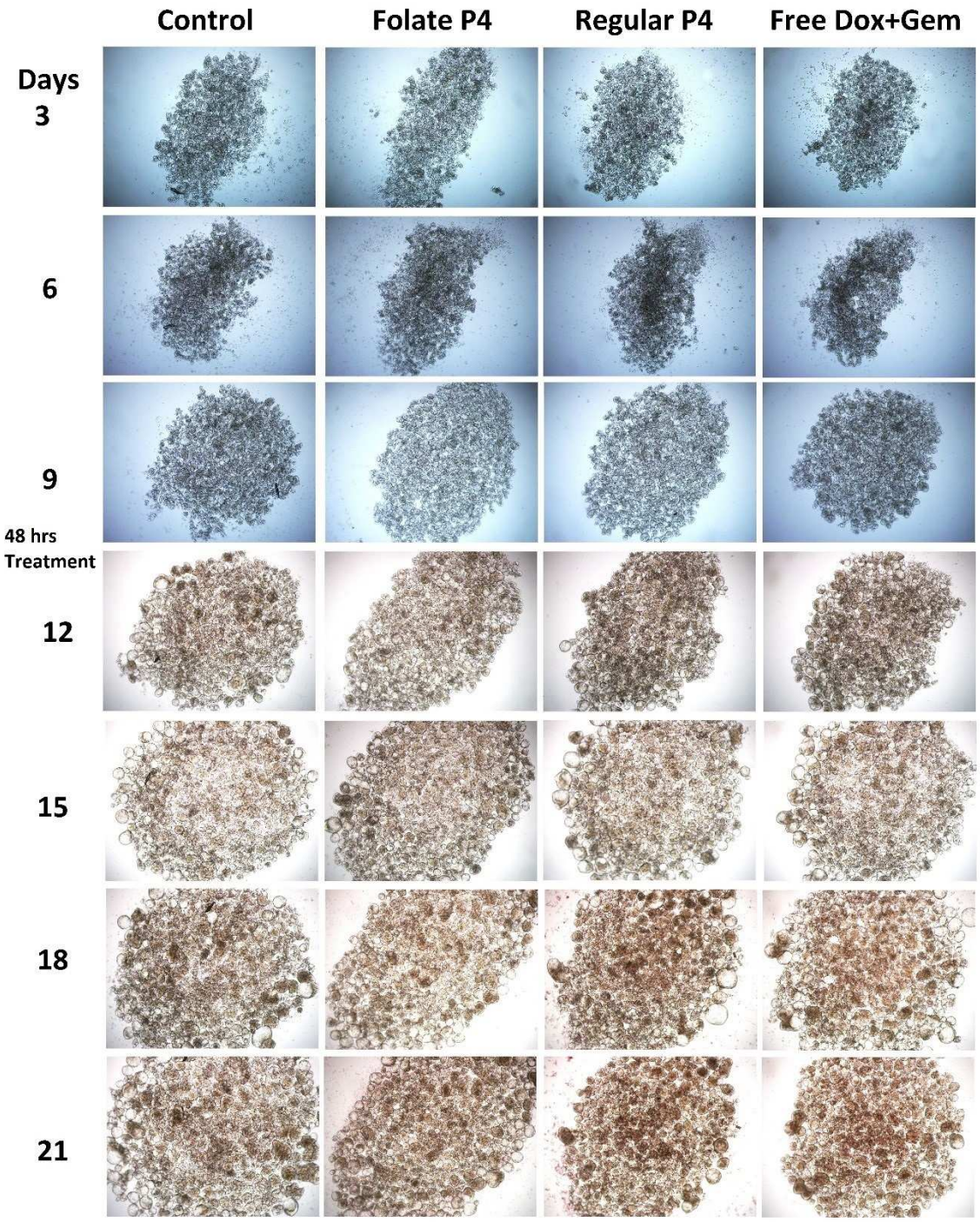

Figure C5. Images of MCF-7 Spheroids treated with P4 polymersomes. Spheroids were exposed to three different treatments for 48 hours on 10th and 11th day.